Volume 49
Number 15
21 April 2020
Pages 4583-4980

# Dalton Transactions

An international journal of inorganic chemistry

rsc.li/dalton

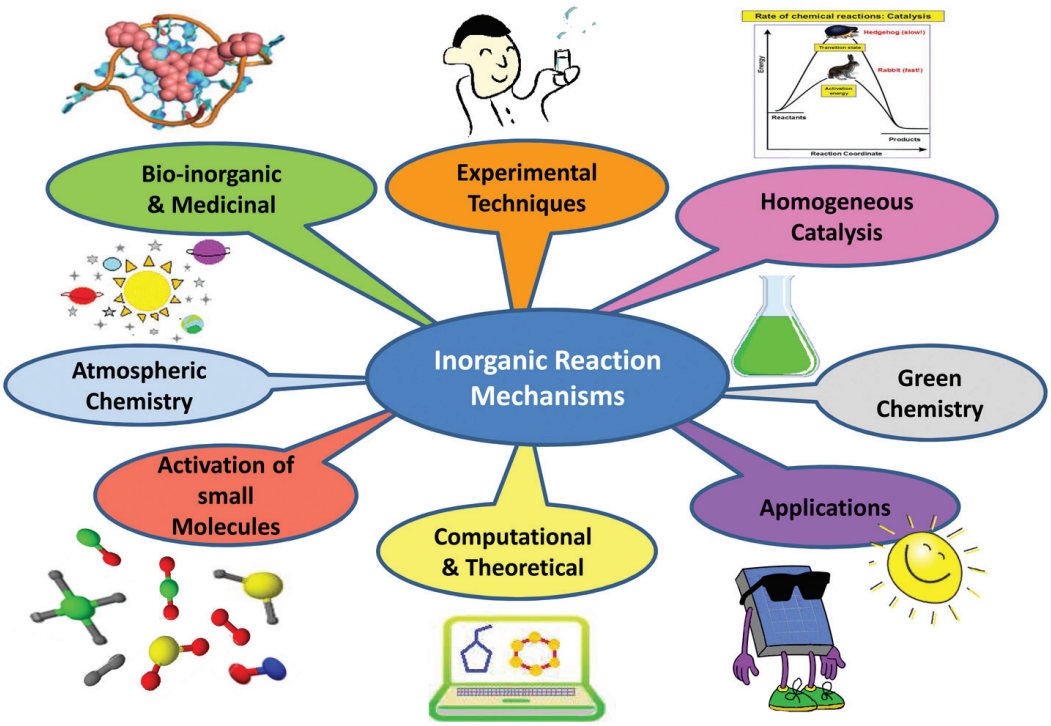


ISSN 1477-9226

ROYAL SOCIETY OF CHEMISTRY

**PERSPECTIVE**
Rudi van Eldik *et al.*
Inorganic reaction mechanisms. A personal journey

Dalton Transactions

ROYAL SOCIETY OF CHEMISTRY

PERSPECTIVE

View Article Online
View Journal | View Issue



Cite this: *Dalton Trans.*, 2020, **49**, 4599

# Inorganic reaction mechanisms. A personal journey†

Colin D. Hubbard,[a,b] Debabrata Chatterjee,[a,c] Maria Oszajca,[d] Justyna Polaczek,[d] Olga Impert,[e] Marta Chrzanowska,[e] Anna Katafias,[e] Ralph Puchta[a] and Rudi van Eldik *[a,d,e]

Received 3rd December 2019,
Accepted 4th March 2020

DOI: 10.1039/c9dt04620h

rsc.li/dalton

This review covers highlights of the work performed in the van Eldik group on inorganic reaction mechanisms over the past two decades in the form of a personal journey. Topics that are covered include, from NO to HNO chemistry, peroxide activation in model porphyrin and enzymatic systems, the wonder-world of $Ru^{III}$(edta) chemistry, redox chemistry of Ru(III) complexes, Ru(II) polypyridyl complexes and their application, relevant physicochemical properties and reaction mechanisms in ionic liquids, and mechanistic insight from computational chemistry. In each of these sections, typical examples of mechanistic studies are presented in reference to related work reported in the literature.



## 1. General introduction

After having received the invitation to write a review on Inorganic Reaction Mechanisms (IRM) for the 50th Anniversary of the RSC Inorganic Reaction Mechanisms Discussion Group Meetings (IRMDGM), my thoughts as corresponding author immediately went back to the nineteen seventies when the family of established mechanistic inorganic chemists such as Martin Tobe, Ralph Wilkins, Fred Basolo, Ralph G. Pearson, Gordon Harris, Harry B. Gray, Henry Taube, John Burgess, Geoffrey Sykes, Thomas Swaddle, and others participated in lively discussions either in the group meetings, or other conferences as well as through publications on the subject of Inorganic Reaction Mechanisms. For more detailed information see: http://homepages.warwick,ac.uk/~mssbq/irmg/irmg_history.htm. For me, being a newcomer to the field of IRM, these meetings among others, were very stimulating and clearly had a big influence on my own academic career. A series of monographs or other forms of publication on IRM have appeared over the years: Martyn V. Twigg, Ed., *Mechanisms of Inorganic and Organometallic Reactions*, vol. 1–8, Plenum, 1983–1994. Ralph G. Wilkins, *Kinetics and Mechanism of Reactions of Transition Metal Complexes*, Wiley-VCH, 1991; James H. Espenson, *Chemical Kinetics and Reaction Mechanisms*, McGraw-Hill, 1995; Jim D. Atwood, *Inorganic and Organometallic Reaction Mechanisms*, Wiley-VCH, 1997; Martin L. Tobe and John Burgess, *Inorganic Reaction Mechanisms*, Addison Wesley Longman, 1999 (this publication is the most comprehensive on IRM); Robert B. Jordan, *Reaction Mechanisms of Inorganic and Organometallic Systems*, 3rd edn, Oxford University Press, 2007. While an abundance of subsequent research on IRM has been published in journals or as reviews since, these works represent a valuable resource for accessing the fundamentals and development as the subject progressed.

As editor of the series Advances in Inorganic Chemistry (Academic Press), we have published a number of thematic issues that deal with IRM in a broader sense: vol. 54 and 70: *Inorganic Reaction Mechanisms*; vol. 64: *Inorganic/Bioinorganic Reaction Mechanisms*; vol. 65: *Homogeneous Catalysis*; vol. 67: *$NO_x$ Related Chemistry*; vol. 73: *Computational Chemistry*; vol. 74: *Water Oxidation Catalysts*; vol. 75: *Medicinal Chemistry*.

The field has expanded to such a degree that it has become impossible for a single author to cover the whole field of IRM. I hope that this concise review of a selection of topics will encourage a group of scientists interested in IRM to tackle the challenge as a team to produce an updated specialist monograph on IRM! In the intervening years, during the emergence of the monograph publications on the subject above, the annual IRMDGM originally held in the UK, while always attracting researchers from outside the UK, expanded in alternate years to venues outside of the UK, to continental Europe,

[a]*Department of Chemistry and Pharmacy, University of Erlangen-Nuremberg, Egerlandstr. 1, 91058 Erlangen, Germany. E-mail: rudi.vaneldik@fau.de*
[b]*Department of Chemistry, University of New Hampshire, Durham, New Hampshire, 03824, USA*
[c]*Vice-Chancellor's Research Group, Zoology Department, University of Burdwan, Burdwan-713104, India*
[d]*Faculty of Chemistry, Jagiellonian University, Gronostajowa 2, 30-387 Krakow, Poland*
[e]*Faculty of Chemistry, Nicolaus Copernicus University in Torun, Gagarina 7, 87-100 Torun, Poland*

†Invited review for the 50th anniversary of the RSC IRMDG for Dalton Transactions.

or to Ireland, for example, Wiesbaden, Strasbourg, Debrecen, Galway and Barcelona, attracting even further members of the veritable Who's Who in IRM, to the meetings. It also presented more opportunities for IRM research students in locations in Europe outside the UK to attend.

Another thought that came to my mind was how to deal with such a review in an objective way? Indeed a huge challenge! As the result of the limited time available, I decided to give the review a personal touch by concentrating on mechanistic high-lights produced in my research group in collaboration with many other leaders in the field of IRM. I extended an invitation to former and present colleagues to assist with writing the review, each one focusing on a specific topic that each was familiar with over the past two decades. The sequence of the selected topics follows an historical development in which the focus is mainly on experimental work and the ensuing results and discussion in the literature.

I ought to indicate, briefly, the route to my "immersion" in IRM. During the seven years I spent at the J. W. Goethe University of Frankfurt (Germany) (Habilitation in 1982), I 'inherited' the high pressure kinetics equipment from the late Prof. Hartwig Kelm and transferred it as it accompanied me to a new position at the University of Witten-Herdecke in 1987, and subsequently to the Friedrich-Alexander University Erlangen-Nuremberg in 1994. The equipment was repeatedly upgraded for contemporary purposes. During that period kinetic and thermodynamic measurements as a function of pressure (usually up to 200 MPa) were used to gain further mechanistic insight in terms of reaction and activation volumes that enabled the construction of volume profiles for inorganic, organometallic and bioinorganic reactions in solution (for more information on the application of high pressure techniques see ref. 1–4). In the subsequent sections of this review, examples will be included in which the application of high pressure techniques revealed unique insight into the detailed nature of the underlying reaction mechanism. Some fascinating and impressive studies were performed with the application of high pressure NMR techniques within our group in collaboration with visiting colleagues from abroad.[5–7]

Recently, I participated in a review on 'mechanistic insight on the chemistry of potential Pt antitumor agents as revealed by collaborative research performed in Kragujevac and Erlangen', in collaboration with colleagues from Kragujevac (Serbia) and Erlangen (Germany), dedicated to Prof. Dr Živadin Bugarčić (1954–2017). This manuscript is published in a special issue of *Inorg. Chim. Acta*, vol. 495, focusing on *Pt antitumor drugs and their chemistry* and edited by Bernhard Lippert, James Hoeschele and Matthew Hall.[8] The chemistry covered in this report will not be reviewed again in the present manuscript.

The selected sequence of the presentation is mostly a historical one based on important mechanistic questions pertinent at the time. The review starts with a section along the line of 'to be or not to be NO' (adapted from the Soliloquy of Shakespeare's Hamlet) and continues with 'from NO to HNO chemistry'. This work was very important in terms of Fe por-

**Colin D. Hubbard**

*Colin D. Hubbard grew up in Norfolk and Sussex. He read Chemistry at the University of Sheffield; B.Sc. (1961), Ph.D. degree with R. G. Wilkins (1964). Following post-doctoral research at MIT and Cornell University, (G. G. Hammes) and at the University of California, Berkeley, (J. F. Kirsch), he joined the faculty at the University of New Hampshire, in 1967, becoming Full Professor in 1979 and Emeritus Professor in 1994. Subsequently he joined the Research Group of Rudi van Eldik, at the University of Erlangen-Nuremberg. This was followed by a period of research at Unilever Research, in Colworth, England. He has served as Co-Editor of several volumes of Advances in Inorganic Chemistry in the period 2003–2019. His research interests include kinetics and mechanism of inorganic reactions and enzyme catalysed reactions. He has published widely in a variety of journals, and is a member of ACS, ASBMB and RSC, as well as The Arts Society (England) and the Triumph Owners' Motorcycle Club.*

**Debabrata Chatterjee**

*Debabrata Chatterjee was the Head of the Chemistry and Biomimetics Group of CSIR-Central Mechanical Engineering Research Institute at Durgapur, India. His research activities mainly include the mechanistic studies of catalytic and bio-chemical reactions in solution. The goal of these studies is to contribute towards a better understanding of these reactions. He has published 175 research papers in peer reviewed SCI journals. He is elected fellow of the National Academy of Science, India (FNASc), West Bengal Academy of Science & Technology (FWAST), and fellow of the Royal Society of Chemistry, UK (FRSC). Childhood polio has left him physically challenged with a considerable mobility problem.*

phyrin and CytP450$_{cam}$ chemistry since it involved kinetic measurements upon fast reactions as a function of temperature and pressure. The experience with NO chemistry formed the basis of detailed studies on 'peroxide activation in model porphyrin and enzymatic systems' reported in the next section. During that time our collaboration with Debabrata Chatterjee (Durgapur, India) produced fascinating Ru(III) chemistry here referred to as 'The wonder-world of $Ru^{III}$(edta) chemistry'. The following two topics come from more recent collaborations with colleagues at the Nicolaus Copernicus University in Torun and deal with 'Redox chemistry of Ru(III) complexes' and 'Ru(II) polypyridyl complexes and their application'. Over the years we have developed an intense interest in the application of ionic liquids (molten organic salts at room temperature) as reaction media to study IRM. Ten years ago we prepared and published a tutorial review on mechanisms in ionic liquids, briefly mentioning organic, organometallic and inorganic reactions.[9] I asked one of the authors of that review, Colin D. Hubbard, of the University of New Hampshire, to now review, with elaboration, our efforts over the past fifteen years, regarding IRM in ionic liquids. He has a longstanding interest in solvent effects and co-solvent effects on reaction kinetics, reactions in mixed solvents, and the importance of solvation effects in mechanism delineation. He has collaborated extensively within our group and also earlier with Edward F. Caldin (University of Kent, Canterbury), and for some forty years with John Burgess (University of Leicester). This review is covered in a section entitled 'relevant physicochemical properties and reaction mechanisms in ionic liquids'. Finally, we highlight some computational studies with Ralph Puchta using DFT calculations under 'mechanistic insight from computational chemistry' and complete the review with some general conclusions.

## 2. From NO to HNO chemistry

### 2.1 Reactions of non-heme Fe(II) complexes with nitric oxide (NO)

Around the turn of the century we got involved in NO chemistry through an industrial collaboration with Akzo Nobel Chemical Research Arnhem and Paques Bio Systems BV, The Netherlands, dealing with homogeneous catalysts for the selective binding and subsequent reduction of NO to dinitrogen in denitrification processes.[10] As homogeneous catalysts, Fe(II) polyaminecarboxylate complexes were used to bind NO efficiently during the wash-process of effluent gases from coal fired power plants. Although the binding constant of NO could be varied from $10^3$ (for $[Fe^{II}(H_2O)_6]^{2+}$) to $10^7$ $M^{-1}$ (for $[Fe^{II}(edta)H_2O]^{2-}$ and $[Fe^{II}(hedtra)H_2O]^{2-}$) using *ca.* 40 different polyaminecarboxylate chelates, the oxygen sensitivity of these complexes increased in the same order by which the Fe(II) complexes were oxidized to the corresponding Fe(III) complexes that showed no ability to bind NO.[10] In subsequent work,[11] detailed kinetic studies on the NO binding rate constants and the corresponding activation parameters[12] were performed to gain further insight into the underlying reaction mechanisms. Most of the studied Fe(II) polyaminecarboxylate complexes are seven-coordinate species in which the water exchange rate constant determines the rate and mechanism of the NO binding process (we will return to this statement later on).

It should be kept in mind that NO is a radical (11 electron species) and a non-innocent ligand. In its interaction with $M^{n+}$ metal ions it can either oxidize the metal ion to form $M^{(n+1)+}$–$NO^-$ or reduce it to $M^{(n-1)+}$–$NO^+$ or bind to it as $M^{n+}$–NO. In the first two cases, $NO^-$ is iso-electronic with dioxygen and coordinates to the metal centre with a bond angle of 120°, and $NO^+$ is iso-electronic with CO and binds to the metal centre

**Maria Oszajca**

*Maria Oszajca is an Assistant Professor at the Faculty of Chemistry of Jagiellonian University where she also obtained her PhD under the supervision of prof. Grażyna Stochel. During her research internships she worked in prof. Rudi van Eldik's group at the University of Erlangen-Nuremberg as well as in the group of prof. Claudine Kieda at CNRS Orléans.*

*She has devoted her scientific career to study the chemical kinetics of various bioinorganic processes relevant to the internal workings of living organisms. Her particular interests lie in the activation mechanisms of small biorelevant molecules (NO, $O_2$* etc.*) on iron-porphyrin model centers.*

**Justyna Polaczek**

*Justyna Polaczek was born in Nowy Targ, Poland, in 1990. She graduated in chemistry in 2014 at the Jagiellonian University in Kraków and started her PhD studies in the Group of* Physicochemistry of Coordination Compounds and Bioinorganic Chemistry *(Prof. Grażyna Stochel). In 2016 she was awarded a PRELUDIUM grant (NCN in Poland). In 2019 she received her PhD on the mechanism of nitrosylcobalamin formation, under the supervision of Prof. Rudi van Eldik. In 2019 she joined the SYMFONIA research project (Prof. Rudi van Eldik, Jagiellonian University) as a post-doctoral fellow and presently studies the influence of air pollution on nitrosylcobalamin interactions.*

with a bond angle of 180°. Thus its non-innocent character allows NO to remain as a radical, or it can be reduced to $NO^-$ or oxidized to $NO^+$.

At this point it is appropriate to refer to high pressure $^{17}$O-NMR experiments by which water exchange rates and activation volumes were determined by way of example for Fe(II) and Fe(III) hexa-aqua and edta complexes.[13,14] The water exchange rate constants at 25 °C were found to be $4.4 \times 10^6$ and $1.6 \times 10^2$ $s^{-1}$ for $[Fe^{II}(H_2O)_6]^{2+}$ and $[Fe^{III}(H_2O)_6]^{3+}$, respectively, with activation volumes of +3.8 and −5.4 $cm^3$ $mol^{-1}$, respectively, demonstrating that the much faster water exchange reaction in the case of Fe(II) follows an $I_d$ mechanism as compared to the less labile Fe(III) complex that follows an $I_a$ mechanism. In the case of the seven-coordinate edta complexes, the water exchange rate constants become rather close, *viz.* $2.7 \times 10^6$ and $6.0 \times 10^7$ $s^{-1}$ for the Fe(II) and Fe(III) complexes, respectively, with activation volumes of +8.6 and +3.6 $cm^3$ $mol^{-1}$, respectively. The large increase in the water exchange rate constant for $[Fe^{III}(edta)H_2O]^-$ compared to the hexa-aqua complex is associated with a mechanistic change-over from an $I_a$ to an $I_d$ (interchange associative to interchange dissociative) mechanism, whereas the more positive activation volume for the $[Fe^{II}(edta)H_2O]^{2-}$ complex indicates a more dissociative character due to the seven-coordinate nature of the complex.

We turned to the application of flash photolysis techniques as a function of temperature and pressure to gain further insight into the detailed nature of the NO binding mechanism. This work was done in collaboration with the group of Prof. Grazyna Stochel at the Jagiellonian University in Krakow, Poland. The rate constants for the 'on' reaction of the studied Fe(II) polyaminecarboxylate complexes required the application of flash photolysis techniques since the reactions with NO ($k_{on}$) are orders of magnitude faster than can be handled by stopped-flow techniques. In the case of the 'off' reaction, an NO-trap technique was used by which a NO scavenger rapidly reacts with the nitrosyl complex such that $k_{off}$ becomes the rate-determining step. These reactions are orders of magnitude slower and can be studied using a stopped-flow instrument as a function of temperature and pressure. Here it was especially the activation parameters $\Delta H^{\ddagger}$, $\Delta S^{\ddagger}$ and $\Delta V^{\ddagger}$ that interested us in terms of the further mechanistic clarification of the 'on' and 'off' reactions.

**Table 1** Rate and activation parameters for the reversible reaction[15]

| Reaction | $k$ at 25 °C | $\Delta H^{\ddagger}$ [kJ $mol^{-1}$] | $\Delta S^{\ddagger}$ [J $mol^{-1}$ $K^{-1}$] | $\Delta V^{\ddagger}$ [$cm^3$ $mol^{-1}$] |
|---|---|---|---|---|
| $Fe(aq)^{2+} + NO$ | $1.4 \times 10^6$ $M^{-1}$ $s^{-1}$ | 37.1 ± 0.5 | −3 ± 2 | +6.0 ± 0.3 |
| $Fe(NO)^{2+} + H_2O$ | $3.2 \times 10^3$ $s^{-1}$ | 48.4 ± 1.4 | −15 ± 5 | +1.2 ± 0.1 |
| $Fe(aq)^{2+} + H_2O$ | $4.4 \times 10^6$ $s^{-1}$ | 41.4 ± 1.2 | +21 ± 5 | +3.8 ± 0.2 |

In the case of the hexa-aqua complex, the rate and activation parameters for the 'on' and 'off' reactions are summarized in Table 1 and compared with that of the water exchange reaction.[15] Based on the kinetic data $k_{on}/k_{off} = 440 \pm 110$ $M^{-1}$ at 25 °C which is of the same order of magnitude as obtained from spectrophotometric measurements, *viz.* $(1.15 \pm 0.05) \times 10^3$ $M^{-1}$ in 0.1 M acetate buffer, pH = 5.0 and 23 °C. In terms of the nature of the mechanism, the volumes of activation for the 'on', 'off' and water exchange reaction are all in line with an $I_d$ mechanism. Furthermore, the water exchange reaction is much faster than the 'on' reaction indicating that the water exchange process controls the rate and mechanism of the 'on' reaction. The zero-field Mössbauer spectrum of the $^{57}$Fe-enriched nitrosylated iron solution measured at 80 K suggested that the electronic structure is best described by the presence of high-spin $Fe^{III}$ antiferromagnetically coupled to $NO^-$ ($S = 1$) yielding the observed spin quartet ground state ($S = 3/2$). A similar structure was proposed for the Fe(edta)NO complex.[16] In a very recent study by Klüfers and Monsch, the crystal structure of the 'brown-ring' chromophore was reported (see Fig. 1) and has an Fe–N–O bond angle of 162°.[17] The authors reported very similar Mössbauer parameters for the nitrosyl complex as in our study,[18] and performed a detailed

**Olga Impert**

*Olga Impert obtained her M.Sc. (2001) and Ph.D. (2007) degrees at the Nicolaus Copernicus University in Torun and did post-doctoral work at the University of Debrecen, Hungary (2010). Her research interests are centered on synthesis and reaction mechanisms of ruthenium complexes, including mixed-valence ion pair complexes.*

**Marta Chrzanowska**

*Marta Chrzanowska was born in Poland in 1991. She received her MS degree in 2015 at the Faculty of Chemistry, Nicolaus Copernicus University in Toruń (Poland). She is currently doing her PhD studies under the supervision of Professors Anna Katafias and Rudi van Eldik in the Chair of Inorganic and Coordination Chemistry at the Nicolaus Copernicus University in Toruń. Her research interests focus on the synthesis, biological application and mechanistic studies of polypyridyl ruthenium complexes.*

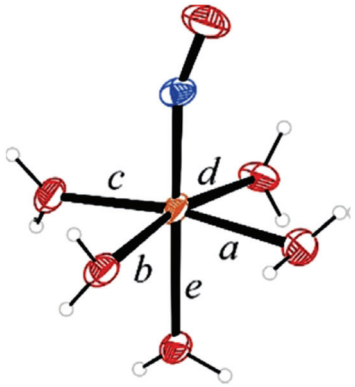


Fig. 1 Crystal structure of $[Fe(H_2O)_5NO]^{2+}$ as reported. Reprinted with permission from ref. 17. Copyright 2019 WILEY-VCH Verlag GmbH & Co. KGaA, Weinheim.

theoretical study to resolve the apparent discrepancy. The authors conclude from their theoretical work that 'there are no mandatory reasons to deprecate the $Fe^{I}(NO^{+})$ formula in favour of the $Fe^{II}(NO^{0})$ or the $Fe^{III}(NO^{-})$ formulation'.[17] Recently, the application of DFT and other computational techniques have been used to study the electronic nature of metal–NO bonds in more detail.[19–23]

$$[Fe(H_2O)_6]^{2+} + NO \rightleftharpoons [Fe(H_2O)_5NO]^{2+} + H_2O \quad (1)$$

In terms of the polyaminecarboxylate complexes for which representative data are reported in Table 2,[12] the activation volumes support the operation of an $I_d$ mechanism for the reversible binding of NO to the seven-coordinate $[Fe^{II}(edta)H_2O]^{2-}$ and $[Fe^{II}(mida)_2H_2O]^{2-}$ complexes, but an $I_a$ mechanism for the six-coordinate $[Fe^{II}(nta)(H_2O)_2]^{-}$ complex. These results demonstrate the role of the coordination number in determining the nature of the reversible NO binding mechanism.

Table 2 Rate and activation parameters for $k_{on}$ for the reversible reactions of $[Fe^{II}(edta)H_2O]^{2-}$, $[Fe^{II}(mida)_2H_2O]^{2-}$ and $[Fe^{II}(nta)(H_2O)_2]^{-}$ with NO at pH = 5 and 25 °C[12]

| Ligand | $k_{on}$ [$M^{-1}$ $s^{-1}$] at 25 °C | $k_{off}$ [$s^{-1}$] at 25 °C | $\Delta H^{\ddagger}$ [kJ $mol^{-1}$] | $\Delta S^{\ddagger}$ [J $mol^{-1}$ $K^{-1}$] | $\Delta V^{\ddagger}$ [$cm^3$ $mol^{-1}$] |
|---|---|---|---|---|---|
| edta | $2.4 \times 10^8$ | 91 | 24 ± 1 | −4 ± 3 | +4.1 ± 0.2 |
| | | | 61 ± 2 | −5 ± 7 | +7.6 ± 0.6 |
| mida | $1.9 \times 10^6$ | 57 | 40 ± 1 | +8 ± 3 | +7.6 ± 0.4 |
| | | | 47 ± 2 | −55 ± 5 | +6.8 ± 0.4 |
| nta | $2.1 \times 10^7$ | 9.3 | 24 ± 1 | −22 ± 3 | −1.5 ± 0.1 |
| | | | 66 ± 1 | −5 ± 4 | −3.5 ± 0.7 |

### 2.2 Reactions of Fe(III) porphyrin complexes with NO

We now turn to a series of Fe(III) porphyrin complexes which exist in solution at pH < 6 in the diaqua form and are labilized by the donor properties of the porphyrin in the axial direction to undergo very fast water exchange reactions. The application of $^{17}O$-NMR techniques enabled the determination of $k_{ex}$ as a function of temperature and pressure. A schematic presentation of the systems studied is given in Fig. 2.[24]

$$[Fe^{III}(Por)(H_2O)_2] + H_2O^{17} \rightleftharpoons [Fe^{III}(Por)(H_2O)(H_2O)^{17}] + H_2O \quad (2)$$

The data reported in Table 3 demonstrate that $k_{ex}$ varies by two orders of magnitude depending on the overall charge on the complex that affects the lability of the axial sites. The activation entropy and activation volume values support the operation of a dissociative ($I_d$ or $D$) mechanism. The activation volume of +11.9 ± 0.3 $cm^3$ $mol^{-1}$ for the TMPS complex is close to that expected for a limiting dissociative mechanism, whereas those obtained for the TPPS and TMPyP complexes are more in the line with an $I_d$ mechanism.[24]

**Anna Katafias**

*Anna Katafias obtained her PhD degree in chemistry (1999) and habilitation in chemistry (2013), speciality – inorganic and coordination chemistry, from the Nicolaus Copernicus University in Torun (Poland). She is currently an Associate Professor at the Faculty of Chemistry of her Alma Mater. Her research interests have centered on the elucidation of inorganic reaction mechanisms, in particular electron transfer processes, activation of small molecules and homogeneous catalysis. Recently, her research involves also the development of polypyridyl non-organometalic ruthenium(II) complexes as models for cellular redox modulation.*

**Ralph Puchta**

*Ralph Puchta studied chemistry at the Friedrich-Alexander University Erlangen-Nuremberg and obtained in 2003 his Ph.D. in organic chemistry on a quantum chemical and experimental study in the field of supramolecular chemistry under the supervision of Tim Clark and Rolf W. Saalfrank. In 2004 he joined the team of Rudi van Eldik at the Institute for Inorganic Chemistry, working computationally on mechanistic problems in coordination chemistry. In addition, he continued his theoretical studies on supramolecular chemistry. Since his habilitation in 2013 he is Privatdozent at the Institute for Inorganic Chemistry, continuing his independent research and a number of fruitful co-operations.*

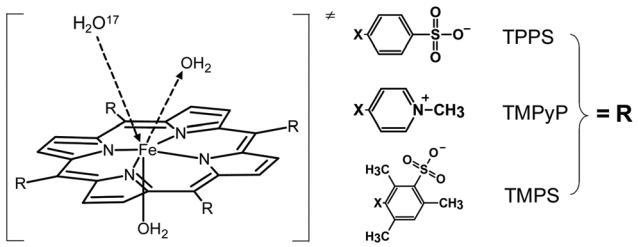


Fig. 2 Schematic presentation of water exchange reactions on a series of Fe(III) porphyrin complexes for which the overall charge is controlled by the substituents R.[24]

Table 3 Summary of rate constants (at 25 °C) and activation parameters for water exchange reactions on the series of Fe(III) porphyrin complexes[24]

| Complex | $k_{ex}$ ($s^{-1}$) | $\Delta H^{\ddagger}$ [kJ $mol^{-1}$] | $\Delta S^{\ddagger}$ [J $mol^{-1}$ $K^{-1}$] | $\Delta V^{\ddagger}$ [$cm^3$ $mol^{-1}$] |
|---|---|---|---|---|
| $[Fe(TPPS)(H_2O)_2]^{3-}$ | $(2.0 \pm 0.1) \times 10^6$ | 67 ± 2 | +99 ± 10 | +7.9 ± 0.2 |
| $[Fe(TMPS)(H_2O)_2]^{3-}$ | $(2.1 \pm 0.1) \times 10^7$ | 61 ± 1 | +100 ± 5 | +11.9 ± 0.3 |
| $[Fe(TMPyP)(H_2O)_2]^{5+}$ | $(4.5 \pm 0.1) \times 10^5$ | 71 ± 2 | +100 ± 6 | +7.4 ± 0.4 |

A reaction scheme for the reaction of the series of Fe(III) porphyrin complexes with NO is presented in Scheme 1. In all cases the final reaction product was identified to be $Fe^{II}$–$NO^+$ as shown by the diamagnetic nature of the product. Table 4 summarizes the $k_{on}$ and $k_{off}$ values along with the thermal and pressure activation parameters. The activation entropies as well as the activation volumes for both the 'on' and 'off' reactions support the operation of an $I_d$ or $D$ mechanism. Since $k_{on}$

**Rudi van Eldik**

*Rudi van Eldik received his PhD from Northwest University, South Africa, followed by a Habilitation at the Goethe University, Frankfurt/Main, Germany. He became a Full Professor of Inorganic Chemistry at the Private University of Witten/Herdecke in 1987, followed by a Chair for Inorganic and Analytical Chemistry at the Friedrich-Alexander University Erlangen-Nuremberg in 1994. After his retirement in 2010 he joined the Faculties of Chemistry at the Jagiellonian University in Krakow and the Nicolaus Copernicus University in Torun, Poland. He received honorary doctoral degrees from: Northwest University (South Africa), University of Kragujevac (Serbia), Jagiellonian University, Krakow (Poland), University of Pretoria (South Africa) and Ivanovo State University of Chemistry and Technology (Russia). He is the author of more than 900 original papers and reviews, and Editor of Advances in Inorganic Chemistry (Academic Press) since vol. 54 of the series.*

$$[Fe^{III}(Por)(H_2O)_2] \underset{k_{-1}}{\overset{k_1}{\rightleftharpoons}} [Fe^{III}(Por)(H_2O)] + H_2O \quad (3)$$

$$[Fe^{III}(Por)(H_2O)] + NO \underset{k_{-2}}{\overset{k_2}{\rightleftharpoons}} [Fe^{III}(Por)(H_2O)(NO^+)] \quad (4)$$

Scheme 1 Reaction scheme for the reversible binding of NO to $[Fe^{III}(Por)(H_2O)_2]$ according to a dissociative mechanism where $k_{on} = k_1k_2/k_{-1}$ and $k_{off} = k_{-2}$.

$= k_1k_2/k_{-1}$, the interpretation of the activation parameters is not straightforward since the parameters are a combination arising from contributions from each of the three reaction steps. A comparison of the data for the water exchange reaction on these complexes shows a good agreement in terms of the reactivity of the different porphyrin complexes and suggests that the water exchange reaction controls the rate and mechanism of the 'on' reaction with NO. In the case of $k_{off}$, both the activation entropy and activation volume data strongly support the operation of a dissociative mechanism, which is in agreement with that expected for an Fe(II) complex.[24]

In the case of the spin-admixed $[Fe^{III}(TMPS)(H_2O)_2]^{3-}$ complex, the p$K_a$ value was found to be 6.9 and an increase in pH > 9 resulted in the formation of a high-spin five-coordinate $[Fe^{III}(TMPS)OH]^{4-}$ complex.[25] This complex was, surprisingly, found to react much slower with NO than the corresponding diaqua complex, but produced the same low-spin product as shown in Scheme 2 with almost the same p$K_a$ value. The overall spin state change accompanying formation of low-spin $[Fe^{II}(TMPS)(NO^+)(OH)]^{4-}$ from purely high-spin $[Fe^{III}(TMPS)OH]^{4-}$ ($S = 5/2 \rightarrow S = 0$) is larger than that occurring upon binding of NO to the spin-admixed complex $[Fe^{III}(TMPS)(H_2O)_2]^{3-}$ ($S = 5/2, 3/2 \rightarrow S = 0$). We suggest that this difference contributes to the observed *ca.* 100-fold decrease in $k_{on}$ at high pH.[25] The volume profile reported in Fig. 3 illustrates the dissociative nature of bond formation of the diaqua complex with NO, as compared to direct coordination of NO with the five-coordinate hydroxo complex and the large volume collapse on going from the high-spin to the low-spin product.

In a subsequent series of studies the selected porphyrins included an octa-cationic ($P^{8+}$),[26] an octa-anionic ($P^{8-}$),[27] and an extremely negatively ($P^{16-}$) charged porphyrin.[28] These complexes all behaved very similarly to the $TMPS^{4-}$ porphyrin in terms of spin-admixed six-coordinate diaqua species and high-spin five-coordinate monohydroxo species. The p$K_a$ value of the diaqua complexes increased along the series $P^{8+}$ (p$K_a$ = 5.0), $TMPyP^{4+}$ (p$K_a$ = 5.5), $TMPS^{4-}$ (p$K_a$ = 6.9), $P^{8-}$ (p$K_a$ = 9.3) and $P^{16-}$ (p$K_a$ = 9.9), indicating that deprotonation of coordinated water becomes more difficult on increasing the negative charge on the porphyrin. Water-exchange rate constants and the associated activation parameters were measured for all the complexes and a summary of the results[28] shows that $k_{ex}$ decreases with increasing positive charge on the porphyrin. The activation entropies and activation volumes are all positive in line with an $I_d$ or $D$ mechanism. Data for the 'on' reactions with NO show that $k_{on}$ decreases with increasing positive charge on the porphyrin as found for the water

 

Table 4 Summary of $k_{on}$ and $k_{off}$ values along with the activation parameters obtained from temperature and pressure dependent measurements[12]

| Complex | $[Fe^{III}(TPPS)(H_2O)_2]^{3-}$ + NO | | $[Fe^{III}(TMPS)(H_2O)_2]^{3-}$ + NO | | $[Fe^{III}(TMPyP)(H_2O)_2]^{5+}$ + NO | |
|---|---|---|---|---|---|---|
| Rate parameters | $k_{on}$ [$M^{-1}$ $s^{-1}$] | $k_{off}$ [$s^{-1}$] | $k_{on}$ [$M^{-1}$ $s^{-1}$] | $k_{off}$ [$s^{-1}$] | $k_{on}$ [$M^{-1}$ $s^{-1}$] | $k_{off}$ [$s^{-1}$] |
| $k$ | $0.50 \times 10^6$ | 500 | $2.8 \times 10^6$ | 900 | $2.9 \times 10^4$ | 66 |
| $\Delta H^{\ddagger}$ [kJ $mol^{-1}$] | 69 ± 3 | 76 ± 6 | 57 ± 3 | 84 ± 3 | 67 ± 4 | 113 ± 5 |
| $\Delta S^{\ddagger}$ [J $mol^{-1}$ $K^{-1}$] | +95 ± 10 | +60 ± 11 | +69 ± 11 | +94 ± 10 | +67 ± 13 | +169 ± 18 |
| $\Delta V^{\ddagger}$ [$cm^3$ $mol^{-1}$] | +9 ± 1 | +18 ± 2 | +13 ± 1 | +17 ± 3 | +3.9 ± 1.0 | +16.6 ± 0.2 |

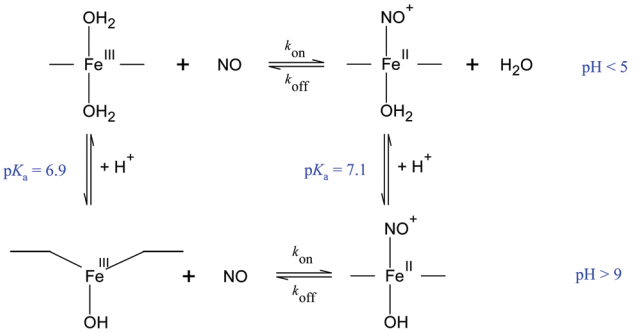


Scheme 2 Schematic presentation of the reversible binding of NO to $[Fe^{III}(TMPS)(H_2O)_2]^{3-}$/$[Fe^{III}(TMPS)OH]^{4-}$ as function of pH.

exchange reactions, whereas the data for the 'off' reaction show that $k_{off}$ as well as $\Delta V^{\ddagger}_{off}$ do not show any trend with increasing positive charge on the porphyrin.[28] The mechanisms of nitrite catalysed reductive nitrosylation of complexes of the type $Fe^{II}(Por)(NO^+)(OH)$, where Por = $P^{8+}$, $P^{8-}$ and $P^{16-}$, were studied in detail.[28,29] In all cases the final product was found to be $Fe^{II}(Por)NO$ as shown in the suggested mechanism in Scheme 3. In addition, it was found that $k_{nit}$ increases, and the corresponding volume of activation changes from negative to positive, on increasing the positive charge on the porphyrin.[28] Thus a comparison from $Fe^{III}(P^{16-})$ to $Fe^{III}(P^{8+})$ clearly shows that the contribution of bond formation is facilitated by negatively charged *meso* substituents, while a decreasing electrostriction prevails over bond-formation in porphyrins containing electron-donating substituents.

### 2.3 Reactions of cytochrome $P450_{cam}$ and functional model porphyrins with NO

The resting state of $CytP450_{cam}$ is a low-spin $Fe^{III}$(porphyrin) complex where the axial sites are occupied by cysteine and a labile water molecule in the *trans* position. During the entrance of camphor (RH) into the active pocket, the labile water molecule is displaced, and a spin-state change from low-spin to high-spin occurs to form a five-coordinate species with the Fe(III) centre out of the porphyrin plane (see Fig. 4).

It was reported in the literature that NO inhibits the catalytic activity of $CytP450_{cam}$ in substrate oxidation processes *via* coordination to the Fe(III) centre. Furthermore, Resonance Raman spectra and theory suggested a low-spin, linear $Fe^{II}$–$NO^+$ centre in CytP450(NO). We performed a detailed kinetic study on the reactions of NO with $CytP450_{cam}$ in the absence and presence of a large excess of camphor in order to distinguish between the ability of $CytP450_{free}$ and $CytP450_{cam}$ to coordinate to NO, respectively.[30] The experiments were performed as a function of temperature and pressure to determine the corresponding activation parameters summarized in Table 5. Flash photolysis techniques were used to study the 'on' reaction and stopped-flow for the 'off' reaction. A combination of $k_{on}$ and $k_{off}$ was used to determine the overall binding constant $K_{NO}$ (= $k_{on}/k_{off}$). The overall reaction can be summarized as follows:

$$CytP450_{free/cam}(Fe^{III}) + NO \underset{k_{off}}{\overset{k_{on}}{\rightleftharpoons}} CytP450_{free/cam}(Fe^{II})(NO^+) \quad (5)$$

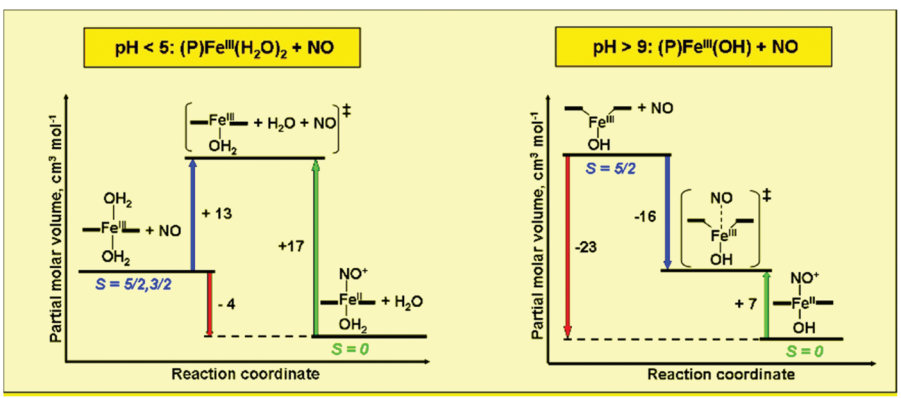


Fig. 3 Volume profiles constructed from activation volumes for the 'on' and 'off' reactions for the reversible binding of NO to $[Fe^{III}(TMPS)(H_2O)_2]^{3-}$/$[Fe^{III}(TMPS)OH]^{4-}$ as function of pH. Blue arrow – 'on' reaction; green arrow – 'off' reaction; red arrow – reaction volume.[25]

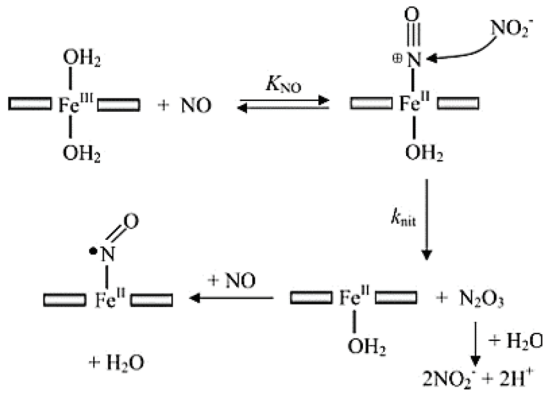

Scheme 3 Suggested mechanism for the nitrite-catalysed reductive nitrosylation of the nitrosyl complex [$Fe^{II}$(P)($NO^+$)] according to an inner-sphere mechanism. Reprinted with permission from ref. 29. Copyright 2006 American Chemical Society.

The results in Table 5 show that $K_{NO}$ is larger for CytP450$_{cam}$ than for CytP450$_{free}$, which demonstrates that substrate binding enhances NO binding. The activation parameters for the reaction of NO with CytP450$_{free}$ indicate very positive activation entropy and activation volume data for both the 'on' and 'off' reactions, suggesting that the transition state involves a five-coordinate species. However, the volume increases are too large to be accounted for by only the release of NO. It was suggested that *ca.* 50% of the volume increase is related to the change in spin-state on going from low-spin CytP450($H_2O$) to high-spin five-coordinate CytP450 in the transition state. In the case of CytP450$_{cam}$ we already start with a five-coordinate species and coordination of NO is characterized by negative activation entropy and activation volume values, whereas the 'off' reaction is characterized by significantly positive activation entropy and activation volume values. The latter results clearly demonstrate a huge volume collapse on going from the five-coordinate high-spin Fe(III) complex to the diamagnetic, low-spin $Fe^{II}(NO^+)$ product. The corresponding volume profiles are reported in Fig. 5 and demonstrate the large volume changes associated with the binding of NO.

In a subsequent study in collaboration with Wolf-D. Woggon (University of Basel), the reversible binding of NO to an enzyme mimic of CytP450$_{cam}$ was studied.[31] This model enzyme carries a $SO_3^-$ ligand coordinated to the Fe(III) complex and mimics the structural nature of CytP450. Furthermore, in toluene it is present as a high-spin five-coordinate species and thereby mimics the camphor bound state of CytP450$_{cam}$ as shown in Scheme 4.

A spectrophotometric study of the reversible binding of NO to the enzyme mimic was performed as a function of temperature and pressure. A summary of the obtained thermodynamic data is $K_{NO}$ = 122 ± 10 $M^{-1}$ at 25 °C, $\Delta H^\circ$ = −72 ± 2 kJ $mol^{-1}$, $\Delta S^\circ$ = −210 ± 7 J $K^{-1}$ $mol^{-1}$ and $\Delta V^\circ$ = −39.5 ± 0.7 $cm^3$ $mol^{-1}$. The binding constant $K_{NO}$ is four orders of magnitude lower than that found for CytP450$_{cam}$ at 25 °C, and increases on lowering the temperature since it is an exothermic reaction as indicated by the negative reaction enthalpy. The significantly negative reaction volume suggests that the five-coordinate high-spin Fe(III) adduct reacts with NO to produce the low-spin six-coordinate $Fe^{II}$–$NO^+$ nitrosyl complex. The kinetics of the binding of NO was studied using flash-photolysis and stopped-

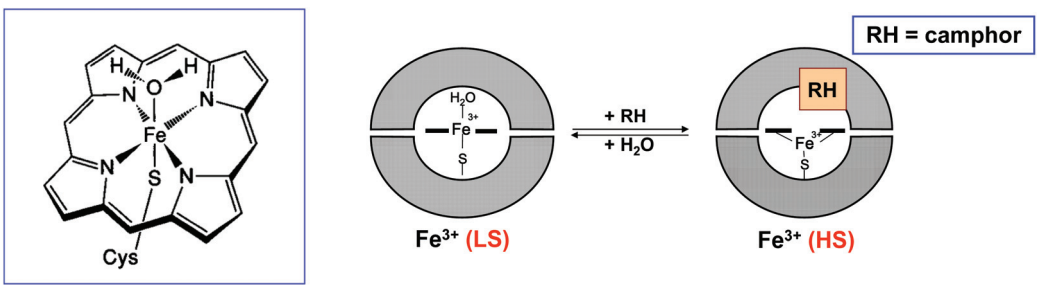


Fig. 4 Schematic presentation of the resting state of CytP450$_{cam}$ (left) and its reversible reaction with camphor (right).

Table 5 Summary of rate constants and activation parameters for the reversible reaction of NO with CytP450$_{free}$ and CytP450$_{cam}$ at 25 °C [30]

| Rate/equilibrium constant at 25 °C | $k_{on}$ [$M^{-1}$ $s^{-1}$] | $k_{off}$ [$s^{-1}$] | $K_{NO}$ [$M^{-1}$] |
|---|---|---|---|
| Cyt P450$_{free}$ LS | (3.5 ± 0.1) × $10^5$ | 0.33 ± 0.06 | (1.1 ± 0.4) × $10^6$ |
| Cyt P450$_{cam}$ HS | (3.4 ± 0.2) × $10^6$ | 1.9 ± 0.3 | (1.8 ± 0.2) × $10^6$ |
| **Activation parameters** | $\Delta H^\ddagger$ [kJ $mol^{-1}$] | $\Delta S^\ddagger$ [J $mol^{-1}$ $K^{-1}$] | $\Delta V^\ddagger$ [$cm^3$ $mol^{-1}$] |
| Cyt P450$_{free}$, $k_{on}$ | 92 ± 1 | +169 ± 4 | +28.3 ± 2.0 |
| Cyt P450$_{free}$, $k_{off}$ | 122 ± 4 | +155 ± 15 | +30.9 ± 1.5 |
| Cyt P450$_{cam}$, $k_{on}$ | 14.1 ± 0.1 | −73.1 ± 0.4 | −7.3 ± 0.2 |
| Cyt P450$_{cam}$, $k_{off}$ | 83.8 ± 0.7 | +41.1 ± 2.2 | +24.2 ± 1.5 |

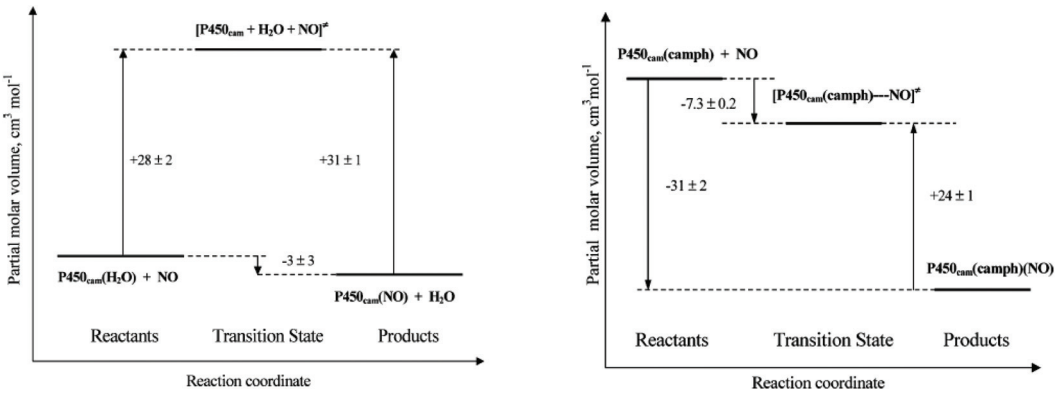


**Fig. 5** Volume profiles for the reversible binding of NO to CytP450$_{free}$ (left) and CytP450$_{cam}$ (right). Reprinted with permission from ref. 30. Copyright 2004 American Chemical Society.



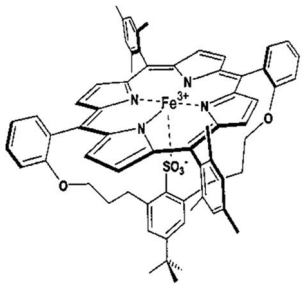


**Scheme 4** Schematic presentation of the five-coordinate high-spin Fe (III) porphyrin complex that mimics the enzymatic activity of CytP450$_{cam}$. Reprinted with permission from ref. 31. Copyright 2006 American Chemical Society.

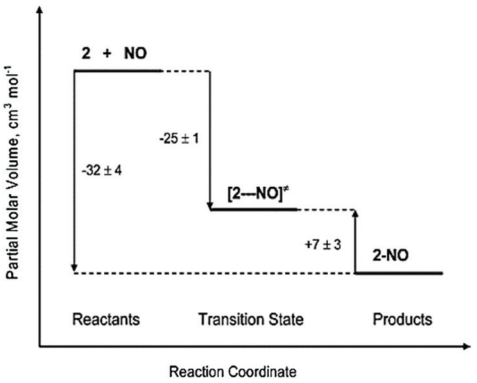


**Fig. 6** Volume profile for the binding of NO to the enzyme mimic **2** in toluene as solvent. Reprinted with permission from ref. 31. Copyright 2006 American Chemical Society.

flow techniques as a function of temperature and pressure. The rate and activation parameters at 25 °C were found to be $k_{on} = (1.80 \pm 0.05) \times 10^6$ M$^{-1}$ s$^{-1}$, $k_{off} = (1.25 \pm 0.01) \times 10^4$ s$^{-1}$, the activation entropy and activation volume for the 'on' reaction $-111 \pm 6$ J K$^{-1}$ mol$^{-1}$ and $-25 \pm 1$ cm$^3$ mol$^{-1}$, respectively, and the same parameters for the 'off' reaction $+29 \pm 5$ J K$^{-1}$ mol$^{-1}$ and $+7 \pm 3$ cm$^3$ mol$^{-1}$, respectively. Both these parameters underline the associative nature of the 'on' reaction as compared to the dissociative nature of the 'off' reaction. The constructed volume profile is reported in Fig. 5, from which it follows that the overall kinetic reaction volume is $-32 \pm 4$ cm$^3$ mol$^{-1}$, *i.e.* a large volume collapse on going from the high-spin five-coordinate reactant state to the low-spin six-coordinate Fe$^{II}$–NO$^+$ product. The reaction volume estimated from the kinetic data is close to that found from the thermodynamic data, *viz.* $-39.5 \pm 0.7$ cm$^3$ mol$^{-1}$. The volume profile in Fig. 6 is characterized by a 'late' transition state in terms of volume changes in contrast to the volume profile reported in Fig. 5 (right) that shows an 'early' transition state. Since both reactions occur from a high-spin five-coordinate reactant state, a likely explanation is related to the magnitude of $K_{NO}$ that differs by four orders of magnitude. This difference resulted from a much faster 'off' reaction in the case of enzyme mimic which accounts for the 'later' transition state.[31]

### 2.4 Reactions of aquacobalamin with NO

During the turn of the century, a highly talented PhD student, Maria Wolak from the Jagiellonian University in Krakow, joined the group in Erlangen to study the reaction between NO and aquacobalamin Cbl(H$_2$O). After a frustrating series of experiments it turned out that NO did not react with Cbl(H$_2$O) at all and the observed reaction was caused by nitrite impurities in solution.[32] On the acidification of solutions of NO to pH 2, the very characteristic fingerprint spectrum of HONO was observed. Apparently the observed reactions reported in the literature,[33–35] were all due to nitrite impurities in solutions of NO! Despite these claims, it was already reported 30 years earlier that NO does not react with Cbl(H$_2$O).[36] Even in an acidic aqueous solution, no evidence was found for the coordination of NO to Cbl(H$_2$O).[37] In a follow-up study, we could show that NO reacts rapidly and efficiently with reduced cobalamin, Cbl(II), in a reversible manner.[38] With the aid of flash-photolysis techniques, the 'on' reaction was found to have a second-order rate constant $k_{on} = 6 \times 10^8$ M$^{-1}$ s$^{-1}$ at 25 °C. The 'off' reaction was studied by stopped-flow using [Fe$^{II}$(edta)(H$_2$O)]$^{2-}$ as an efficient scavenger for NO, with $k_{off}$ =

$2\ s^{-1}$ at 25 °C, such that $K_{NO} = k_{on}/k_{off} = 3 \times 10^8\ M^{-1}$. The well-resolved $^1$H-, $^{31}$P-, and $^{15}$N-NMR spectra for the nitrosyl complex indicated that the complex is diamagnetic. Furthermore, the $^{15}$N-NMR signal at 785 ppm is very characteristic for square-pyramidal Co(II) complexes with a bent nitrosyl ligand. This results from the combination of the unpaired electron of the paramagnetic $d^7$ Co(II) centre with the odd electron residing on the $\pi^*$ orbital of nitrosyl, with subsequent formation of the Co–NO bond. These findings suggest that Co(II) is oxidized to diamagnetic Co(III) and NO is reduced to $NO^-$, *i.e.* iso-electronic with dioxygen, and binds to the Co(III) centre in a bent mode. DFT calculations suggested the bond-angle to be between 118 and 121°.[39] A few years later, Brasch and co-workers were successful to obtain the crystal structure of Cbl(NO) and reported a bond-angle of 117 to 121°.[40,41] At that point the authors referred to 'nitroxyl' cobalamin to stress the 'nitroxyl' ($NO^-$) character of the 'nitrosyl' complex. We adopted this notation in our later work on the Cbl(NO) system,[42,43] and were criticized by a reader of JBIC for doing so. Subsequently, we answered the reader in a commentary to clarify where the 'nitroxyl' notation originated from,[44] and agreed to refer to the Cbl(NO) complex in future as a 'nitrosyl' complex with substantial 'nitroxyl' character!

During the early stages of the described work, we published a review on 'to be or not to be NO in coordination chemistry', since NO is a non-innocent ligand and can formally coordinate as $NO^+$, $NO^\bullet$ or $NO^-$.[45] During the same year we also published a review on the application of flash photolysis techniques in the study of nitrosyl complexes.[46] Five and ten years later we updated our work on nitrosyl chemistry in the form of two micro reviews.[47,48]

### 2.5 Reactions of pentacyanoferrate(II/III) with NO

In collaboration with Federico Roncaroli and José Olabe from the University of Buenos Aires, we performed a series of studies on the formation with and release of NO during its reaction with pentacyanoferrate(II/III). In the first study, we investigated the interaction between $[Fe^{III}(CN)_5(H_2O)]^{2-}$ and NO which is controlled by an outer-sphere electron transfer reaction to form $[Fe^{II}(CN)_5(NO^+)]^{2-}$, the classic nitroprusside anion.[49] The $[Fe^{II}(CN)_5(H_2O)]^{3-}$ complex could be trapped as a reactive intermediate in the reaction of $[Fe^{III}(CN)_5(H_2O)]^{2-}$ with NO, by using pyrazine and thiocyanate as scavengers for this intermediate. In a subsequent study, the interaction of pentacyanoferrate(II) with NO was investigated.[50] The reaction product $[Fe^{II}(CN)_5(NO)]^{3-}$ is the well characterized nitrosyl complex, described as low-spin Fe(II) bound to the NO radical. The reported activation parameters support a dissociative mechanism, with rate-controlling dissociation of coordinated water, and subsequent fast coordination of NO. The volume profile for the reversible coordination of NO is presented in Fig. 7, which clearly demonstrates the operation of a dissociative mechanism.

In the final paper, the release of NO by the reduced form of nitroprusside, $[Fe^{II}(CN)_5(NO)]^{3-}$, was studied in detail.[51] Evidence was presented that the reduction product contains

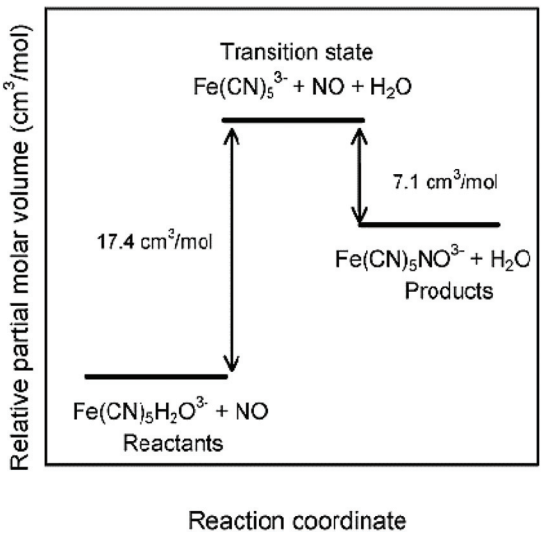


**Fig. 7** Volume profile for the reversible coordination of NO. Reprinted with permission from ref. 50. Copyright 2003 American Chemical Society.

an equilibrium mixture of $[Fe(CN)_4(NO)]^{2-}$ and $[Fe(CN)_5(NO)]^{3-}$ ions. In the pH range 4–10, the first complex predominates at pH < 8 and is formed by the rapid release of the *trans*-cyanide from $[Fe(CN)_5(NO)]^{3-}$, which is the main product at pH > 9–10. Both nitrosyl complexes decay by first-order kinetics with rate constants around $10^{-5}\ s^{-1}$ (pH 6–10) related to the dissociation of NO. The study revealed conditions that favour rapid release of NO, in order to promote vasodilator effects on the injection of nitroprusside. It further described new processes related to dinitrosyl complex formation and NO disproportionation, which are relevant to the diverse biological processes involved with NO and $N_2O$ processing.[51]

### 2.6 Reactions of aquacobalamin with nitrite and HNO

The formation of nitroxylcobalamin CblNO *via* the reaction between reduced cobalamin CblCo(II) and nitric oxide was shown by Wolak *et al.* almost 20 years ago.[38] The possibility of CblNO generation *via* reduction of nitrocobalamin $CblNO_2$ still remains an open question.

The possible intracellular production of CblNO *via* reduction of $CblNO_2$ was studied for the reducing agents glutathione (GSH) (Brasch *et al.*),[52] L-cysteine ethyl ester, glucose, formate and ascorbate.[42,43] It was demonstrated that the products of the reaction between nitrocobalamin and GSH or Cys-OEt lead to thiol derivatives of vitamin $B_{12}$, but not nitroxylcobalamin as wanted. It can be concluded that in these cases instead of redox processes, substitution reactions are observed. However, when ascorbic acid as a strong reducing agent known as an intracellular antioxidant was used in the reaction with nitrocobalamin, it allowed us to obtain totally different and very interesting results.

The reaction between $CblNO_2$ and ascorbic acid was first studied in the pH range 4–7. The results obtained suggested that the conditions used in these experiments have a big influ-

 

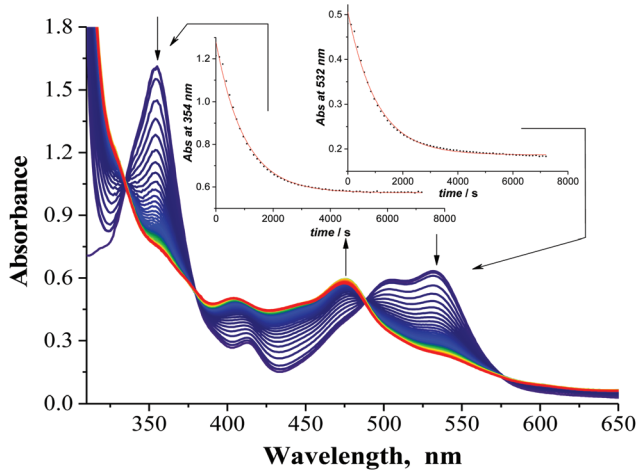


Fig. 8 Spectral changes observed for the reaction between $CblNO_2$ ($7.6 \times 10^{-5}$ M) and Asc ($2.10 \times 10^{-2}$ M) at pH = 7.2 (25 °C, 0.1 M Tris buffer, Ar atmosphere). Spectra were recorded every 2 min. Inset: Plots of absorbance at 354 (left) and 532 nm (right) *versus* time.

ence on the mechanism of the observed reaction. To initiate the reaction, a solution of ascorbic acid (Asc) was added to the solution of $CblNO_2$ at an appropriate pH. Reactions were carried out under an Ar atmosphere since it was shown that traces of atmospheric oxygen in the reaction mixture caused the rapid re-oxidation of the reaction products to $CblNO_2$.

When the reaction between $CblNO_2$ and Asc was monitored at pH = 7.2, the UV-Vis spectral changes indicated that $CblNO_2$ ($\lambda_{max}$ = 354, 413 and 532 nm) was converted to reduced cobalamin, CblCo(II) ($\lambda_{max}$ = 312, 407 and 476 nm).[42] Isosbestic points were observed at 335, 372, 487 and 571 nm. Fig. 8 shows the recorded UV-Vis spectra and insets present first-order absorbance *vs.* time traces at 354 and 532 nm.

Kinetic data collected as a function of Asc and $NO_2^-$ concentrations are shown in Fig. 8. The $k_{obs}$ *versus* [Asc] dependence in Fig. 9a shows a saturation behaviour typical for an outer-sphere electron transfer reaction. The profile within this plot suggests that the reaction proceeds *via* a rapid pre-equilibration ($K$) to form an encounter complex which subsequently undergoes an outer-sphere electron transfer reaction ($k$), *i.e.* the observed rate constant reaches a limiting value at high Asc concentration, $k = (3.3 \pm 0.3) \times 10^{-3}$ $s^{-1}$ at 25 °C. Based on the presented results, it can be assumed that CblCo(II) is formed as a product of the reaction given in (6).

$$CblNO_2 + Asc \overset{K}{\rightleftarrows} [CblNO_2 \cdot Asc] \xrightarrow{k} CblCo(II) + DHAsc + NO_2^- \quad (6)$$

The plot presented in Fig. 9b shows the dependence of $k_{obs}$/[Asc] on $NO_2^-$ concentration and indicates that free nitrite in the equilibrated solution has an influence on the observed rate constant. Increasing $NO_2^-$ concentration in the reaction mixture significantly slows down the reaction of CblCo(II) formation. The data presented in Fig. 9b were fitted to eqn (7):

$$\frac{k_{obs}}{[Asc]} = \frac{k_2 + k_3 K_1 [NO_2^-]}{1 + K_1 [NO_2^-]} \quad (7)$$

The obtained value of $k_2$ (17.3 ± 0.4 $M^{-1}$ $s^{-1}$) upon keeping $K_1$ constant at $2 \times 10^5$ $M^{-1}$ agrees with the rate constant for CblCo(II) formation in the reaction between $CblOH_2$ and Asc. The other obtained value $k_3$ is approx. 200 times lower, *viz.* 0.13 ± 0.01 $M^{-1}$ $s^{-1}$. The data suggest that formation of CblCo(II) is the result of the two parallel processes summarized in Scheme 5. According to the proposed mechanism, $CblOH_2$ is in rapid equilibrium with $CblNO_2$ and on addition of Asc to the equilibrium mixture, both $CblOH_2$ and $CblNO_2$ can be reduced by Asc to form CblCo(II) and DHAsc. The nitrite concentration controls the contributions of the $CblOH_2$ and $CblNO_2$ pathways to the overall reduction process. At low concentration of $NO_2^-$, $k_{obs(2)}/[Asc] = k_2$ and only the reduction of

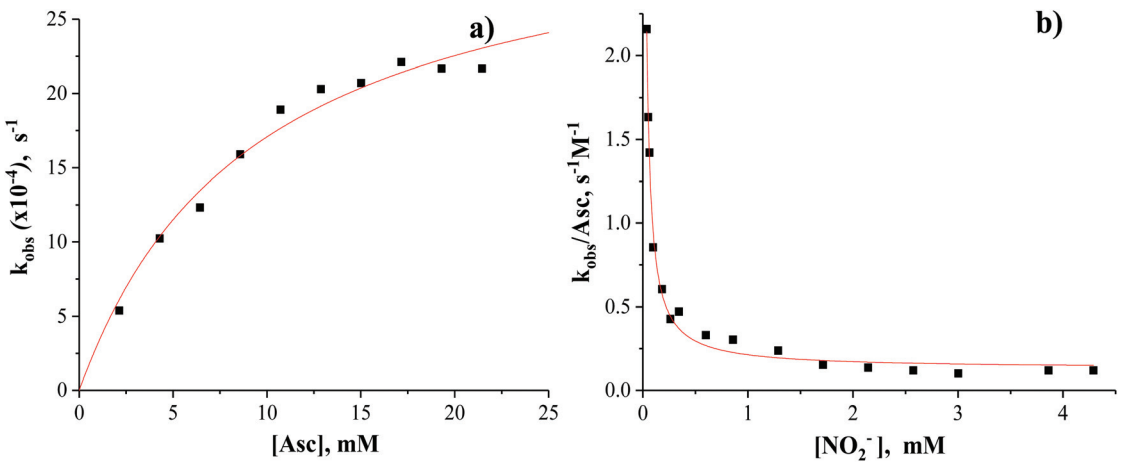


Fig. 9 Dependence of (a) $k_{obs}$ on Asc concentration and (b) $k_{obs}$/[Asc] on $NO_2^-$ concentration for the reaction between $CblNO_2^-$ and Asc. Experimental conditions: pH = 7.2 (25 °C, 0.1 M Tris buffer); (a) $8.5 \times 10^{-5}$ M $CblNO_2$, ($NO_2^-/CblOH_2$ = 10), $2.1 \times 10^{-3}$–$2.6 \times 10^{-2}$ M Asc, (b) $8.5 \times 10^{-5}$ M $CblOH_2$, $8.5 \times 10^{-5}$–$4.3 \times 10^{-3}$ M $NO_2^-$, $2.1 \times 10^{-3}$ M Asc.

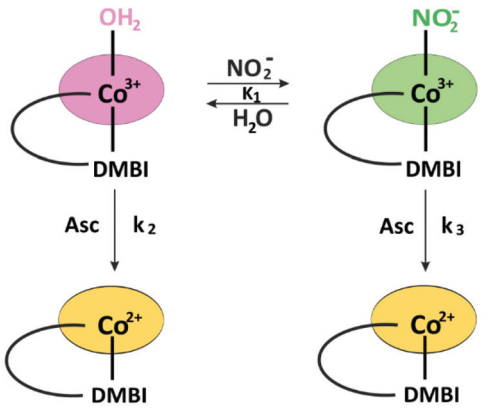


**Scheme 5** Proposed mechanism for the reaction between $CblNO_2$ and Asc.

$CblOH_2$ is observed, whereas at high concentration of $NO_2^-$, $k_{obs(3)}/[Asc] = k_3$ and only the reduction of $CblNO_2$ is observed.

Significantly different results were obtained when the reaction was studied under more acidic conditions (pH < 5, 0.1 M acetate buffer, 25 °C, Ar atmosphere). This can be explained in the context of ascorbic acid properties, since under these conditions, ascorbic acid is mainly present in the mono- and diprotonated forms of ascorbic acid, *i.e.* $HAsc^-$ and $H_2Asc$ ($pK_{a1}$ = 4.1 and $pK_{a2}$ = 11.3 [53]). The mixture of $HAsc^-$ and $H_2Asc$ has a much weaker reducing property than at pH ~ 7, where ascorbic acid is mainly present as $HAsc^-$ and traces of the much stronger reducing agent $Asc^{2-}$.[53–58]

Under the above-mentioned conditions, addition of $HAsc^-$ to nitrocobalamin does not lead to the formation of CblCo(II), as shown at pH ~ 7,[42] but appears to be converted directly to nitroxylcobalamin, CblNO ($\lambda_{max}$ = 316, 344 and 475 nm)[38] with isosbestic points at 335, 373, 490 nm (Fig. 10a). Interesting is the fact that under the selected conditions, CblNO was formed within 100 min from the start of the reaction and was present in the reaction mixture during the next 300 min. However, spectral changes recorded between 400 and 800 min from the start of the reaction indicated the reformation of $CblNO_2$ (Fig. 10b).

Based on the results of further studies, the formation and stability of CblNO depends on the concentration of both $HAsc^-$ and free $NO_2^-$ in the reaction mixture. In summarizing briefly the assembly of results, it should be mentioned that while higher concentrations of nitrite slow down the conversion of $CblNO_2$ to CblNO, an increasing $HAsc^-$ concentration accelerates the reaction and stabilizes CblNO in solution. Moreover, further studies showed that it is possible to reduce the final $CblNO_2$ product by the addition of a new portion of ascorbic acid after almost 20 h from the start of the reaction (see Fig. 11).

The spectral changes shown above suggest that the observed formation of CblNO is a simple reduction of the coordinated nitrite to nitroxyl. However, additional studies demonstrated that the mechanism is more complex, for example during the reaction evidence for the presence of nitric

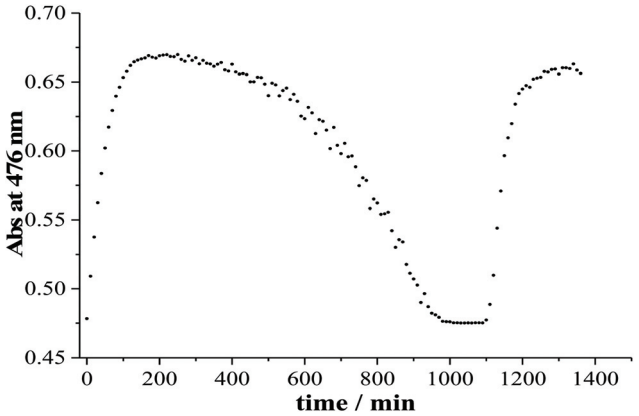


**Fig. 11** Plot of absorbance at 476 nm *vs.* time for the reaction between $CblNO_2$ and $HAsc^-$ with addition of a new portion of $HAsc^-$ after 1100 min from the start of the reaction.

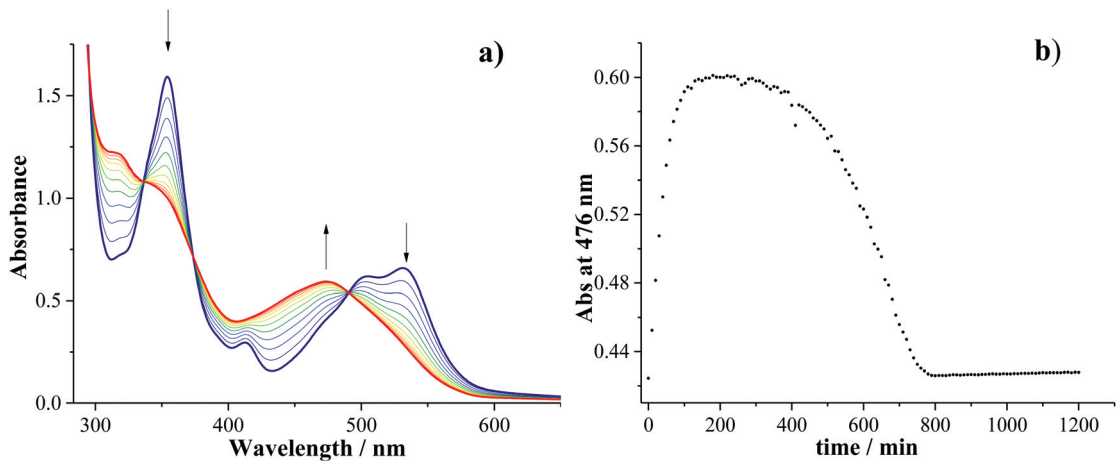


**Fig. 10** (a) Spectral changes observed for the reaction between $CblNO_2$ ($8.6 \times 10^{-5}$ M) and $HAsc^-$ ($8.6 \times 10^{-4}$ M) at pH = 4.3 (0.1 M acetate buffer, 25 °C, Ar atmosphere) during the first 100 min. Spectra were recorded every 1 min. (b) Plot of absorbance at 476 nm *vs.* time.

 

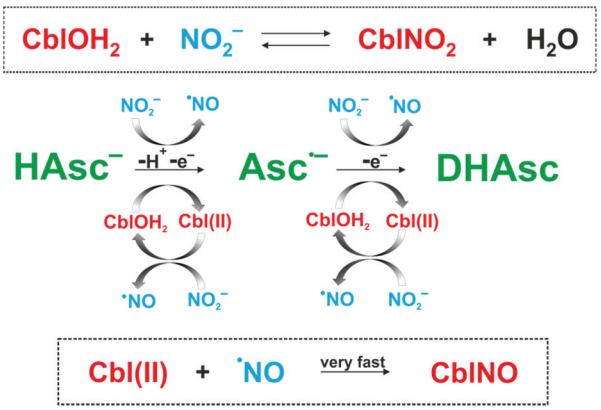


**Scheme 6** Overall reaction sequence for the redox cycling of $CblNO_2$, CblNO and $CblOH_2$ in the presence of ascorbate.

oxide was found.[43] As a result of these studies the most probable reaction sequence was proposed (Scheme 6). This is based on a series of one-electron reduction processes: both nitrite and $CblOH_2$ present in the reaction mixture are reduced by $HAsc^-$ to CblCo(II) and •NO, respectively. In a subsequent, very fast reaction ($k = 7.4 \times 10^8$ $M^{-1}$ $s^{-1}$),[6] CblCo(II) and •NO form the final product, *viz*. the nitroxyl complex, $Co^{III}$–$NO^-$.

Nitroxylcobalamin was demonstrated to also be a product of the reaction between aqua/hydroxocobalamin and nitroxyl (HNO, azanone), a highly reactive NO sibling molecule.[59–62] However, due to the short lifetime of nitroxyl during the reaction with cobalamin, several sources of HNO such as $R_2N$-NONOates (1-(*N*,*N*-dialkylamino)diazen-1-ium-1,2-diolates),[59] Angeli's salt (sodium trioxodinitrate, $Na_2N_2O_3$, AS)[62] and Piloty's acid,[61] had to be used. In these reports, the formation of CblNO was shown to follow different reaction routes and mechanisms.

Whereas the reaction of aquacoabalamin with $R_2N$-NONOate proceeds *via* an NONOate-cobalamin intermediate,[59] the reaction with AS was found to follow transfer of the nitroxyl group to the cobalt(III) centre at pH < 9.9, or by direct interaction of cobalamin with HNO generated at pH > 10.8.[62] Formation of CblNO was also observed on reacting the reduced forms of vitamin $B_{12}$, *viz*. CblCo(II) and CblCo(I), with Piloty's acid (benzenesulfohydroxamic acid, *N*-hydroxy-benzenesulfonamide, $PhSO_2NHOH$, PA).[61] In this case the rate-determining step of the reaction of CblCo(II) with PA, was found to be decomposition of PA to HNO and benzenesulfinate. This reaction is followed by reduction of CblCo(II) by HNO to $CblCo(I)^-$ and oxidation of HNO to •NO. The $CblCo(I)^-$ intermediate in turn, is oxidized back to CblCo(II) by a second molecule of HNO and then CblCo(II) reacts with •NO to give nitroxylcobalamin, *i.e.* $Co^{III}$–$NO^-$.[61]

The latest study on the reaction of aquacobalamin/hydroxocobalamin with PA provided some very interesting results.[54] When a buffered anaerobic solution of $CblOH_2$/OH (0.1 M appropriate buffer pH = 4–10, 25 °C, Ar atmosphere) was added to an aqueous anaerobic solution of PA, the recorded UV-Vis spectral changes clearly indicated the formation of CblNO ($\lambda_{max}$ = 321, 480 nm)[38,62] (Fig. 12a).

The value of $k_{obs1}$ is *ca*. 14 times faster than $k_{obs2}$. The main and faster reaction step is ascribed to the direct reaction of $CblOH_2$ with PA to form CblNO (Scheme 7). The parallel and slower reaction step is ascribed to the decomposition of PA to give HNO and $PhSO_2^-$, where $PhSO_2^-$ can also react with $CblOH_2$. The absorbance *versus* time trace in Fig. 12b clearly shows that the overall reaction consists of more than one step which causes the isosbestic point at 367 nm to show some deviation at longer reaction times (see Fig. 12a). The second process was identified as the parallel slower reaction of $CblOH_2$ with $PhSO_2^-$.[63] Furthermore, pH dependent experiments in the range 4–10 enabled the determination of $pK_a$(Cbl-PA) = 5.38 ± 0.03, which is *ca*. 4 units lower than the $pK_a$(PA) = 9.3 due to the fact that PA is coordinated to the Co(III) centre of $CblOH_2$.

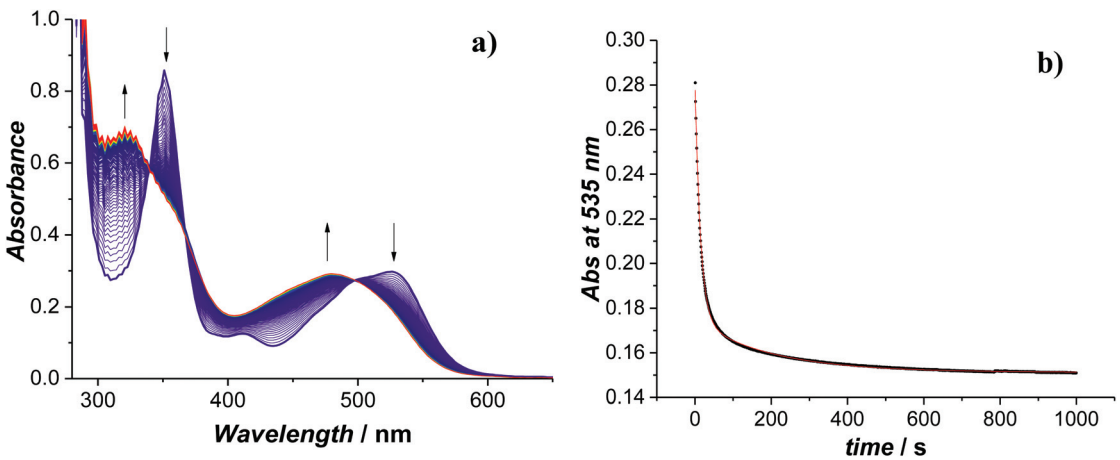


**Fig. 12** (a) UV-Vis spectra for the reaction between $CblOH_2$ and PA at pH 7.2 (0.1 M Tris buffer, 25 °C, Ar atmosphere). (b) Typical kinetic trace recorded at 535 nm for the reaction between $CblOH_2$ ($4.3 \times 10^{-5}$ M) and PA ($2.2 \times 10^{-3}$ M) at pH = 7.2 (25 °C, 0.10 M Tris buffer). The data were fitted to a double exponential function for two parallel reactions giving $k_{obs1}$ = (70.6 ± 0.3) × $10^{-3}$ $s^{-1}$ and $k_{obs2}$ = (5.12 ± 0.04) × $10^{-3}$ $s^{-1}$. Experimental data – black curve; double exponential fit – red curve.

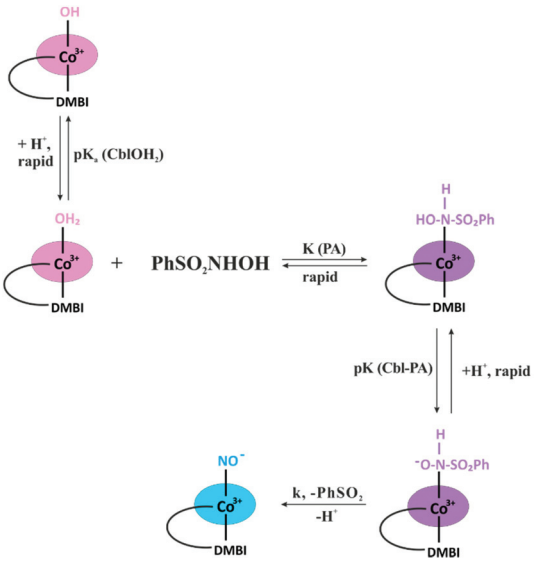


**Scheme 7** Proposed reaction scheme for the direct reaction between $CblOH_2$ and PA to form CblNO and $PhSO_2^-$.

## 3. Peroxide activation in model porphyrin and enzymatic systems

### 3.1 Introduction

Studies on the mechanistic details of the catalytic cycles of cytochrome P450, catalases and heme peroxidases with the application of model iron(III) porphyrin complexes date back to the early eighties.[64–67] Interest in the subject of enzymatic catalysis of these enzymes is not surprising considering their very important role in many metabolic processes, *e.g.* oxidation of a variety of xenobiotics or hydrogen peroxide utilization. Catalytic cycles of these enzymes especially cytochromes P450, pose significant challenges to mechanistic chemistry mainly due to their high instability and high reactivity of transient intermediates.[68–71] In the catalytic cycle of cytochrome P450, three transient intermediates have been identified: iron(III) hydroperoxide (compound 0), iron(IV)-oxo porphyrin π–cation radical (compound I) and iron(IV)-oxo (compound II), of which compound I is widely recognized as the most reactive species.[67] At a certain stage compound 0 has also been perceived as a competitive player in oxidation reactions, which gave rise to intensive discussions in the scientific world and motivated researchers to further perform experimental and theoretical studies on the catalytic cycle of cytochrome P450.[72–75]

Particular attention was also devoted to the elucidation of the factors that determine the O–O bond scission mode (homolytic *vs.* heterolytic) in iron(III) peroxide intermediates, [$Fe^{III}$(Por)(OOR)], to specify the nature of the initially formed reactive intermediates (iron(IV)-oxo *vs.* iron(IV)-oxo porphyrin π–cation radical). Factors such as the porphyrin ring type, chemical nature of the peroxo group undergoing cleavage (hydroperoxo, alkylperoxo, acylperoxo, as well as side-on *versus* end-on coordination in $Fe^{III}$(O–O)), the type of axial ligand coordinated to iron, spin state of the iron centre, solvent polarity and acidity, have all been identified as affecting the mode of O–O bond scission as well as the nature of the accumulating reactive species.[67] A wide range of model studies with the application of ferric porphyrins following their reactivity toward terminal oxidants such as hydrogen peroxide or organic peroxides, has been performed.[67] A significant proportion of the experiments were done under catalytic conditions without direct observation of the time-dependent evolution of the reactive intermediates.[76–83] In such approaches, conclusions about the mechanism of O–O bond cleavage in [$Fe^{III}$(Por)OOR] leading to particular reactive species generation (either [$Fe^{IV}$(Por)(O)] or [$Fe^{IV}$($Por^{+\bullet}$)(O)]), were drawn indirectly from qualitative and quantitative analyses of the oxidation products. However, it is important to note that the nature of the catalytically active species may not always reflect the initial mode of O–O bond cleavage under particular experimental conditions.

This was our motivation to take up the challenge of tuning the reaction conditions in such a way to allow direct observation and tracking of the reactivity of the three crucial intermediates in the cytochrome P450 catalytic cycle (compound 0, compound I and compound II) considered to be capable of promoting the oxidation of organic species. The studies were performed with the application of model iron(III) porphyrins as well as cytochrome P450.

### 3.2 Peroxide activation by model iron(III) porphyrin complexes

Our journey with mechanistic studies on peroxide activation by iron(III) porphyrins started with the challenge to study the impact of pH on the mechanism of O–O bond cleavage. Studies with the application of a water-soluble iron porphyrin ($Fe^{III}$(TMPS), TMPS = [*meso*-tetrakis(sulfonatomesityl)porphyrinato]iron(III)) performed over a broad pH range (1–13), revealed that the acidity of the medium strongly affects the nature of the resulting reactive product. At an acidic pH < 5.5, the iron (IV)-oxo porphyrin cation radical [$Fe^{IV}$($TMPS^{+\bullet}$)(O)] was observed as the dominant species formed in the reactions of $Fe^{III}$(TMPS) with various oxidants such as $H_2O_2$, *m*-chloroperoxybenzoic acid (*m*-CPBA), and iodosylbenzene (PhIO). Increasing the pH > 7.5, resulted in the accumulation of iron (IV)-oxo porphyrin [$Fe^{IV}$(TMPS)(O)] as the sole reactive species.[84] The results obtained were correlated with the pH-dependent changes of $E^{o\prime}$ for electrochemical oxidation of [$Fe^{III}$(TMPS)] reported by Liu and Su (Fig. 13).[85] On this basis a schematic diagram comparing the pH sensitivity of the metal centre oxidation process ($Fe^{III} \rightarrow Fe^{IV}$) *vs.* porphyrin-centred (P → $P^{+\bullet}$) oxidation process was constructed. Analysis of the diagram clearly indicates that by selecting appropriate pH conditions, one can tune the nature of the oxidized form of [Fe(TMPS)] through changes in the relative values of $E^{o\prime}_{Fe(IV)/Fe(III)}$ and $E^{o\prime}_{Por(+\bullet)/Por}$. The diagram presents three pH ranges indicating the most thermodynamically favourable oxidation reactions, (i) O–O bond homolysis at pH < 3.5 leading to an one

 

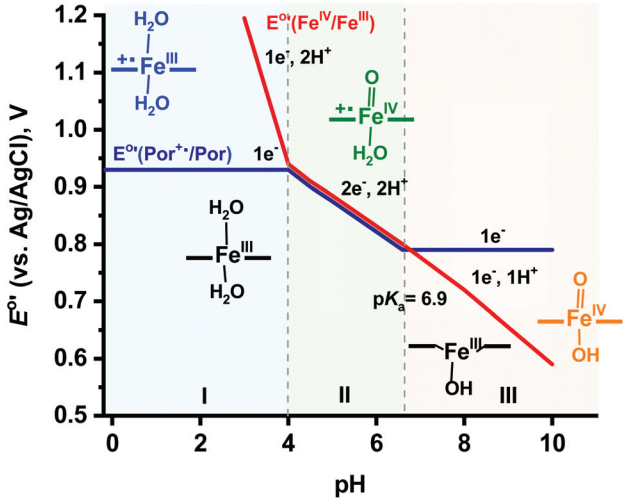


Fig. 13 Schematic diagram for the pH dependent electrochemical oxidation of $Fe^{III}$(TMPS) in aqueous solution. Reprinted with permission from ref. 84 and 85. Copyright 2007 WILEY-VCH Verlag GmbH & Co. KGaA, Weinheim.

electron oxidation of the porphyrin ring, (ii) O–O bond heterolysis at pH 3.5–7 resulting in the accumulation of iron(IV)-oxo porphyrin cation radical, and (iii) O–O bond homolysis at pH > 7 resulting in the generation of iron(IV)-oxo species as the most thermodynamically stable species under basic conditions.[84,85]

These studies also drew attention to a very important issue, namely that the initial mechanism of O–O bond cleavage may not always correspond to the final reactive product observed under specific reaction conditions. For example, application of an appropriately strong oxidant under basic conditions will result in the initial generation of iron(IV)-oxo porphyrin cation radical species; however, this intermediate will tend to decompose to a more thermodynamically favoured form of iron(IV)-oxo species under these conditions. This may occur either *via* comproportionation/disproportionation equilibria of high-valent iron porphyrins resulting from the relationship shown in Fig. 13 (eqn (8)) or through other redox reactions with the components of the system.

$$Fe^{IV}(Por^{+\bullet})(O) + Fe^{III}(Por)(L) \underset{\text{(low pH: } n=2,\ L=2H_2O;\ \text{high pH: } n=1,\ L=OH^-)}{\overset{\text{comproportionation}}{\rightleftharpoons}} 2Fe^{IV}(Por)(O) + nH^+ \quad (8)$$

The pH sensitivity of the O–O bond scission mode has also been reported by others,[76,77] but our work for the first time, focused on the redox characteristics of iron porphyrin and its pH sensitivity with regard to oxidation to iron-oxo porphyrin forms, as well as consideration of the iron porphyrin and oxidant as redox partners.[84]

Strong evidence for this conclusion was provided by studies performed in aqueous/methanol and aqueous/acetonitrile solvents showing that heterolytic cleavage of the O–O bond of *m*-CPBA by [Fe(TMPS)] occurs regardless of the acidity of the reaction medium. The results substantiate that for a sufficiently strong oxidant under the studied solvent conditions, acidity change may not result in a mechanistic changeover in O–O bond cleavage and the observed final reaction product is a result of subsequent reduction.[86] Therefore, reasonable doubt should exist on considering mechanisms of O–O bond cleavage determined solely on the product-analysis, since under catalytic reaction conditions, subsequent reactions may in some cases occur much faster than oxygen atom transfer from the primary oxidation product to specific oxidized substrates.

The pH-dependence under aqueous conditions for the formation of high-valent iron(IV)-oxo species, clearly indicated that by a judicious choice of the reaction conditions with regard to solvent acidity/basicity, one can favour formation of either the iron(IV)-oxo porphyrin cation radical or iron(IV)-oxo species. Taking advantage of that, we were able to tune the nature of the high-valent iron(IV)-oxo species by tuning the pH and to perform for the first time a comparative study on the reactivity of both [$Fe^{IV}$(Por)(O)] and [$Fe^{IV}$($Por^{+\bullet}$)(O)] in an aqueous medium. Oxidation of three water-soluble substrates 4-methoxybenzaldehyde (4-MB-ald), 4-methoxybenzylalcohol (4-MB-alc) and 1-phenylethanol (1-PhE) was studied at pH 5 and 10, providing stability of models for compounds I and II, respectively. Temperature and pressure dependence studies allowed the determination of the activation enthalpy ($\Delta H^{\ddagger}$), entropy ($\Delta S^{\ddagger}$) and volume ($\Delta V^{\ddagger}$) (Table 6).[87]

The determined activation volumes revealed different mechanisms for C–H abstraction reactions conducted by [$Fe^{IV}$(Por)(O)] and [$Fe^{IV}$($Por^{+\bullet}$)(O)]. Small negative values of $\Delta V^{\ddagger}$ for the reactions with [$Fe^{IV}$($Por^{+\bullet}$)(O)] pointed to a stepwise reaction mechanism with dominant role of O–H bond formation. This was in contrast to reactions with [$Fe^{IV}$(Por)(O)] for

Table 6 Rate constants and activation parameters for the oxidation of selected substrates by compounds I and II mimics generated by the application of [$Fe^{III}$(TMPS)] under aqueous conditions[87]

| | $k$ [$M^{-1}$ $s^{-1}$], at 5 °C | $\Delta H^{\ddagger}$ [kJ $mol^{-1}$] | $\Delta S^{\ddagger}$ [J $mol^{-1}$ $K^{-1}$] | $\Delta V^{\ddagger}$ [$cm^3$ $mol^{-1}$] | $-T\Delta S^{\ddagger}_{(5°C)}$ [kJ $mol^{-1}$] | $\Delta G^{\ddagger}_{(5°C)}$ [kJ $mol^{-1}$] |
|---|---|---|---|---|---|---|
| **Compound I** | | | | | | |
| **1-PhEt** | 219 ± 2 | 33 ± 1 | −80 ± 2 | −2.3 ± 0.2 | 22.2 ± 0.5 | 55 ± 2 |
| **4-Mb-alc** | 7762 ± 137 | 22.4 ± 0.4 | −89 ± 1 | −2 ± 1 | 24.7 ± 0.3 | 47 ± 1 |
| **4-Mb-ald** | 9094 ± 319 | 24 ± 1 | −80 ± 2 | — | 22.2 ± 0.5 | 46 ± 2 |
| **Compound II** | | | | | | |
| **1-PhEt** | 2.2 ± 0.1 | 52 ± 1 | −51 ± 4 | +16.6 ± 0.6 | 14 ± 1 | 66 ± 2 |
| **4-Mb-alc** | 11.8 ± 0.4 | 46 ± 1 | −59 ± 3 | +12.6 ± 1.2 | 16.4 ± 0.8 | 62 ± 2 |
| **4-Mb-ald** | 87.6 ± 2.3 | 45 ± 1 | −45 ± 3 | +9.9 ± 0.8 | 12.5 ± 0.8 | 57 ± 2 |

which positive activation volumes were determined, indicating a domination of C–H bond homolysis coupled to reduction of the iron centre. The temperature dependent study allowed us to compare the contribution of $-T\Delta S^{\ddagger}$ *vs.* $\Delta H^{\ddagger}$ to the overall activation barrier ($\Delta G^{\ddagger}$). For [$Fe^{IV}$($Por^{+\bullet}$)(O)] species, but not for [$Fe^{IV}$(Por)(O)], the contribution of the $T\Delta S^{\ddagger}$ and $\Delta H^{\ddagger}$ terms were comparable, indicating that their impact on $\Delta G^{\ddagger}$ is markedly temperature sensitive. Furthermore, the oxidation of two out of three studied substrates was entropy-controlled within the room and physiological temperature range.

These results drew further attention to the issue raised earlier by Takahashi,[88] who warned against hasty interpretation of theoretical calculations, which are based on the calculated $E_a$ values. Such precaution arose from the studies showing entropy-controlled chemo-selectivity of cyclohexane oxidation by iron(IV)-oxo porphyrin cation radical species, indicating that $\Delta H^{\ddagger}$ is not always the dominant factor in the height of the activation barrier. These results also provided an explanation for the 'chameleon-like' behaviour of the compound I mimic observed by Song *et al.*,[89] who also reported the temperature dependent product distribution of C=C epoxidation *versus* C–H hydroxylation for the oxygenation of cyclohexene by [$Fe^{IV}$($Por^{+\bullet}$)(O)] species. Recently, Nam and co-workers on the basis of deuterium kinetic isotope effect studies on the oxidation of cyclohexene concluded that the switchover of the reaction pathway (C=C epoxidation *vs.* C–H hydroxylation) is the result of tunnelling effects on the H-atom abstraction for hydroxylation.[90]

Further support for these conclusions was provided by temperature dependent studies, performed in acetonitrile with the application of iron(III) *meso*-tetra(2,4,6-trimethylphenyl) porphyrin hydroxide [$Fe^{III}$(TMP)(OH)]. Comparison of the reactivity of [$Fe^{IV}$($TMP^{+\bullet}$)(O)] and [$Fe^{IV}$(TMP)(O)] in epoxidation and C–H abstraction reactions, revealed that reaction rates depend on both the chemical nature of the substrate and the reactive intermediate. Most of the studied reactions were enthalpy-controlled (Table 7); however, in the case of C–H abstraction conducted by [$Fe^{IV}$($TMP^{+\bullet}$)(O)] species, domination of the enthalpy term cannot be taken for granted. For example, the reaction with 9,10-dihydroanthracene is dominated by the $\Delta H^{\ddagger}$ term, whereas C–H abstraction in xanthene exhibits a large contribution from the $\Delta S^{\ddagger}$ term.[91]

### 3.3 The role of compound 0

Another intriguing question about the reactive intermediates in the catalytic cycle of cytochrome P450 is whether the hydroperoxo iron(III) intermediate (compound 0) is a potent reactive agent capable of participating in oxygenation of organic substrates. This dilemma was approached by both experimental and theoretical studies that resulted in the emergence of the so-called multi-oxidant-hypothesis (also referred to as the multiple-oxidant dilemma).[92–96] Several contradictory conclusions about the potency of compound 0 reactivity have been published. Cryle and De Voss reported results of fatty acid and thio-fatty acid oxidation by $P450_{BM3}$ and its T268A mutant, and concluded that compound 0 is the oxidant responsible for sulfoxidation.[72,97] On the other hand, Shaik *et al.*[73] opposed the findings of this report by presenting results from their theoretical calculations, which demonstrate that compound 0 is an inferior oxidant in comparison to compound I. The results remain in agreement with the studies reported by Nam, which exclude compound 0 as a reactive intermediate.[74,75]

These contradictory results stimulated interest in examining the reactivity of compound 0 towards various types of oxidation reactions in the course of direct oxidation reactions. By selecting appropriate reaction conditions, we were able to report for the first time on the reactivity of the compound 0 mimic [$Fe^{III}$(TMP)(*m*-CPBA)], in direct oxidation reactions of organic substrates, as well as under catalytic conditions.[98] The first phase of the work focused on the epoxidation and sulfoxidation reactions for which the multiple-oxidant dilemma was emphasized. The results of the study left no doubt that in these types of oxidation reactions [$Fe^{III}$($TMP^{+\bullet}$)(O)] ($k^{Cpd\ I/stilbene} = 66 \pm 2\ M^{-1}\ s^{-1}$ at −15 °C, $k^{Cpd\ I/DMS} = (1.7 \pm 0.1) \times 10^4\ M^{-1}\ s^{-1}$ at −35 °C) is a much more powerful oxidant than [$Fe^{III}$(TMP)(*m*-CPBA)] ($k^{Cpd\ 0/stilbene} = 0.142 \pm 0.006\ M^{-1}\ s^{-1}$ and $k^{Cpd\ 0/DMS} = 9.7 \pm 0.1\ M^{-1}\ s^{-1}$ at −15 °C).[98] In the next step, all of the three most discussed reactive intermediates (compounds 0, I and II) were prepared in solution and their reactivity with respect to epoxidation, sulfoxidation, C–H and O–H abstraction, as well as to hydride-transfer reactions, was evaluated. Kinetic studies on the reactivity of these three intermediates were performed with the application of a single model complex [$Fe^{III}$(TMP)] under identical experimental conditions, which provided a full comparability of the determined rate

**Table 7** Rate constants and activation parameters for the oxidation of selected substrates by mimics of compounds I and II generated by application of [$Fe^{III}$(TMP)] in acetonitrile as solvent[91]

| | $k$ [$M^{-1}\ s^{-1}$] at −15 °C | $\Delta H^{\ddagger}$ [kJ $mol^{-1}$] | $\Delta S^{\ddagger}$ [J $mol^{-1}\ K^{-1}$] | $-T\Delta S^{\ddagger}_{(-15°C)}$ [kJ $mol^{-1}$] | $\Delta G^{\ddagger}_{(-15°C)}$ [kJ $mol^{-1}$] |
|---|---|---|---|---|---|
| **Compound I** | | | | | |
| ***cis*-Stilbene** | 15.8 ± 0.6 | 46 ± 1 | −43 ± 4 | 11 ± 1 | 57 ± 2 |
| **DHA** | (1.01 ± 0.04) × $10^2$ | 42 ± 1 | −41 ± 5 | 11 ± 1 | 53 ± 2 |
| **Xanthene** | (6.5 ± 0.7) × $10^2$ | 24.4 ± 0.9 | −100 ± 4 | 25 ± 1 | 49 ± 5 |
| **Compound II** | | | | | |
| ***cis*-Stilbene** | 0.094 ± 0.001 | 52.9 ± 0.5 | −57 ± 2 | 14.7 ± 0.5 | 68 ± 1 |
| **DHA** | 1.5 ± 0.1 | 51 ± 3 | −41 ± 5 | 11 ± 2 | 62 ± 5 |
| **Xanthene** | 6.2 ± 0.3 | 37 ± 3 | −85 ± 5 | 22 ± 2 | 59 ± 3 |

DHA – 9,10-dihydroanthracene.

 

constants. The obtained results confirmed that for most of the studied reaction types compound I exhibited the highest reactivity, since the second-order rate constants for substrate oxidation exceed the rate constants for compounds 0 and II by several orders of magnitude. The reactivity of the compound I mimic proved to be dominant with the exception of the hydride transfer reactions, for which compound II turned out to be the most reactive species. The reactivity order for the hydride transfer reaction turned out to be the opposite (Cpd **II** > Cpd 0 > Cpd **I**) than for the other reaction types. Since for the hydride transfer reaction with 10-methyl-9,10-dihydroacridine (AcrH2), proton transfer is the rate-determining step, such behaviour was accounted for as a consequence of the ability of each reactive intermediate to promote the proton-abstraction step.[99]

Numerous experimental and theoretical studies provide results that prove the important role of the anionic ligand nature in the O–O bond cleavage process. Due to the fact that compound 0 in the catalytic cycle of heme enzymes is a six-coordinate *hydroperoxo*-iron(III) species, syntheses of [Fe(Por)(OOH)] models with hydroxo or imidazole ligands in the *trans* position to the $OOH^-$ group was desired. Such systems were successfully obtained by several groups; however, very low stability under extreme low temperature conditions excluded the possibility to study their reactivity.[100–105] Following this need, we were able for the first time to obtain a relatively stable hydroperoxo iron(III) intermediate with the application of an electron-withdrawing porphyrin TPFPP (TPFPP = 5,10,15,20-tetrakis(pentafluorophenyl)-21*H*,23*H*-porphyrin) as a model catalyst. By carefully tuning the reaction conditions, the generation of two forms of the model compound 0 in acetonitrile at −15 °C could be followed spectrophotometrically, *viz*. six-coordinate, low-spin [Fe(TPFPP)(OH)(OOH)] and five-coordinate, high-spin [Fe(TPFPP)(OOH)]. The reactivity of these two forms revealed to be completely different. Heterolysis of the O–O bond was observed for the six-coordinate [Fe(TPFPP)(OH)(OOH)] species, whereas five-coordinate [Fe(TPFPP)(OOH)] underwent O–O bond homolysis. Such a difference in reactivity was assigned to the influence of the axial ligand and spin-state on the mode of O–O bond cleavage in hydroperoxo intermediates.[106]

Further studies revealed that the six-coordinate Compound 0 mimic obtained with the electron-withdrawing porphyrin TPFPP, is very stable and completely unreactive towards *cis*-stilbene and dimethyl sulphide. This is in contrast to the reactivity of [$Fe^{III}$(TMP)(*m*-CPBA)], for which, although very slow, oxygenation of these substrates could be followed.[98,99] Such a completely different reactivity of the electron-withdrawing porphyrin model of compound 0 in comparison to electron-donating porphyrins, was observed for the complex with the hydroperoxo ligand bound in the end-on mode to the iron centre, as well as for the side-on peroxide complex.[107,108]

### 3.4 The influence of axial ligands

Heme-containing mono-oxygenases differ in the proximal-axial ligand nature, which significantly affects their ability to catalyse various types of oxidation reactions. Therefore, another aspect widely discussed in the literature concerns the influence of axial ligand nature on the formation and reactivity of high-valent iron(IV)-oxo species. Since histidine is one of the common ligands in heme mono-oxygenases, *e.g.* horseradish peroxidase, various derivatives of imidazole are often used in order to mimic the active site. For that reason, we undertook studies to check the influence of *N*-methylimidazole on the formation and reactivity of high-valent iron(IV)-oxo intermediates.[109] Spectrophotometric studies covering the complete catalytic cycle in which a compound II model with *N*-methylimidazole or hydroxo ligands oxidize selected substrates, were performed with the application of water-soluble [$Fe^{III}$(TMPS)] and hydrogen peroxide as oxidant. Results for the second-order rate constants obtained as a function of *N*-methylimidazole (*N*-MeIm) concentration, revealed that the mono-imidazole [$Fe^{III}$(TMPS)($H_2O$)(*N*-MeIm)] substituted complex is much more reactive than the five-coordinate high-spin [$Fe^{III}$(TMPS)(OH)] and six-coordinate low-spin [$Fe^{III}$(TMPS)(*N*-MeIm)$_2$] complexes. The *N*-methylimidazole substituted compound II model, was obtained in two reaction pathways, *viz*. *via* the reaction of $H_2O_2$ with [$Fe^{III}$(TMPS)(*N*-MeIm)$_2$] or *via* the reaction of [$Fe^{IV}$(TMPS)(O)(OH)] with *N*-methylimidazole, and its reactivity was studied toward selected organic substrates. Kinetic studies on the reactivity of both compound II models revealed a lack of influence of the axial ligand nature (*N*-methylimidazole *vs.* $OH^-$) on substrate oxidation. Experimental results were further confirmed by theoretical calculations. The energy barrier for the dehydrogenation, being the rate-determining step for the studied reactions, did not exhibit a dependence on the selected axial ligands.[109] In the light of numerous studies showing significant influence of the axial ligands on the reactivity of Compound I, we do not deny that this observation was quite surprising to us since a significant influence of both anionic axial ligands, as well as imidazole, on the reactivity of compound I was reported.[110–114]

In order to perform a comparative analysis of the reactivity of compound I and compound II mimics as key active species of horseradish peroxidase, studies with the application of [$Fe^{III}$(TMP)(2-MeIm)] in acetonitrile were performed. Functional models for reactive intermediates of this enzyme, *viz*. [$Fe^{IV}$($TMP^{+\bullet}$)(O)(2-MeIm)] and [$Fe^{IV}$(TMP)(O)(2-MeIm)], were generated *in situ* and their reactivity studied towards epoxidation, C–H bond activation, and heteroatom oxidation reactions. The results obtained revealed not only the difference in the reactivity efficiency of these two high-valent iron species, but also in the product distribution in the case of DMS oxidation. Sulfoxidation was the favourable process in the case of oxidation by compound I, whereas C–H bond activation dominated in the case of oxidation by compound II. A comparison of the energy barriers determined theoretically for sulfoxidation and C–H abstraction for both iron-oxo species with $\Delta G^{\ddagger}$ values obtained experimentally, confirmed satisfyingly the differences in the observed product distribution. Such diverse product distribution was explained by regio-selec-

tive conversion between sulfoxidation and C–H bond activation that occurs at the level of the initial rate-determining step.[115]

### 3.5 Functional models for cytochrome P450

The distinct feature of cytochrome P450 which is perceived to be crucial for facilitation of heterolytic O–O bond cleavage, is the axial thiolate ligand which decreases the reduction potential of the active site and stabilizes iron(IV)-oxo porphyrin π–cation radical species.[116] However, to obtain iron(III) heme-thiolate models turned out to be challenging due to the high instability of such macrocycles. Several research groups took up the challenge of synthesis of functional models for cytochrome P450.[64,117–120] One of them was Higuchi's group who were able to synthesize alkanethiolate-coordinated ferric porphyrin with the thiolate ligand sterically protected by bulky pivaloyl groups (**SR** complex) (Fig. 14).[121] Woggon *et al.*[122–124] in order to overcome the problem with low stability of such complexes, exchanged the $RS^-$ group with $RSO_3^-$ and proposed two complexes, one with electron-withdrawing (**$RSO_3^-$-1**) and the second one with electron-donating (**$RSO_3^-$-2**) substituents on the porphyrin ring (Fig. 14).

Our fruitful collaboration with both these groups resulted in in-depth understanding of the reactivity of these complexes as models for P450 enzymes. Kinetic studies on the reactivity of the **SR**-complex with organic peroxides, revealed a substantial effect of the thiolate group on the formation and reactivity of the iron(IV)-oxo porphyrin cation radical. The results obtained revealed that the complex has a unique ability to undergo heterolytic O–O bond cleavage independent of solvent polarity. Kinetic studies on the catalytic oxidation of *tert*-butylphenol (TBPH), *cis*-stilbene, 9,10-dihydroanthracene (DHA) and dimethyl sulphide (DMS), showed a very fast oxygen atom transfer or hydrogen atom abstraction by compound I, $[(SR^{+\bullet})Fe^{IV}{=}O]$, and pointed to the formation of the $[(SR^{+\bullet})Fe^{IV}{=}O]$ intermediate being the rate-determining step. Unfortunately, the **SR** complex prevailed to be highly unstable; under an excess of peroxide the complex loses the coordinated thiolate group, most probably due to oxidation to $SO_3^-$ (**dec-SR**), and in the subsequent step undergoes decomposition. In the presence of *m*-CPBA in excess over the SR complex, the thiolate-lacking **dec-SR** complex may also undergo oxidation to reactive $[(\mathbf{decSR}^{+\bullet})Fe^{IV}{=}O]$ species, which however is a much less powerful oxidant than the parent complex (Fig. 15).[126]

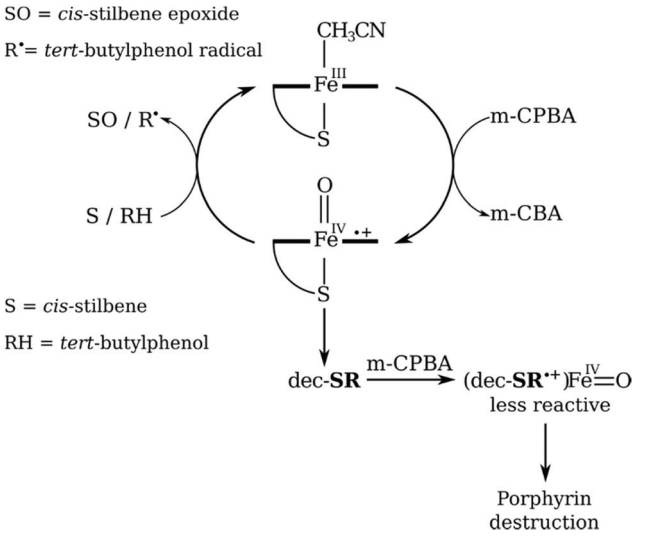


**Fig. 15** Catalytic cycle of the **SR** complex in acetonitrile. Reprinted with permission from ref. 126. Copyright 2009 WILEY-VCH Verlag GmbH & Co. KGaA, Weinheim.

Complexes synthesized by the Woggon group, besides the exchange of the $RS^-$ group for $RSO_3^-$, turned out to be valuable models for cytochrome P450 showing good reactivity towards hydrocarbon hydroxylation, *N*-dealkylation, alkene epoxidation and diol cleavage.[123,124] Application of a rapid scan, low-temperature stopped-flow technique, allowed to follow spectrophotometrically the whole catalytic cycle of **$RSO_3^-$-1** including the formation of the acylperoxo intermediate. Kinetic studies on the formation and reactivity of the iron (IV)-oxo intermediate with the application of **$RSO_3^-$-1**, allowed to determine the formation constant for the acylperoxo Fe(III) complex, the first-order rate constant for heterolytic O–O bond cleavage and the second-order rate constant for *cis*-stilbene oxidation.[127]

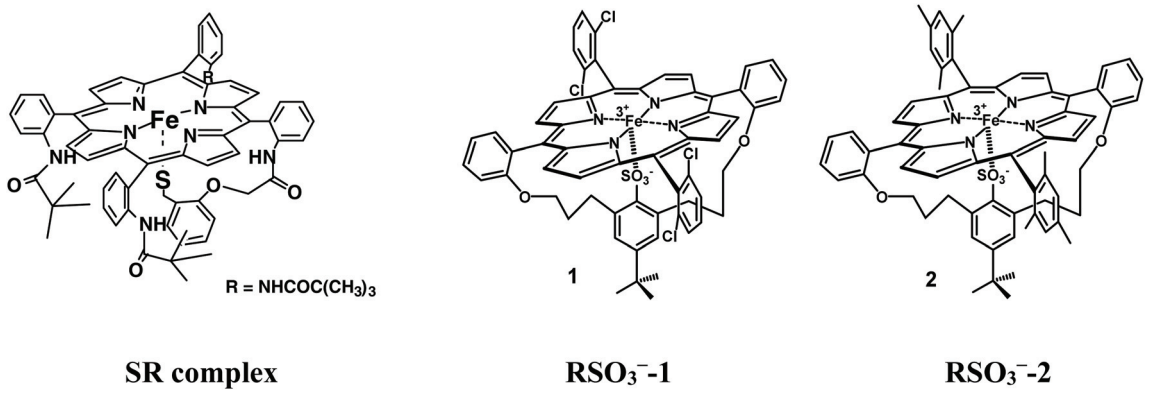


**Fig. 14** Models of cytochrome P450 active site bearing $RS^-$ or $RSO_3^-$ groups.[121–125]

 

Detailed studies on the kinetics, formation mechanism and reactivity of the iron(IV)-oxo cation radical generated in the reaction of *m*-CPBA with $\mathbf{RSO_3^-}$**-1** and $\mathbf{RSO_3^-}$**-2**, were performed in various solvents (toluene, acetonitrile, dichloromethane, methanol). Comparison of the rate constants and activation parameters obtained for both complexes in the selected solvents, revealed a strong influence of the electronic nature of the porphyrin ring, as well as solvent properties on the stability/reactivity of the corresponding iron(IV)-oxo porphyrin cation radical complexes. The $\mathbf{RSO_3^-}$**-2** species with electron-donating substituents on the porphyrin ring exhibited significantly higher rate constants for the formation of the $[Fe^{IV}(Por^{+\bullet})(O)]$ intermediate in comparison to $\mathbf{RSO_3^-}$**-1** bearing electron-withdrawing substituents. In contrast, the reactivity towards organic substrates was reversed. Comparison of the results obtained in various solvents allowed to point toward acetonitrile as the best choice due to fast formation of iron(IV)-oxo species and extended stability.[128]

### 3.6 Experiments with cytochrome $P450_{cam}$

Our interest in the understanding of the detailed mechanism of the catalytic cycle of cytochrome $P450_{cam}$ led us to perform experiments with cytochrome $P450_{cam}$ itself, besides studies with the application of model porphyrin systems as reported above. Since the catalytic cycle of cytochrome P450 starts with natural substrate (camphor) binding, which is associated with the expulsion of the water molecule coordinated at the sixth position of the heme iron, which is accompanied by a change in spin state from low spin to high spin. In a first step the detailed kinetic and thermodynamic description of the reversible binding of camphor to cytochrome $P450_{cam}$ was studied.[129]

In order to contribute to a better understanding of the cytochrome $P450_{cam}$ catalytic cycle, our studies subsequently focused on the generation of the key reactive intermediates *via* the oxidation of the enzyme by the application of the so called 'peroxide shunt' approach commonly used in model studies. By precise selection of the reaction conditions, we were able to generate the hydroperoxo iron(III) intermediate (compound 0, P450-$Fe^{III}$-OOH) through oxidation of the substrate-free enzyme by hydrogen peroxide.[130] Studies performed under basic conditions, revealed the formation of the hydroperoxo iron(III) intermediate in a concerted way, namely coordination of $OOH^-$ was preceded by $H_2O_2$ deprotonation at the hydroxo ligand coordinated to the iron(III) centre, followed by $H_2O$ substitution by $OOH^-$ (Fig. 16). The proposed mechanism differs from the typical $H_2O_2$ coordination mode observed in heme proteins possessing distal histidine in the active centre acting as general acid–base catalyst.

Formation and reactivity of compound 0 was studied as a function of pH, $[H_2O_2]$, [camphor] and $[K^+]$. The mild basic conditions applied in the study, resulted in the suppression of the formation of compound I which is a consequence of the suppression of a distal proton relay system. So far, only indirect evidence for the formation of cytochrome P450 compound I has been provided in an approach based on the formation of the iron(II)dioxygen complex and its subsequent reduction using various irradiation techniques and cryo-reduction of oxo-P450. The extended life-time of compound 0 was exploited to study its reactivity toward the natural substrate (camphor) of cytochrome $P450_{cam}$. Camphor oxidation was conducted at pH = 8.2 for substrate-bound P450 being in equilibrium with the substrate-free form (Fig. 16). The results obtained showed that under the selected conditions, suppressing the heterolytic O–O bond cleavage, the cytochrome $P450_{cam}$ $Fe^{III}$–OOH intermediate (compound 0) may act as an oxygen donor. These studies for the first time provide evidence for the catalytic activity of a true compound 0 transient intermediate and not its oxidant-dependent mimics.[130]

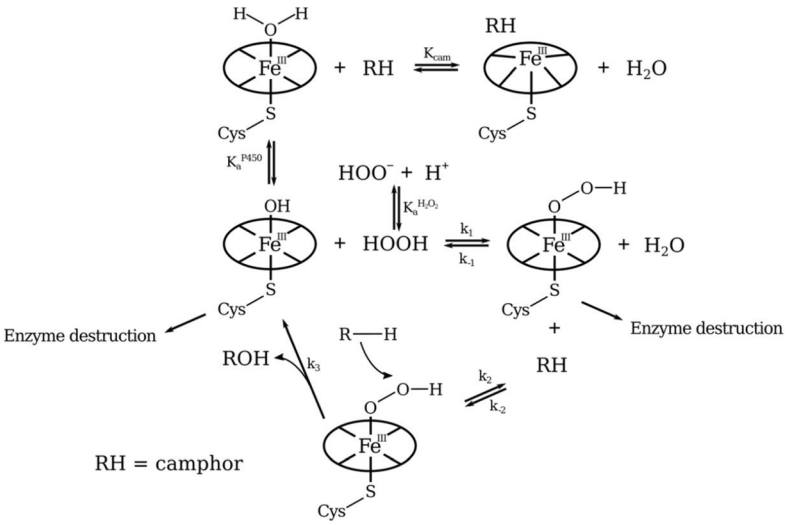


Fig. 16 Suggested reaction mechanism for camphor oxidation catalysed by Compound 0. Reprinted with permission from ref. 130. Copyright 2015 WILEY-VCH Verlag GmbH & Co. KGaA, Weinheim.

### 3.7 Conclusions

In conclusion, detailed studies on the kinetics and mechanism of the reactivity of simple and more advanced models of mono-oxygenase enzymes as well as cytochrome $P450_{cam}$ itself, allowed us to identify crucial reactive intermediates in the catalytic cycle of this enzyme family *viz.* compounds 0, I and II. Furthermore, by judicious tuning of the reaction conditions, we were able to control successfully the formation and reactivity of these species. We strongly believe that our studies contributed to resolve the important problems related with the nature and mechanism of the reactivity of these catalytically active intermediates.

## 4. The wonder-world of $Ru^{III}$(edta) chemistry

### 4.1 Introduction

The chemistry of the 'edta' ($edta^{4-}$ = ethylenediaminetetraacetate) complexes of ruthenium(III) is wonderful in many ways. As a consequence of its kinetic lability towards the aqua substitution reaction, it affords a facile and straightforward method of preparation of mixed-ligand compounds, especially with some biological molecules.[131] Furthermore, a range of accessible and stable oxidation states made $Ru^{III}$(edta) of abiding importance to kinetic and mechanistic studies for the past four decades concerning the elucidation of inorganic reactions mechanisms. Most of the work published in earlier periods was limited to the aqueous chemistry of these compounds, mainly concerning the reactivity of $Ru^{III}$(edta) complexes towards aqua- substitution reactions[132–136] and catalytic studies[137] which were thoroughly reviewed earlier.[138] However, a major impetus toward development of $Ru^{III}$(edta) chemistry has been undertaken by the authors of this article who have collaborated for the past two decades. The ability of $Ru^{III}$(edta) in mediating reactions of biological importance and unravelling their mechanistic characteristics, has been demonstrated in the recent past, and this review mainly covers the application of $Ru^{III}$(edta) complexes as catalysts or mediators in peroxide activation, oxidation of thiols and thio-molecules, NO production, *S*-nitrosylation of cysteine and $H_2S$. Since, kinetic information on the aforementioned reactions appears to be of great significance to understand preferential reaction pathway (s), this review will focus on the kinetics and mechanism of the $Ru^{III}$(edta) mediated activation and catalytic transformation of the species that are mentioned.

### 4.2 Background chemistry

The donor character of the 'edta' ligand is quite comparable to many biological enzymes, which make use of carboxylate and amine donors from amino acids to bind to the metal centre. The 'edta' ligand forms a very stable 1 : 1 metal complex with ruthenium. The pale yellow solid $K[Ru^{III}(Hedta)Cl]$ complex rapidly converts into the $[Ru^{III}(Hedta)(H_2O)]$ species when dissolved in water.[132,133] It was shown earlier,[132,133] and later established by crystallographic studies,[139] that the 'edta' ligand functions as a pentadentate ligand towards Ru(III) with a protonated pendant acetate arm. The sixth coordination site of the ruthenium centre in the $Ru^{III}$(edta) complex is occupied by a water molecule at low pH or by an hydroxide ion at high pH (see Scheme 8).

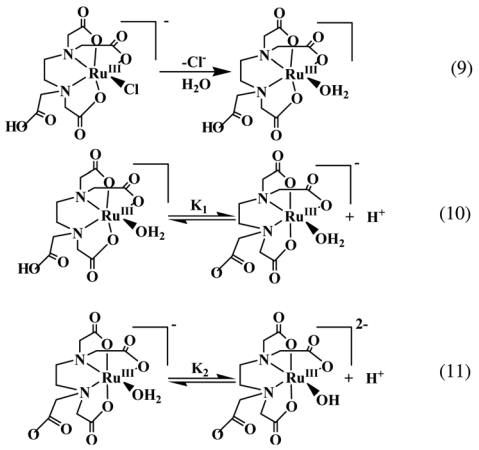


Scheme 8 Acid-dissociation equilibria of $[Ru^{III}(Hedta)(H_2O)]$.

The $pK_a$ values related to the acid-dissociation equilibria of the pendant carboxylic acid arm and the coordinated water molecule are 2.4 and 7.6, respectively, at 25 °C.[132,133] The $[Ru^{III}(Hedta)H_2O]$ complex exhibited a remarkable lability towards substitution in the pH range 4–6, because in this pH range the ruthenium(III) complex exists in its most labile form, $[Ru(edta)(H_2O)]^-$.[138] The pendant carboxylate group, was suggested to be responsible for the lability with regard to the displacement of the water molecule from $[Ru^{III}(edta)(H_2O)]^-$ involving an associative interchange ($I_a$) mechanism.[138] The $[Ru^{III}(edta)(H_2O)]^-$ complex, due to its lability towards aqua substitution, could be of oncological significance as it could bind DNA constituents[140] as well as thiols[141] in a facile and straightforward manner, and show protease inhibition activities.[141,142]

Electrochemical studies of the $Ru^{III}$(edta) complex have shown that the electron transfer process is rapid and reversible for the $Ru^{III}/Ru^{II}$ couple ($E_{1/2}$ = −0.04 V *vs.* NHE).[132] It is noteworthy that although Ru(III) is the predominant oxidation state under physiological conditions, Ru(II), Ru(IV) and Ru(V) oxidation states are readily accessible in the presence of biological reductants (*e.g.*, ascorbate or thiols)[143] or oxidants (*e.g.*, $O_2$ or $H_2O_2$), respectively.[138]

### 4.3 $Ru^{III}$(edta) mediated peroxide activation

The catalytic ability of the $Ru^{III}$(edta) complex towards mimicking the $H_2O_2$-metabolizing enzymes peroxidases and catalases, is shown schematically in Scheme 9.

The reaction of the $[Ru^{III}(edta)(H_2O)]^-$ complex with $H_2O_2$ was followed kinetically using stopped-flow and rapid-scan techniques.[144,145] Time-resolved spectral studies revealed that the reaction of $[Ru^{III}(edta)(H_2O)]^-$ with $H_2O_2$ proceeds through

 

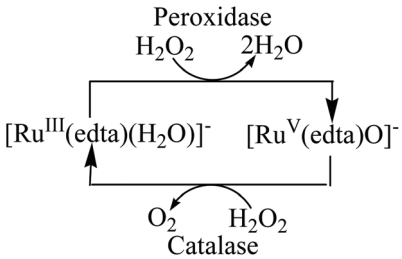


**Scheme 9** Schematic representation of peroxidase and catalase activities of $[Ru^{III}(edta)(H_2O)]^-$.

the rapid formation of a band at 425 nm (Fig. 17a) which was assigned to the formation of the $[Ru^{III}(edta)(OOH)]^{2-}$ species and the kinetic trace at 425 nm (Fig. 17b) clearly demonstrates the intermediate nature of the species.[145] The $[Ru^{III}(edta)(OOH)]^{2-}$ species subsequently undergoes heterolysis of the O–O bond to form $[Ru^{V}(edta)(O)]^-$ as characterized by the strong band at 390 nm ($\varepsilon_{max}$ = 8000 ± 20 $M^{-1}$ $cm^{-1}$).[137] It is worth mentioning here that $[Ru^{III}(edta)(OOH)]^{2-}$ and $[Ru^{V}(edta)(O)]^-$ are capable of functioning in a similar way as compounds 0 and I, respectively, in biomimetic oxidation processes.

The kinetic profile of the reaction of $[Ru^{III}(edta)(H_2O)]^-$ with other oxidants, *viz.* $^t$BuOOH and $HSO_5^-$ containing the peroxide (O–O) bond, was found to be similar to that observed for the reaction of $[Ru^{III}(edta)(H_2O)]^-$ with $H_2O_2$. The $[Ru^{V}(edta)(O)]^-$ species was produced almost quantitatively for both oxidants, $^t$BuOOH and $HSO_5^-$.[146] Based on the results of spectral and kinetic studies taken together for the reactions of $[Ru^{III}(edta)(H_2O)]^-$ with the precursor oxidant ROOH (ROOH = $H_2O_2$, $^t$BuOOH and $HSO_5^-$),[144–146] a generalized mechanism (Scheme 10) involving the formation of the $[Ru^{III}(edta)(OOR)]^{2-}$ (R = H, $^t$Bu, $HSO_3^-$) intermediate in a rapid pre-equilibrium step, followed by the subsequent heterolytic cleavage of the O–O bond to produce $[Ru^{V}(edta)(O)]^-$ as the major product, was proposed.

The reactivity order expressed in terms of *kK*, *i.e.* the product of the equilibrium constant *K* for the formation of $[Ru^{III}(edta)(OOR)]^{2-}$ and the rate constant *k* for the subsequent heterolytic cleavage of the O–O bond to form $[Ru^{V}(edta)(O)]^-$ and ROH, is as follows: $H_2O_2$ ($kK$ = 26.5 $M^{-1}$ $s^{-1}$)[144,145] ≫ $HSO_5^-$ ($kK$ = 7.0 $M^{-1}$ $s^{-1}$) ≫ $^t$BuOOH ($kK$ = 1.45 $M^{-1}$ $s^{-1}$) at 25 °C.[146] Since, the overall reaction is a two-step process as outlined in Scheme 10, the nucleophilicity of the oxidants (ROOH) to form $[Ru^{III}(edta)(OOR)]$ (R = H, $^t$Bu and $HSO_3^-$) *via* the aqua substitution reaction (eqn (12)) presumably governs the efficiency of the precursor oxidants (ROOH) to produce $[Ru^{V}(edta)(O)]^-$ in the reaction system. However, the reduction potential of the precursor oxidants, *i.e.* $^t$BuOOH ($E°$ = 1.15 V), $H_2O_2$ ($E°$ = 1.78 V) ≤ $HSO_5^-$ ($E°$ = 1.82 V)[147] could also contribute towards heterolytic cleavage of the O–O bond in $[Ru^{III}(edta)(OOR)]$ that leads to the formation of $[Ru^{V}(edta)(O)]^-$.[146] In addition to the aforesaid thermodynamic factors, steric hindrance on $^t$BuOOH and $HSO_5^-$ as compared to $H_2O_2$ should account for the smaller values of kK for $^t$BuOOH and $HSO_5^-$ as compared to $H_2O_2$.

While studying the peroxidase activity of $[Ru^{III}(edta)(H_2O)]^-$, the catalase mimicking ability of $Ru^{III}(edta)$ to promote the disproportionation of $H_2O_2$ into dioxygen and water was also observed at high concentrations of $H_2O_2$.[148] It was further noticed that an increase in $H_2O_2$ concentration increased the amount of $O_2$ generated in the reaction system (Table 1), and the amount of $O_2$ produced is close, as might be

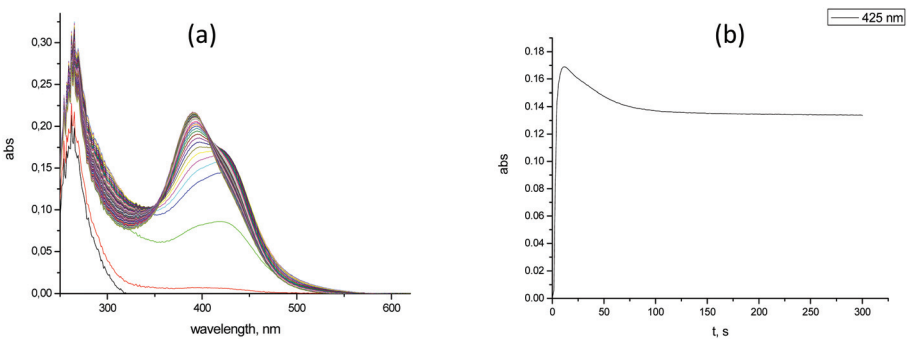


**Fig. 17** (a) Spectral changes observed in the reaction of $[Ru^{III}(edta)(H_2O)]^-$ with a large excess of $H_2O_2$ at 23 °C. (b) Absorbance *versus* time trace at 425 nm. $[Ru^{III}]$ = 2 × $10^{-5}$ M, $[H_2O_2]$ = 1 × $10^{-2}$ M, pH = 4.0 (0.001 M acetate buffer). Reprinted with permisson from ref. 145. Copyright 2011 the Royal Society of Chemistry.

$$[Ru^{III}(edta)(H_2O)]^- + ROOH \underset{}{\overset{K}{\rightleftharpoons}} [Ru^{III}(edta)(OOR)]^{2-} + H_3O^+ \quad (12)$$

$$[Ru^{III}(edta)(OOR)]^{2-} \xrightarrow[+\,H^+]{k_{het(O\text{-}O)}} [Ru^{V}(edta)O]^- + ROH \quad (13)$$

**Scheme 10** Proposed mechanism for the reaction of $[Ru^{III}(edta)(H_2O)]^-$ with ROOH. Reprinted with permission from ref. 146. Copyright 2008 the Royal Society of Chemistry.

Table 8 Results of $O_2$ evolution studies as a function of $H_2O_2$ concentration at 25 °C and pH = 5.0 (10.0 mM acetate buffer). [$Ru^{III}$] = 2.0 μmol. Reprinted with permission from ref. 148. Copyright 2014 the Royal Society of Chemistry

| $H_2O_2$ (mmol) | $O_2$ produced (mmol) after 4 h |
|---|---|
| 0.1 | 0.043 |
| 0.2 | 0.111 |
| 0.4 | 0.190 |
| 1.0 | 0.440 |
| 2.0 | 0.825 |

$$[Ru^{III}(edta)(H_2O)]^- + H_2O_2 \overset{K}{\rightleftharpoons} [Ru^{III}(edta)(OOH)]^{2-} + H_2O + H^+ \quad (14)$$

$$[Ru^{III}(edta)(OOH)]^{2-} \xrightarrow{+H^+} [Ru^{V}(edta)(O)]^- + H_2O \quad (15)$$

$$[Ru^{V}(edta)(O)]^- + H_2O_2 \xrightarrow{k_{cat}} [Ru^{III}(edta)(H_2O)]^- + O_2 \quad (16)$$

Scheme 11 Mechanism for the catalytic disproportionation of $H_2O_2$ by $[Ru^{III}(edta)(H_2O)]^-$. Reprinted with permission from ref. 148. Copyright 2014 the Royal Society of Chemistry.

expected, to half of the initial amount of $H_2O_2$ used (Table 8).[148]

Based on the experimental observations above and by analogy with the reported mechanism for the disproportionation of $H_2O_2$ into $O_2$ and $H_2O$, a working mechanism for the catalase activity of $[Ru^{III}(edta)(H_2O)]^-$ is outlined in Scheme 11. As suggested, a 'compound I' like species, $[Ru^{V}(edta)(O)]^-$ is formed *via* peroxidase activity (reactions (14) and (15) in Scheme 11). In a subsequent step, $[Ru^{V}(edta)(O)]^-$ reacts with another molecule of $H_2O_2$ (in the presence of a high concentration of $H_2O_2$) to convert it to dioxygen and water, thus mimicking catalase activity (reaction (16)). Under turnover conditions, the $[Ru^{III}(edta)(H_2O)]^-$ catalyst was regenerated at the end of the catalytic cycle (reaction (16)) and immediately reacted further with $H_2O_2$ to produce $[Ru^{V}(edta)(O)]^-$ in the reaction system, by which a steady state concentration of $[Ru^{V}(edta)(O)]^-$ was reached. Once this concentration of $[Ru^{V}(edta)(O)]^-$ is attained, no appreciable further spectral changes were observed,[148] but evolution of dioxygen ($O_2$) was clearly visible at the higher $H_2O_2$ concentration.

It was observed that the catalase activity is strongly controlled by the $H_2O_2$ concentration, and a small amount of $[Ru^{V}(edta)(O)]^-$ could trigger the catalase activity at higher $H_2O_2$ concentration. Noteworthy here is that catalase has one of the highest turnover numbers of all enzymes; one catalase molecule can convert millions of hydrogen peroxide molecules to water and oxygen in a second. The catalytic turn-over number achieved by $Ru^{III}$(edta) system is 1400, only surpassed by the $Fe^{III}$(TAML) system.[149]

### 4.4 $Ru^{III}$(edta) mediated oxidation of thiols

Kinetics of substitution reactions of the $Ru^{III}$(edta) complex with thiols play a crucial role in the catalysis of thiol-oxidation by the $Ru^{III}$(edta)/$H_2O_2$ system as it is associated with the making and breaking of metal–sulphur bonds. Moreover, the nucleophilicity of the coordinating thiols governs the reactivity of the oxidation process. Therefore, substitution kinetics of the $Ru^{III}$(edta) complex with various biologically important thiols (RSH), though studied quite some time ago,[136,141,150] are included in this review. The reaction of $[Ru^{III}(edta)(H_2O)]^-$ with thiols occurs rapidly in a straightforward manner and results in the formation of S-bonded red-coloured $[Ru^{III}(edta)(SR)]^{2-}$ complexes which are quite stable in the absence of an oxidant. However, it may be noted here that a similar, but substitution inert $[Ru^{III}(edta)(pz)]^-$ complex (pz = pyrazine) could oxidize thiols (RSH = cysteine, glutathione) in an outer-sphere manner to a disulphide RSSR product.[151]

While the redox thiol-disulphide inter-conversions are the basis of many energy transfer cycles, the oxidation of thiols (RSH) by hydrogen peroxide ($H_2O_2$) has been recognized to be the most important process with regard to cellular signal transduction pathways.[152] The catalytic ability of $Ru^{III}$(edta) towards oxidation of thiols (RSH) using $H_2O_2$ as precursor oxidant has been explored in the recent past.[153,154] Addition of $H_2O_2$ to the red solution of $[Ru^{III}(edta)(SR)]^{2-}$ (where RSH = cysteine) resulted in rapid de-coloration of the solution accompanied by the oxidation of coordinated cysteine. Kinetic traces pertaining to the $Ru^{III}$(edta) catalysed oxidation of cysteine are shown in Fig. 18. Typically, sigmoid-shaped kinetic traces recorded at 510 nm as shown in Fig. 18a and b as a function of $H_2O_2$ concentration as well as cysteine concentration signify the occurrence of a catalytic oxidation process.[153]

The length of the induction period as observed in Fig. 18a shortens with increasing concentration of $H_2O_2$; however, it increased with increasing cysteine concentration (Fig. 18b) as a result of the rapid reformation of the $[Ru^{III}(edta)(SR)]^{2-}$ complex resulting in a longer recycling of the catalyst under turnover conditions [RSH] > [$Ru^{III}$]. These observations substantiate the occurrence of a catalytic process in the oxidation of thiols by $H_2O_2$ in the presence of $[Ru^{III}(edta)(H_2O)]^-$. Both $RSO_2H$ (cysteine sulfinic acid) and RSSR (cystine) were reported to be the major oxidation products of cysteine;[153] however, the product ratio [RSSR]/[$RSO_2H$] increased with increasing [RSH].[153]

The mechanism outlined in Scheme 12 was proposed as a consequence of the findings above.[153,154] The values of the second-order rate constant ($k_{ox}$) and the activation parameters reported for $Ru^{III}$(edta) catalysed oxidation of different thiols (RSH = cysteine, glutathione, *N*-acetylcysteine and penicillamine)[154] are summarised in Table 9. Activation entropies pertaining to the heterolytic cleavage of the O–O bond, followed by the 2e/O-atom transfer process, requires much more geometric reorganization to reach the transition state. The values of the activation parameters, particularly the highly negative values of $\Delta S^{\ddagger}$ (Table 9), are in good agreement with the oxygen atom transfer reactions involving heterolytic cleavage of the O–O bond.[155]

The steric hindrance on the coordinated thiols with regard to the approach of $H_2O_2$ probably governs the rate of oxidation

 

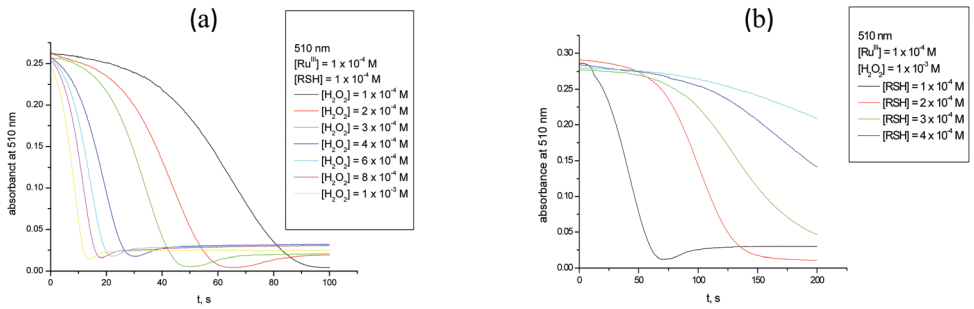


**Fig. 18** Typical absorbance–time traces for the oxidation of $[Ru^{III}(edta)(CyS)]^{2-}$ (a) at different concentrations of $H_2O_2$ where $[Ru^{III}]$ = 0.1 mM, [CySH] = 1 mM, $[H_2O_2]$ = (1–10) mM (increasing from right to left), pH 5.1, $T$ = 20 °C and (b) at different [CySH] = (1–5) mM (increasing from left to right) where, $[Ru^{III}]$ = 0.1 mM, $[H_2O_2]$ = 1 mM, pH 5.1, $T$ = 20 °C. Reprinted with permission from ref. 153. Copyright 2011 the Royal Society of Chemistry.



$$[Ru^{III}(edta)(H_2O)]^- + RSH \underset{}{\overset{K_{RSH}}{\rightleftharpoons}} [Ru^{III}(edta)SRH]^- + H_2O \quad (17)$$

$$[Ru^{III}(edta)(SRH)]^- + H_2O_2 \xrightarrow{k_{ox}} [Ru^{III}(edta)S(OH)R]^- + H_2O \quad (18)$$

$$[Ru^{III}(edta)S(OH)R]^- + H_2O_2 \longrightarrow [Ru^{III}(edta)(H_2O)]^- + RSO_2H \quad (19)$$

$$[Ru^{III}(edta)S(OH)R]^- + RSH \longrightarrow [Ru^{III}(edta)(H_2O)]^- + RSSR \quad (20)$$

**Scheme 12** Mechanism for the oxidation of thiols (RSH) by the $Ru^{III}$(edta)-$H_2O_2$ system. Reprinted with permission from ref. 154. Copyright 2016 Taylor & Francis.

**Table 9** Rate and activation parameters for the oxidation of $[Ru^{III}(edta)(SR)]^{2-}$ by $H_2O_2$ at 25 °C. Reprinted with permission from ref. 154. Copyright 2016 Taylor & Francis

| RSH | $k_{ox}$ [$M^{-1}$ $s^{-1}$] at 25 °C | $\Delta H^{\ddagger}$ [kJ $mol^{-1}$] | $\Delta S^{\ddagger}$ [J $K^{-1}$ $mol^{-1}$] |
|---|---|---|---|
| Cysteine | 25.0 | 45 ± 1 | −67 ± 3 |
| Glutathione | 17.3 | 46 ± 2 | −66 ± 5 |
| *N*-Acetylcysteine | 2.9 | 64 ± 2 | −20 ± 6 |
| Penicillamine | 1.32 | 62 ± 3 | −29 ± 7 |

by the $Ru^{III}$(edta)/$H_2O_2$ catalytic system. Typically penicillamine is the least reactive (Table 9) as the S-atom is sterically more encumbered (presence of two methyl groups adjacent to the S-atom in penicillamine) towards the approach of $H_2O_2$ which accounts for the observed lower rate constant value for the $Ru^{III}$(edta) catalysed oxidation of penicillamine. The kinetic data provided in Table 9 further suggest that cysteine could be more reactive than glutathione towards the heterolytic cleavage of the O–O bond of $H_2O_2$. Noteworthy here, is that in all cases the catalytically active intermediate species $[Ru^{III}(edta)(OOH)]^{2-}$ and $[Ru^{V}(edta)O]^-$ (equivalent to compounds 0 and compounds I, respectively) do not play a crucial role in the aforementioned catalytic oxidation of thiols (RSH). It is the oxidant, $H_2O_2$ that directly attacks the sulphur atom of the coordinated thiols in $[Ru^{III}(edta)SR]^{2-}$ leading to the formation of the S-bonded sulfenato $[Ru^{III}(edta)S(O)R]^{2-}$ species *via* nucleophilic scission of the O–O bond. A similar type of kinetic intermediate was also reported for the oxidation of thiols coordinated to chromium(III) and cobalt(III).[156,157] The $[Ru^{III}(edta)S(O)R]^{2-}$ intermediate reacts further either with another molecule of substrate or oxidant in kinetically indistinguishable step(s) to produce the ultimate oxidation product.

Apart from the thiols mentioned above, oxidation of some other biochemically significant thio-species such as thiourea (TU), thiocyanate ($SCN^-$) and thiosulphate ($S_2O_3^{2-}$) which can coordinate to $Ru^{III}$(edta) directly through the S-donor, and thereby produce the red coloured complexes $[Ru^{III}(edta)(L)]^{n-}$ (L = thiourea, thiocyanate and thiosulphate), was also reported.[158–160] The values of the rate constant reported for the oxidation of coordinated thiourea, thiocyanate and thiosulphate are 3.4 $M^{-1}$ $s^{-1}$,[158] 3.11 $M^{-1}$ $s^{-1}$ (ref. 159) and 0.93 $M^{-1}$ $s^{-1}$ (ref. 160) at 25 °C, respectively.

### 4.5 $Ru^{III}$(edta) mediated NO production

Nitric oxide (NO) seems to play an important role in many disease states. Whereas a decrease in NO production could lead to acute hypertension, sepsis and toxic shock are caused by the overproduction of NO. The thermodynamics and kinetics that characterise $Ru^{III}$(edta) as an efficient NO scavenger in aqueous solution were reported,[161] and more recently the kinetics and mechanism of NO production in $Ru^{III}$(edta) mediated oxidation of L-arginine with $H_2O_2$ in resemblance to NOS activity were reported.[162]

Formation of $[Ru^{III}(edta)(NO)]^-$ *via* the oxidation of azide ion ($N_3^-$) by $Ru^{III}$(edta)/$H_2O_2$ has also been described.[162] However, $[Ru^{III}(edta)(NO)]^-$ was found to be stable under the specified conditions[163] and therefore, did not liberate NO in the manner of the NO-releasing catalase-NO complex. A working mechanism (Scheme 13) pertaining to the oxidation of coordinated azide ion leading to the formation of $[Ru^{III}(edta)(NO)]^-$ has been proposed. This accounts for the experimental observations reported for the formation of this Ru(III) species during azide ion oxidation by the $Ru^{III}$(edta)/$H_2O_2$ system.[163]

The $NO_2^- \rightarrow NO$ pathway is emerging as an important mediator of blood flow regulation,[164,165] and related to this the catalytic role of $Ru^{III}$(edta) in NO formation from nitrite has recently been explored.[166] It was shown that the reaction of

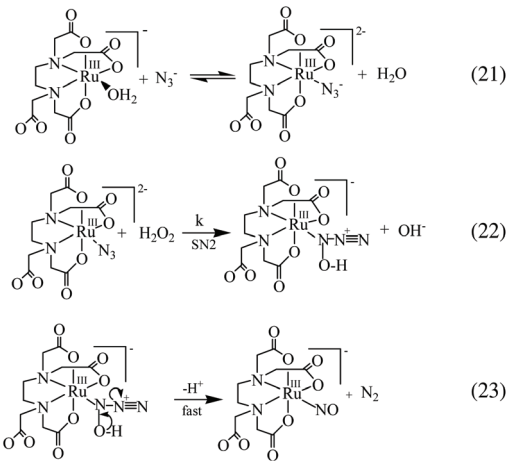

Scheme 13 Mechanism for the oxidation of $[Ru^{III}(edta)N_3]^{2-}$ by $H_2O_2$. Reprinted with permission from ref. 163. Copyright 2014 the Royal Society of Chemistry.

$[Ru^{III}(edta)(H_2O)]^-$ with $NO_2^-$ rapidly produces $[Ru^{III}(edta)(NO_2)]^{2-}$ (a second-order rate constant of 272 $M^{-1}$ $s^{-1}$ at 25 °C and pH 4.5), which is, however, unstable at pH values lower than 5.0 and converts to $[Ru^{III}(edta)(NO^+)]$ species in a nitrite concentration independent pathway.[166] Spectral changes pertaining to the conversion of $[Ru^{III}(edta)(NO_2)]^{2-}$ to $[Ru^{III}(edta)(NO^+)]$ are shown in Fig. 19. The value of the observed rate constant ($k'_{obs}$) reported for this conversion ($[Ru^{III}(edta)(NO_2)]^{2-}$ to $[Ru^{III}(edta)(NO^+)]$) is $2.2 \times 10^{-3}$ $s^{-1}$ at 25 °C and pH = 4.5. At higher pH (>6.5) the $[Ru^{III}(edta)(NO_2)]^{2-}$ species undergoes decomposition in the presence of biological thiols, RSH (RSH = cysteine and glutathione) resulting in the formation of the $[Ru^{II}(edta)(NO)]^{2-}$ species with the concomitant formation of disulfido species, RSSR, the oxidation product of the corresponding thiols, RSH.[166]

The following mechanistic Scheme 14 accounts for all of the aforementioned findings. Noteworthy here is that $Ru^{III}$(edta) is reported to be the first example of a Ru(III) complex that accomplishes nitrite activation through rapid coordination of nitrite ion to the $Ru^{III}$-centre thus effecting

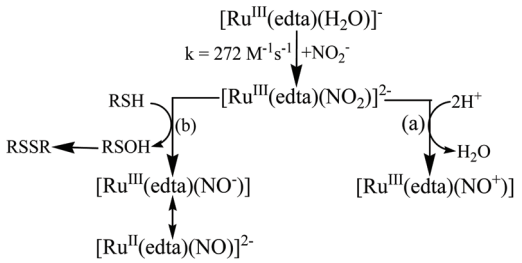

Scheme 14 Proposed mechanism for nitrite activation and the O-atom transfer reaction by the $[Ru^{III}(edta)(H_2O)]^-$ complex. Reprinted from ref. 166 with permission from the Royal Society of Chemistry.

O-atom transfer towards oxidation of biological thiols, cysteine and glutathione.[166]

### 4.6 $Ru^{III}$(edta) mediated *S*-nitrosylation of cysteine and $H_2S$

Incorporation of an NO moiety onto the thiol (SH) group of cysteine residues (*S*-nitrosylation) plays an important role in regulation of protein functions. Recently $Ru^{III}$(edta), as the first-ever example for a Ru(III) complex, has been shown to mediate the *S*-nitrosylation of cysteine in the presence of sodium nitrite at pH 4.5.[167]

Spectral changes reported for the reaction of $NaNO_2$ with $[Ru^{III}(edta)(CyS)]^{2-}$ at pH 4.5 and the corresponding kinetics profiles are displayed in Fig. 20a and b, respectively. Formation of the *S*-nitrosylated product, $[Ru^{III}(edta)S(NO)Cy]^-$ was confirmed by ESI-MS analysis of the reaction mixture at the end of the reaction.[167]

The value of the second-order rate constant corresponding to the *S*-nitrosylation of cysteine estimated from the maximum slope of the kinetics traces (Fig. 20b)[167] was 93 ± 4 $M^{-1}$ $s^{-1}$ at 25 °C and pH 4.5. A working mechanism proposed to embody the spectroscopic and kinetic data is presented in Scheme 15 for the $[Ru^{III}(edta)(H_2O)]^-$ mediated *S*-nitrosylation of cysteine.[167]

The above findings suggest that $[Ru^{III}(edta)(H_2O)]^-$ not only binds NO, but also stores NO as an *S*-nitroso (SNO) conjugate of the $[Ru^{III}(edta)(CyS)]^{2-}$ complex, thereby mimicking heme-

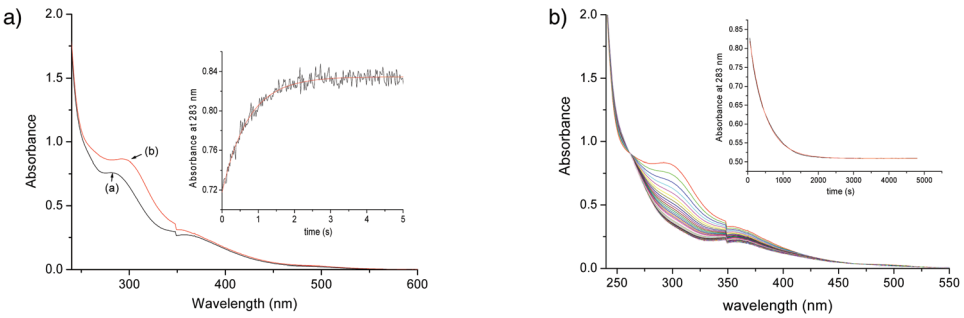


Fig. 19 (A) Spectra of (a) $[Ru^{III}(edta)(H_2O)^-]$ and (b) recorded immediately after addition of nitrite to a solution of $[Ru^{III}(edta)(H_2O)]^-$ at 25 °C and pH = 4.5, $[Ru^{III}]$ = 0.2 mM, $[NO_2^-]$ = 2.0 mM. Inset. Kinetic trace corresponding to formation of $[Ru^{III}(edta)(NO_2)]^{2-}$ and (B) decay of spectral feature that is observed upon mixing $[Ru^{III}(edta)(H_2O)]^-$ with $NO_2^-$ under the conditions specified in (A). Inset. Kinetic trace corresponding to the decay of $[Ru^{III}(edta)(NO_2)]^{2-}$ under the same conditions as for (A). Reprinted with permission from ref. 166. Copyright 2014 the Royal Society of Chemistry.

 

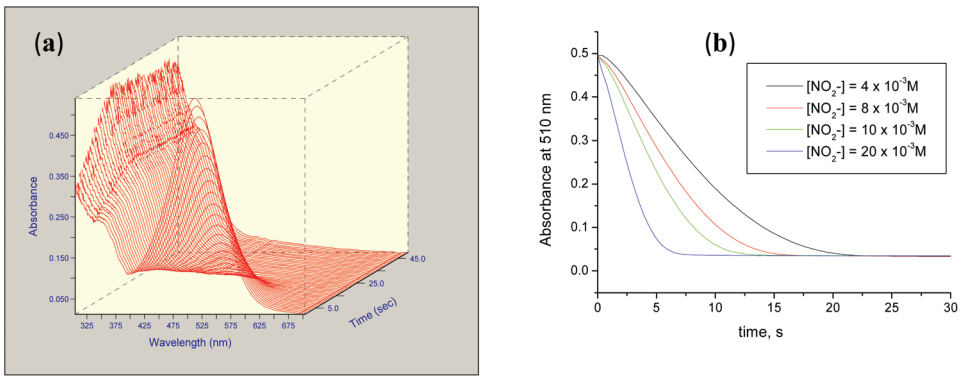


**Fig. 20** (a) Spectral changes for the reaction of $[Ru^{III}(edta)(CyS)]^{2-}$ (0.2 mM) with $NO_2^-$ (2.0 mM) at 25 °C, pH 4.5 and (b) effect of nitrite concentration on the kinetic traces' profiles pertaining to the *S*-nitrosylation of the coordinated cysteine in $[Ru^{III}(edta)(CyS)]^{2-}$ (0.2 mM) with $NO_2^-$ at 25 °C, pH (4.5). Reprinted with permission from ref. 167. Copyright 2014 the Royal Society of Chemistry.

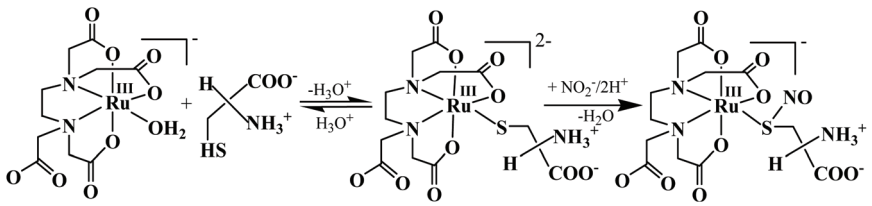


**Scheme 15** Mechanism for the $[Ru^{III}(edta)(H_2O)]^-$ mediated *S*-nitrosylation of cysteine by nitrite ion. Reprinted with permission from ref. 167. Copyright 2014 the Royal Society of Chemistry.

assisted *S*-nitrosylation of a proximal thiolate in a nitric oxide transport protein.[168]

While nitric oxide (NO) acts as a vasodilator and intrinsic signalling molecule,[169] hydrogen sulphide ($H_2S$), the smallest thiol is currently recognized as a physiologically relevant gasotransmitter that governs a variety of physiological functions.[170] It is now well documented in the literature that $H_2S$ could interfere with NO signalling by reacting with NO[171] or $NO_2^-$.[172] In this regard the role of metal ions in the interaction of nitrite and sulphide has not yet been explored, albeit there is an important report describing the formation of HSNO/HNO in the heme-iron-catalysed *S*-nitrosylation of $H_2S$ with nitrite.[173] The ability of the $Ru^{III}(edta)$ complex to mediate *S*-nitrosylation of bisulfide ion ($HS^-$) to yield $[Ru^{III}(edta)(SNO)]^{2-}$ in aqueous solution, has recently been explored.[174] Initially, the reaction of $Ru^{III}(edta)$ with NaHS at pH 8.2 resulted in the formation of a bluish-green coloured disulfur bridged dinuclear complex, $[(edta)Ru^{III}SSRu^{III}(edta)]^{4-}$ which was characterised by Raman spectroscopy and the ESI-MS method.[174] Subsequently, the $[(edta)Ru^{III}SSRu^{III}(edta)]^{4-}$ complex reacts rapidly with NO under anaerobic conditions to yield the S-bonded $[Ru^{III}(edta)(SNO)]^{2-}$ product complex which was confirmed by ESI-MS measurements and further characterised by FTIR and EPR spectral studies in solution.[174] The results from the studies[174] that revealed the formation of $[Ru^{III}(edta)(SNO)]^{2-}$, unprecedented for the ruthenium system, opens the way for the possibility of using transition metals other than iron[173] for the coupling of $HS^-/H_2S$ with NO. It was further reported that the reaction of $[Ru^{II}(edta)(NO^+)]^-$ ($\leftrightarrow[Ru^{III}(edta)(NO)]^-$) with $HS^-$ could not produce N-bonded $[Ru^{III}(edta)N(O)SH]^-$ in a parallel resemblance to Fe-HSNO.[172] Nevertheless, it was reported very recently that the formation of N-bonded $[Ru^{III}(edta)N(O)SH]^-$ is feasible when $[Ru^{III}(edta)(NO^+)]$, the Ru(III)-analogue of $[Ru^{II}(edta)(NO^+)]^-$, is reacted with $HS^-$ in aqueous solution.[174] This may be due to the fact that under the identical coordination environment of the 'edta' ligand, the coordinated nitrosonium ion ($NO^+$) in $[Ru^{III}(edta)(NO^+)]$ is more electrophilic than the coordinated 'NO' (in $[Ru^{III}(edta)(NO)]^-$) to be able to react with a nucleophile (Nu) to form the [Ru(edta)(NO-Nu)] adduct (Nu = $HS^-$). Although $[Ru^{III}(edta)(NO)]^-$ has $[Ru^{II}(edta)(NO^+)]^-$ character, the lower oxidation state of the metal centre does not impart enough electrophilicity onto the $NO^+$ bound to Ru(II) to enable $[Ru^{II}(edta)(NO^+\text{-}Nu)]$ to be formed. It was reported that the addition of NaHS to the solution of $[Ru^{III}(edta)(NO^+)]$ (preformed by lowering the pH of the solution of $[Ru^{III}(edta)(NO_2)]^{2-}$ to 3.5), resulted in the formation of the N-bonded $[Ru^{III}(edta)N(O)SH]^-$. It was identified by ESI-MS studies, and further characterised by FTIR and EPR studies in solution.[175] Noteworthy is that the EPR signals of the N-bonded $[Ru^{III}(edta)N(O)SH]^-$ species are different[175] from those reported for the S-bonded $[Ru^{III}(edta)S(NO)]^{2-}$.[174] The following mechanistic Scheme 16 was proposed to account for the results.

The stability of both N- and S-bonded thionitrous acid/thionitrite complexes of $Ru^{III}(edta)$ have been assessed by performing comprehensive DFT calculations,[175] and in the geometric

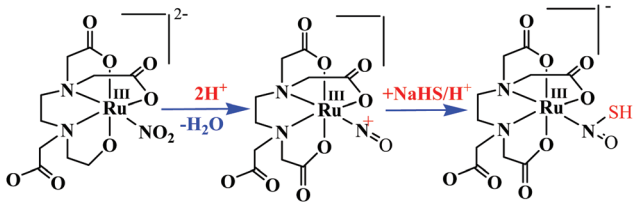


**Scheme 16** Schematic representation of the reactions of $[Ru^{III}(edta)(NO_2)]^{2-}$ with NaHS. Reprinted with permission from ref. 175. Copyright 2019 the Centre National de la Recherche Scientifique (CNRS) and the Royal Society of Chemistry.

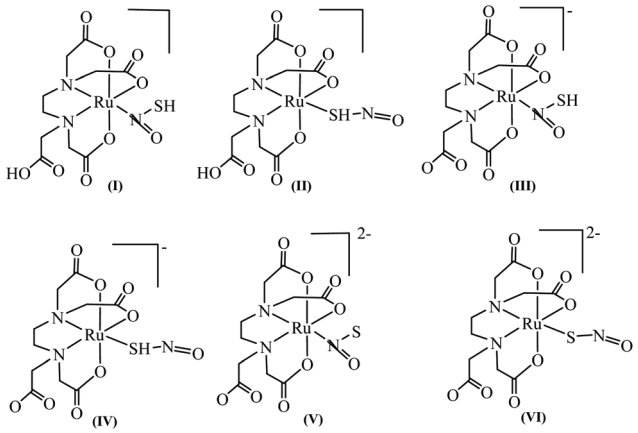


**Fig. 21** Pictorial representations of different HSNO/$SNO^-$ complexes of $Ru^{III}$(Hedta/edta) wherein three carboxylate groups and two N-atoms of the ethylenediamine collar are coordinated and one carboxylate group remains in the dangling position. Reprinted with permission from ref. 175. Copyright 2019 the Centre National de la Recherche Scientifique (CNRS) and the Royal Society of Chemistry.

arrangements the Ru(III) centre is coordinated to the oxygen atoms of three carboxylate groups and nitrogen atoms of the two amine groups pictorially represented in Fig. 21, whereas optimised structures of **I–VI** are shown in Fig. 22. It is noteworthy that in all the six structures **I–VI**, one carboxylate group remains in the dangling position.

From the calculation of their relative free energies, it is seen that the N-coordinated isomers (**I**, **III**, **V**) are always more stable than their S-coordinated isomers (**II**, **IV**, **VI**) as shown in Fig. 22. The relative free energy of **I**, **III** and **V** are −11.6, −12.9 and −2.9 kcal $mol^{-1}$ more stable in comparison to **II**, **IV** and **VI**, respectively. A free energy profile for the conversion of the S-bonded isomer, $[Ru^{III}(edta)SH(NO)]^-$ to the N-bonded isomer, $[Ru^{III}(edta)N(O)SH]^-$ is shown in Scheme 17. The calculated energy barrier for the conversion mentioned (Scheme 17) is around 15.4 kcal $mol^{-1}$, whereas the energy barrier for the reverse process, *i.e.* N- to S-bonded isomer, should be 26.1 kcal $mol^{-1}$ (Scheme 17). This suggests that the conversion of the N- to the S-bonded isomer is energetically unfavourable.

Experimental findings together with the results of DFT calculations have amply demonstrated that the formation of

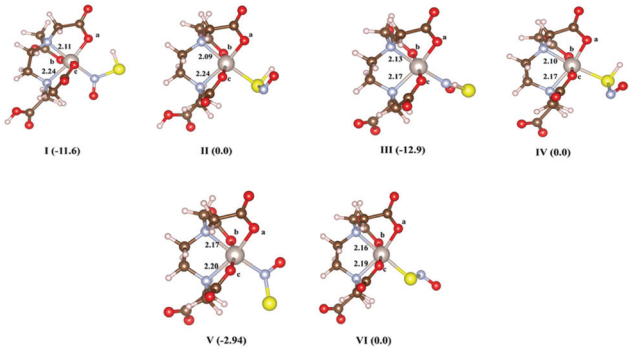


**Fig. 22** Optimised structures of **I–VI**. Red, grey, yellow, blue and pink colours represent O, C, S, N and H atoms, respectively. Oxygen atoms which are coordinated to the Ru-centre are denoted as a, b and c, respectively. Numbers in the parentheses are free energies in kcal $mol^{-1}$. Reprinted with permission from ref. 175. Copyright 2019 the Centre National de la Recherche Scientifique (CNRS) and the Royal Society of Chemistry.

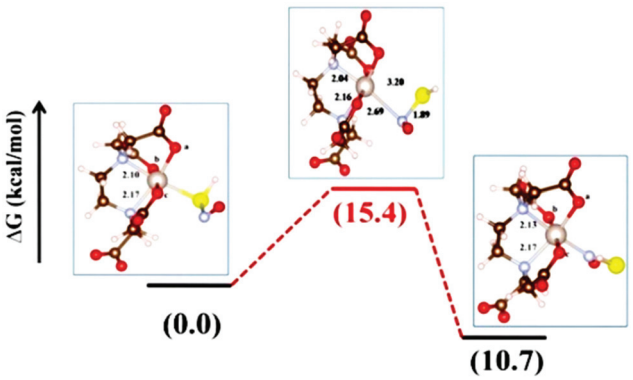


**Scheme 17** Gibbs free energy profile pertaining to the transformation of the S-bonded thionitrous acid complex $[Ru^{III}(edta)S(NO)H]^-$ to the N-bonded isomer. Reprinted with permission from ref. 175. Copyright 2019 the Centre National de la Recherche Scientifique (CNRS) andthe Royal Society of Chemistry.

N-bonded thionitrous acid bound to $Ru^{III}$(edta) in aqueous solution is feasible in the reaction of $[Ru^{III}(edta)(NO^+)]$ with sulphide at lower pH (~3.5),[175] whereas the S-bonded isomer, $[Ru^{III}(edta)(SNO)]^{2-}$ could be formed effectively in a higher pH range (8–9) by reacting the sulphide bridged $[(edta)Ru^{III}SSRu^{III}(edta)]^{4-}$ complex with NO.[174] Results of these studies taken together,[174,175] though unprecedented for the Ru(III) system, would be of significance in regard to the chemical understanding of the role of metal complexes in the cross talk of the two gasotransmitters, NO and $H_2S$.

### 4.7 Conclusions

In this review, reactions that have done most to change the wonder-world of $Ru^{III}$(edta) chemistry are straightforward. Their scientific significance was reviewed infusing some intriguing perspectives. The work described in this review confirms the amazing ability of $Ru^{III}$(edta) towards substrate binding –

 

an important feature that governs its catalytic activity. We have systematically summarized the performance of $Ru^{III}$(edta) complexes which afford a wide scope for an increased understanding of mechanistic possibilities concerning the nature of the active intermediate involved in the catalytic process. Overall these results and conclusions could be of significance in the mechanistic understanding of the action of a group of enzymatic reactions in terms of redox regulation.

# 5. Redox chemistry of Ru(III) complexes

## 5.1 Introduction

Many d-electron metal complexes are used with great success as catalysts in the control of industrial processes and environmental effluents, and as metallodrugs for the treatment of for instance arthritis, autoimmune diseases and cancers.[176,177] In the most cases the mechanisms of such chemical and biological processes are not well understood at the molecular level and much of the development of such complexes is done by trial and error.

In general, it is postulated that metal complexes are 'prodrugs' that become transformed by ligand substitution and redox processes before they reach the target site. However, since the application of the first anticancer metal-based drugs in the middle of the 20th century, it has been challenging to define the 'pharmacophores' for metal complexes, *i.e.* the steric and electronic features necessary for target recognition and for triggering the biological response.[178] If this can be achieved, then metal-based drug design offers unique features not available to purely organic drugs.

The potential application of ruthenium complexes as anticancer or antiviral drugs is being widely explored. Promising drug candidates have been found within the diversity of families of ruthenium compounds developed, ranging from inorganic Ru(III) and Ru(II) octahedral complexes, to several types of organometallic Ru(II) species. They show multiple targets and diverse mechanisms of action which in fact are still unclear.[179] Even compounds that are structurally very similar display different behaviour and surprisingly different biological properties.[180] Some Ru(III) complexes are postulated to be activated by reduction to usually more labile Ru(II) species in hypoxic tumour microenvironments, which may promote their possible interaction with proteins, DNA and other biological targets.[176,177] The 'activation by reduction' hypothesis was recently critically discussed by Alessio and cannot be generalized for all Ru(III) complexes.[178] Walsby and co-authors[176] reported that an obvious correlation between the redox potentials and half maximal inhibitory concentration ($IC_{50}$) of Ru(III) complexes studied lately by them, was not noticed and the redox potential is not the main discriminator of Ru(III) species. Nevertheless, they concluded that a contribution of Ru(II) complexes to the observed activity of the investigated Ru(III) complexes could not be excluded. In turn, other recently reported studies have shown that the Ru(III) oxidation state may predominate *in vivo*.[181] Furthermore, it is noteworthy to mention that the redox activity of ruthenium complexes may also interfere in the cellular redox balance.[177,180]

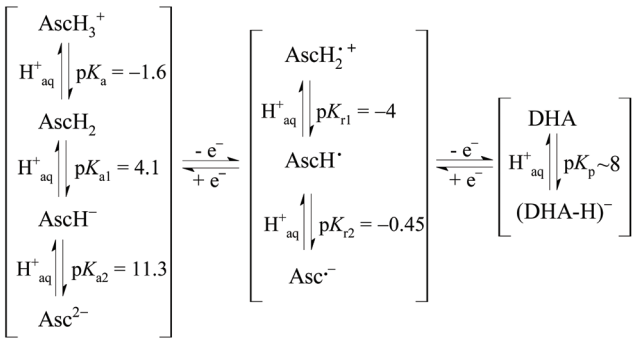


**Scheme 18** Protolytic forms of various redox forms of L-ascorbic acid. Adapted from ref. 53.

## 5.2 L-Ascorbic acid as a reducing agent

Ru(III) can be reduced to Ru(II) *in vivo* by physiological reducing agents such as glutathione and L-ascorbic acid. This chapter summarizes the results of mechanistic studies on three Ru(III) – L-ascorbic acid systems performed in our group. L-Ascorbic acid (hereafter generally referred to as $AscH_2$) commonly known as vitamin C, is a mild two electron reductant. In general, it can exist in four protolytic forms presented along with the corresponding p$K_a$ values in Scheme 18. Note that the terms 'L-ascorbic acid' and '$AscH_2$' used throughout the paper refer to all protolytic forms of the reductant unless otherwise stated.

Three of them, *viz.* $AscH_2$, $AscH^-$ and $Asc^{2-}$ can occur in aqueous solution in the pH range 0–14. Therefore, the redox potential of L-ascorbic acid is strongly affected by the acidity of the solution. Its redox chemistry is summarised in Fig. 23 and Table 10. As expected, the more protonated form of L-ascorbic acid, the lower the redox potential and the weaker the reducing properties: $Asc^{2-}$ > $AscH^-$ > $AscH_2$. A one electron oxidation of L-ascorbic acid results in the formation of the ascorbyl radical, a strong acid present within the 0–14 pH range as the $Asc^{\bullet-}$ anion radical (Fig. 23). This radical exhibits interesting redox properties that highly depend on the solution acidity. On one hand, it oxidises further to the stable dehydroascorbic acid (DHA) in a solution of pH up to 8, or to a hydrolytically unstable dehydroascorbate $(DHA\text{-}H)^-$ in more alkaline media (Fig. 23b). Note that 'DHA' used hereafter refers to dehydroascorbic acid or dehydroascorbate unless otherwise stated. This step is the thermodynamic driving force for the overall L-ascorbic acid oxidation process. On the other hand, the $Asc^{\bullet-}$ radical with a redox potential that increases strongly with decreasing pH, may be a strong oxidant especially in acidic media (Fig. 23c).[53,182]

## 5.3 Mechanistic studies on reduction of Ru(III) complexes by L-ascorbic acid

In recent years we were engaged in mechanistic studies on the L-ascorbic acid reduction of a series of Ru(III) complexes.[53,183,184] Kinetics and mechanism of such reactions

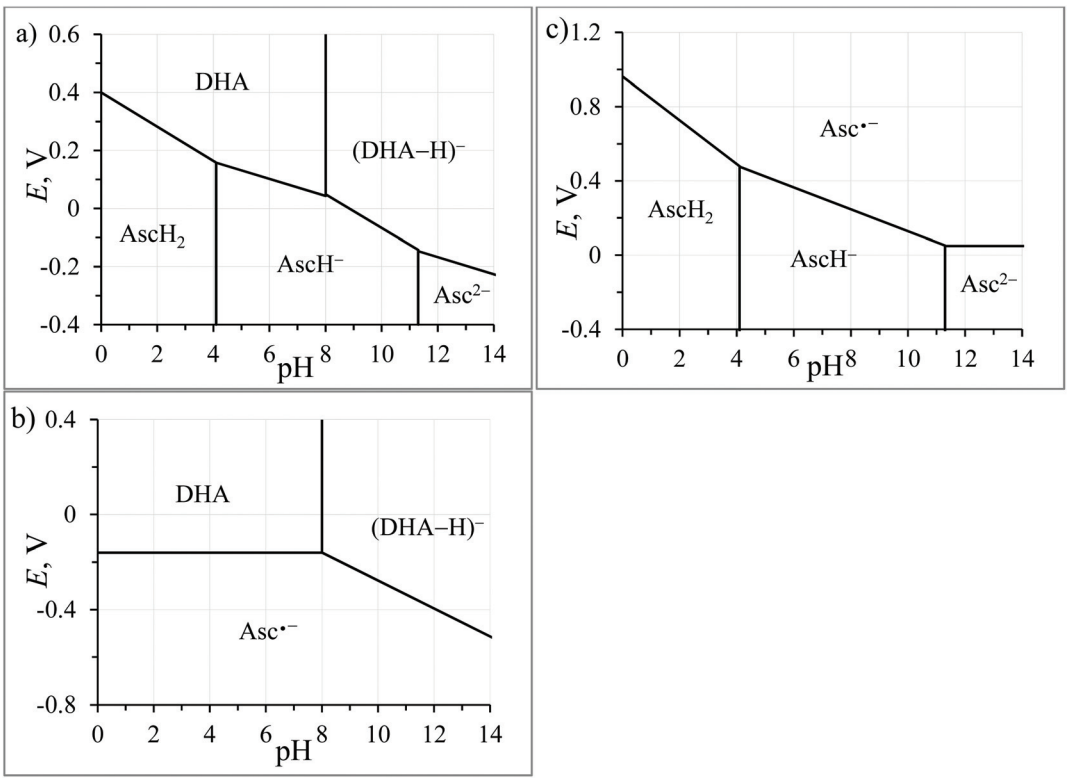


**Fig. 23** Pourbaix diagrams for (a) L-ascorbic acid ⇌ dehydroascorbic acid/dehydroascorbate; (b) ascorbyl radical ⇌ dehydroascorbic acid/dehydroascorbate; (c) ascorbyl radical ⇌ L-ascorbic acid. Adapted from ref. 53.

**Table 10** Redox potentials of L-ascorbic acid, ascorbate and ascorbyl radical *vs.* SHE calculated using data given in Scheme 18 and Fig. 23. Reprinted with permission from ref. 183. Copyright 2016 Wiley-VCH Verlag GmbH & Co. KGaA

| Redox couple | $E^\circ$ [V] | Redox couple | $E^\circ$ [V] |
|---|---|---|---|
| DHA/$AscH_2$ | +0.40 | $(DHA\text{-}H)^-/Asc^{\bullet-}$ | +0.31 |
| $DHA/AscH^-$ | +0.28 | $DHA/Asc^{\bullet-}$ | −0.16 |
| $DHA/Asc^{2-}$ | −0.05 | $Asc^{\bullet-}/Asc_2$ | +0.96 |
| $(DHA\text{-}H)^-/AscH^-$ | +0.52 | $Asc^{\bullet-}/AscH^-$ | +0.72 |
| $(DHA\text{-}H)^-/Asc^{2-}$ | +0.19 | $Asc^{\bullet-}/Asc^{2-}$ | +0.05 |

were examined earlier by other groups.[185–193] However, the lability of the employed ruthenium species in terms of ligand substitution was very high and/or reduction processes were very fast. As a consequence, reaction conditions applied were restricted to solutions of a pH where fully protonated $AsH_2$ and the ascorbate mono-anion $AscH^-$ exist. A comparison of the reactivity of the different protolytic forms was in most cases qualitative and limited to a drastic increase in reactivity with deprotonation of the acid. Therefore, our goal was to examine complexes that would enable a quantitative comparison of the redox abilities of the three protolytic forms of L-ascorbic acid and to expand our knowledge on the underlying mechanistic behaviour of the Ru(III) – L-ascorbic acid systems. We have studied three Ru(III) complexes with *N*,*O*-donor chelating pyridine-carboxylate chelates (see Fig. 24).[53,183,184]

We selected picolinate (pic) as the first chelate, *i.e.* the anion of pyridine-2-carboxylic acid (known also as 2-picolinic acid). It is an endogenous prime natural ligand, coordinating efficiently to many metals, among them Zn, Cr, Mn, Fe, Cd and Cu,[194–196] and used as a way of introducing bioactive metals into biological systems.[176,195–198] We first synthesized *mer*-$[Ru^{III}(pic)_3]$ complex **1**, reported earlier in the literature.[199,200] Sufficiently high stability of the complex in both the +3 and +2 oxidation states and redox properties of **1**, offered the advantage to investigate its reaction with L-ascorbic acid over a wide pH range. As a follow-up to the studies on the trispicolinatoruthenium(III), we synthesised its derivative, a new *cis*-$[Ru^{III}Cl_2(pic)_2]^-$ complex, **2**.[201] The unexpected behaviour of the dichloridobispicolinato-ruthenate(III)-L-ascorbic acid system[183] inspired us to continue our studies using the previously reported $[Ru^{III}(dipic)_2]^-$ complex[185] (where dipic = anion of pyridine-2,6-dicarboxylic acid, dipicolinate anion) as a modification of **2**. However, our attempts to prepare this complex failed. Instead of the envisaged $[Ru^{III}(dipic)_2]^-$, we obtained a new *trans*-$[Ru^{III}Cl_2(dpicOEt)_2]^-$ complex, **3** (where dpicOEt = monoesterified dipicolinate anion).[184] This happened since one carboxylate group of each dipicolinato ligand was esterified by ethanol used as solvent in the synthetic work. The complexes were identified and characterised in the solid state and in solution applying a wide range of techniques, *viz.* single crystal X-ray diffraction, elemental analysis, IR and EPR spectroscopy, mass spectrometry (ESI-MS or LC-MS) and

 

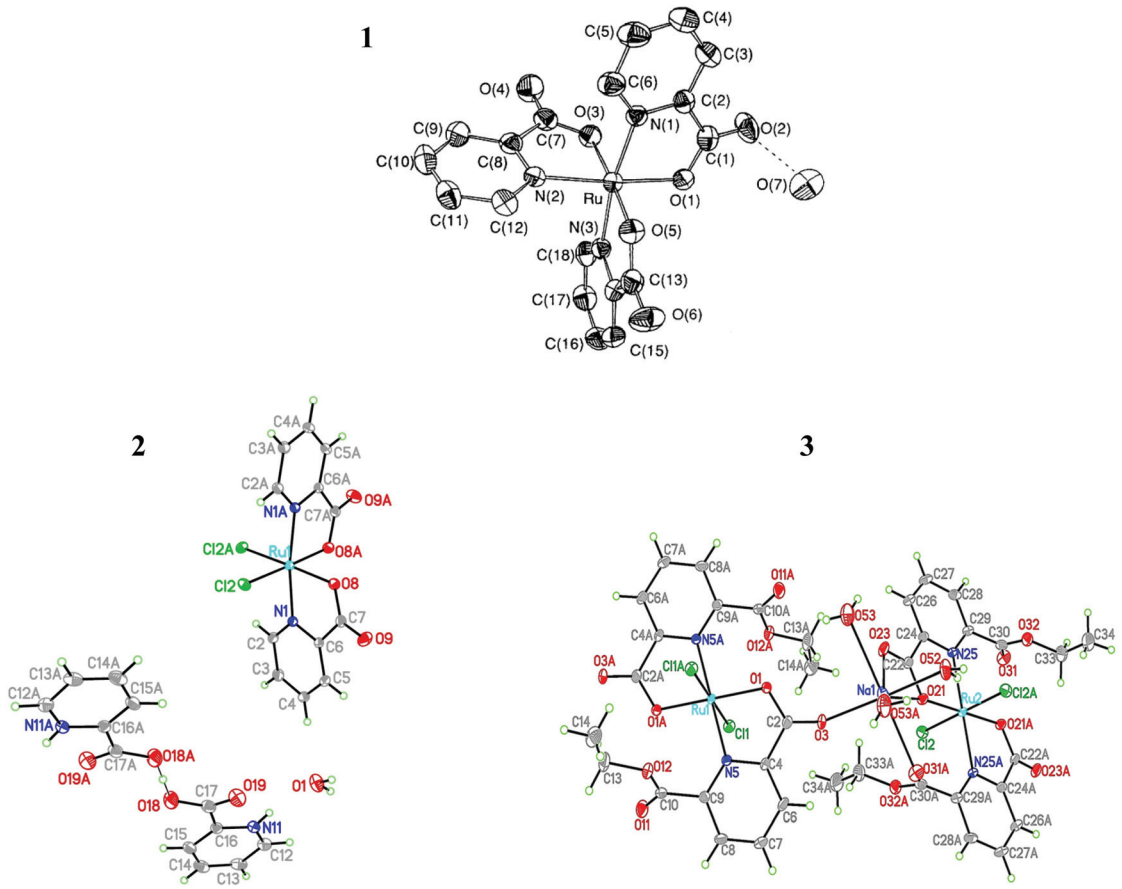


**Fig. 24** Structures of *mer*-[$Ru^{III}(pic)_3$], **1** (Reprinted with permission from ref. 203. Copyrigth 1991 The Royal Society of Chemistry), H(Hpic)$_2$[*cis*-$RuCl_2(pic)_2$]·$2H_2O$, **2** (Reprinted with permission from ref. 201. Copyright 2016 Taylor and Francis), and {[$Na(H_2O)_2$][*trans*-$RuCl_2(dipicOEt)_2$]}$_n$, **3** (Reprinted with permission from ref. 184. Copyright 2017 Wiley-VCH Verlag GmbH & Co. KGaA). The latter complex exists in aqueous solution in the monomeric *trans*-$[RuCl_2(dipicOEt)_2]^-$ form. The hydrogen atoms are omitted for clarity.

UV-VIS spectroscopy. Cyclic voltammetry was used to estimate their redox properties. The following values of $E_{1/2}$ 0.330, 0.030 and 0.052 V *vs.* SHE were found for *mer*-[$Ru^{III}(pic)_3$]/*mer*-[$Ru^{II}(pic)_3$]$^-$, *cis*-[$Ru^{III}Cl_2(pic)_2$]$^-$/*cis*-[$Ru^{II}Cl_2(pic)_2$]$^{2-}$ and *trans*-[$Ru^{III}Cl_2(dpicOEt)_2$]$^-$/*trans*-[$Ru^{II}Cl_2(dpicOEt)_2$]$^{2-}$ couples, respectively.[184,201,202] It follows that **1** is a much stronger oxidant than **2** and **3**, which could be accounted for in terms of its higher stability. Similar oxidising properties of **2** and **3** are due to the close similarity of these complexes.

Prior to the studies on electron transfer processes in the Ru(III) – L-ascorbic acid systems, the stability of **1**, **2** and **3** was examined under conditions selected for the subsequent kinetic experiments. All starting complexes turned out to be inert in terms of any ligand substitution reactions within the applied 1.0–7.4 (**1**), and 6.8–9.7 (**2**–**3**) pH ranges. However, since the product of the reduction of **3** seemed to be dioxygen sensitive, to avoid any mechanistic complications, the redox process between **3** and L-ascorbic acid was carried out under anaerobic conditions. All systems were investigated applying electron absorption spectroscopy. Formation of an intense absorption band upon addition of the reductant to pale solutions of **1**–**3**, documented generation of the red corresponding Ru(II) species (Fig. 25).

Kinetics of the reactions were followed under pseudo-first-order conditions as a function of L-ascorbic acid concentration over a wide pH range. Since the timescale of the processes varied between 0.2–1000 s, either conventional mixing or stopped-flow techniques were used. The absorbance *vs.* time profiles were recorded at the wavelengths corresponding to the maxima of the generated Ru(II) absorption bands. All kinetic traces obtained for **1** could be satisfactorily reproduced by a single exponential function (eqn (24a)). Although the spectral changes registered for all systems were similar at first glance, surprisingly, kinetic traces observed for **2** and **3** did not obey pseudo-first-order kinetics. Moreover, they could not be satisfactory fitted with a double exponential function. Only application of a triple exponential function, outlined in eqn. (24b), gave excellent fits under all experimental conditions. Results of the absorbance-time data fitting are exemplarily shown in Fig. 26.

$$A = A\exp(-k_{obs}t) + C \quad (24a)$$

$$A = A_1\exp(-k_{obs1}t) + A_2\exp(-k_{obs2}t) + A_3\exp(-k_{obs3}t) + C \quad (24b)$$

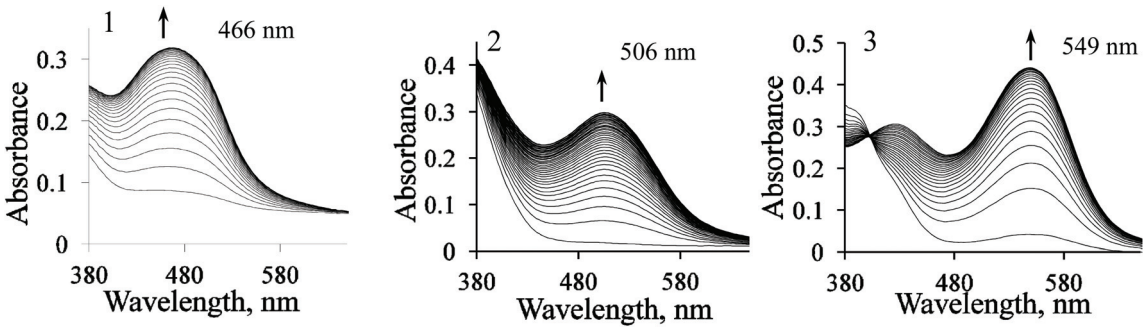


Fig. 25 Typical spectral changes observed during the reaction of **1**, **2** and **3** with 1 mM $AscH_2$ at 25 °C. Experimental conditions: [**1**] = 4 × $10^{-5}$ M, pH 2, $I$ = 1.0 M ($NaClO_4$), scanned every 45 s; [**2**] = 0.1 mM, pH = 7.5, $I$ = 0.1 M (NaCl), scanned every 1 s; [**3**] = 0.1 mM, pH = 9.1, $I$ = 0.1 M (NaCl), argon atmosphere, scanned every 1.2 s. Reprinted with permission from ref. 53, 183 and 184. Copyright 2017 Wiley-VCH Verlag GmbH & Co. KGaA.

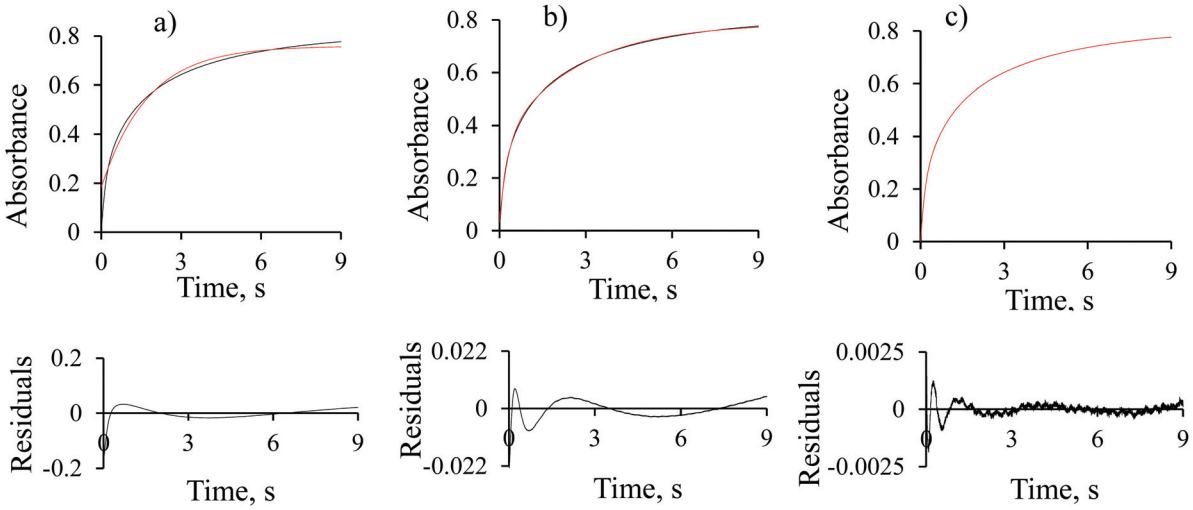


Fig. 26 Typical experimental kinetic trace (black) for the reaction of 0.1 mM **3** with 2 mM $AscH_2$ along with fits (red) to a single exponential function (a), the sum of two exponential functions (b), and the sum of three exponential functions (c); pH = 9.60, $I$ = 0.1 M (NaCl), $T$ = 25 °C. Note the expanded scale used for the reported residuals, which clearly shows the quality of the fit especially in (b) and (c). Reprinted with permission from ref. 184. Copyright 2017 Wiley-VCH Verlag GmbH & Co. KGaA.

This finding suggests the existence of a mixture of three Ru(III) species differing in reactivity towards L-ascorbic acid in solutions of **2** and **3**, and being converted into a common Ru(II) product. However, with the aid of a wide range of analytical techniques, such as mass spectrometry, UV/Vis spectroscopy, combined with chromatographic methods as well as capillary electrophoresis, the presence of only a single Ru(III) species in the solutions of **2** and **3** was definitely proven. Therefore, another explanation is required for the unexpected complex kinetic behaviour of these two systems and the apparent three parallel reaction phases ($k_{obs1}$, $k_{obs2}$ and $k_{obs3}$).

Values of the observed rate constants calculated for **1** (from eqn (24a)) are directly proportional to the total ascorbic acid concentration, $[AscH_2]_T$, over the whole pH range studied (eqn (25)). Even at the highest concentration of the reductant, no saturation effect was observed (see Fig. 27a). Values of the second rate constants $k$ are collected in Table 11.

$$k_{obs} = k[AscH_2]_T \quad (25)$$

Moreover, the total concentration of L-ascorbic acid did not affect the observed total absorbance increase, indicating the complete conversion of **1** into its +2 oxidation state.

In contrast, the effect of $[AscH_2]_T$ on the concentration of Ru(II) species formed and observed rate constants found for the systems involving complexes **2** and **3**, depended on the acidity of the solutions. At the lower pH studied, *viz.* 7.2–8.5 and 6.8–8.3 for **2** and **3**, respectively, plots of all $k_{obs}$ (eqn (24b)) *vs.* $[AscH_2]_T$ are linear with significant intercepts (see Fig. 27b, eqn (26)). Furthermore, under these conditions the degree of conversion of **2** and **3** increased with both the total concentration of the reductant and pH of the solution. Values

 

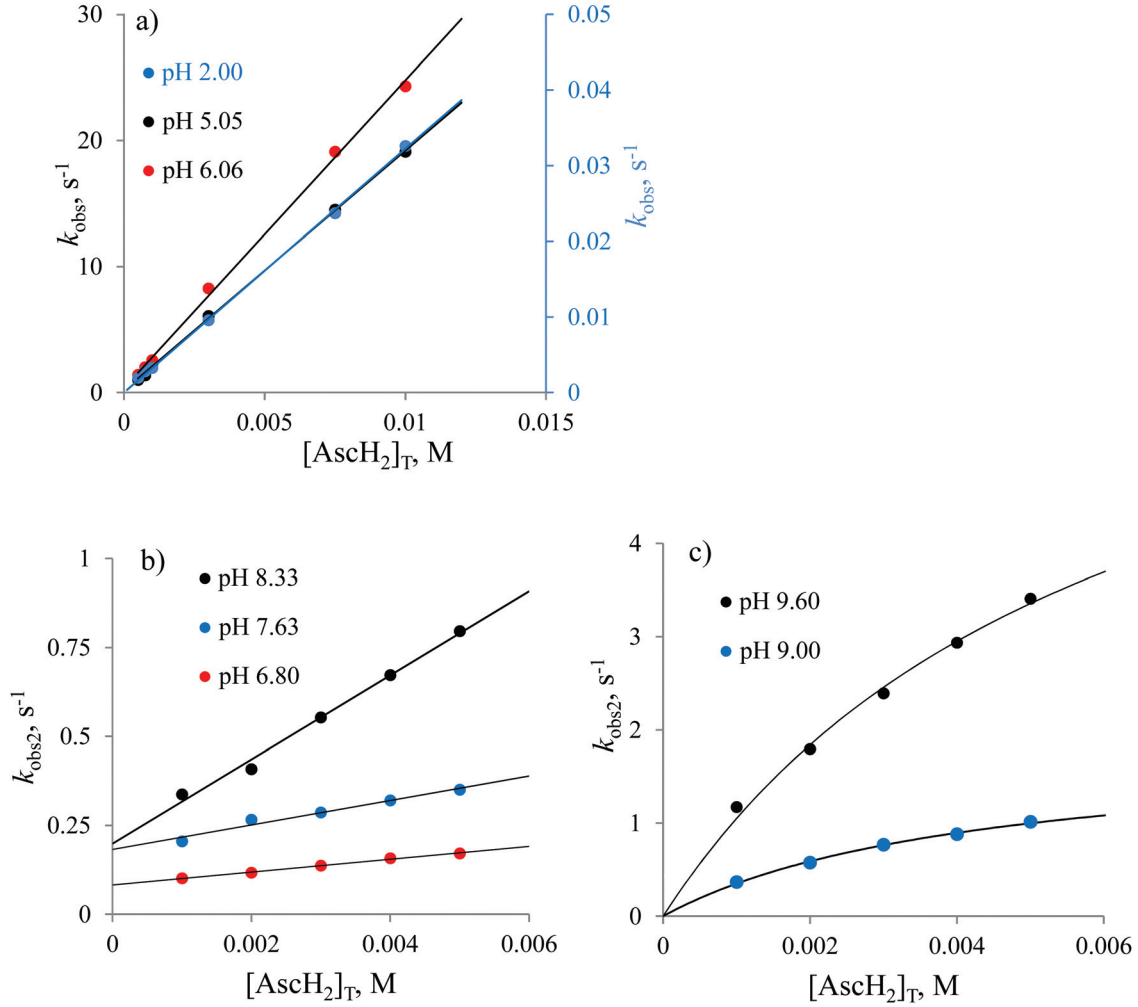


**Fig. 27** Total ascorbic acid concentration dependence of $k_{obs}$ for the reduction of **1** (a) and $k_{obs2}$ for the second (major) phase of the process in system **2** (b and c); (a) $I$ = 1 M ($NaClO_4$), (b) and (c) $I$ = 0.1 M (NaCl), $T$ = 25 °C.

of the second-order rate constants $k_b$ for the forward reaction and intercepts $k_a$ for the reverse reaction are listed in Table 11.

$$k_{obs} = k_a + k_b[AscH_2]_T \quad (26)$$

At higher pH, *viz*. 9.3–9.7 and 9.0–9.6 for **2** and **3**, respectively, values of all the observed rate constants for the three parallel reaction phases ($k_{obs1}$, $k_{obs2}$ and $k_{obs3}$) show a non-linear saturation dependence on $[AscH_2]_T$ and pass through the origin within error limits (see Fig. 27c, eqn (27)).

$$k_{obs} = \frac{k_c K[AscH_2]_T}{1 + K[AscH_2]_T} \quad (27)$$

Moreover, in the alkaline solutions the yield of generation of Ru(II) species is independent of both the total concentration of the reductant and pH of the solution. Values of $k_c$ and $K$ (eqn (27)) are summarised in Table 11. It should be noted that at a given pH, all the $k_{obs1}$, $k_{obs2}$ and $k_{obs3}$ dependencies on the total L-ascorbic acid concentration are very similar. Since the $k_{obs2}$ data represent the major part of the kinetic trace, *i.e.* the largest part of the overall spectral change, we use it hereafter as a representative quantity for the discussion of the results obtained. Plots of $k_{obs2}$ *vs.* $[AscH_2]_T$ shown in Fig. 27b and c exemplify the behaviour of the systems involving complexes **2** and **3**. The nonzero intercepts ($k_a$) found for these plots in the lower pH range (eqn (26), Fig. 27b) indicate a back reaction or a parallel aquation of the starting chlorido complexes. Interestingly, on increasing pH the values of $k_a$ play a less important role compared to $k_b$. As mentioned above, (i) the collected spectroscopic data demonstrated stability of **2** and **3** under all applied conditions, and (ii) the concentration of the Ru(II) species formed in both systems increased with $[AscH_2]_T$ and pH. What is more, some kinetic experiments conducted in the presence of a large excess of either chloride or picolinate, did not reveal any evidence for a contribution of hydrolysis of **2**

Table 11 Kinetic parameters obtained for the systems **1** ($I$ = 1 M, $NaClO_4$), **2** and **3** ($I$ = 0.1 M, NaCl) at 25 °C. Data taken from ref. 53,183 and 184

**1**

| pH | $k$, $M^{-1}$ $s^{-1}$ | pH | $k$, $M^{-1}$ $s^{-1}$ | pH | $10^3k$, $M^{-1}$ $s^{-1}$ |
|---|---|---|---|---|---|
| 1.00 | 0.445 | 1.52 | 1.09 ± 0.01 | 5.05[a] | 1.90 ± 0.02 |
| 1.10 | 0.531 | 1.70 | 1.73 ± 0.02 | 6.06[a] | 2.44 ± 0.05 |
| 1.19 | 0.556 | 2.00 | 3.18 ± 0.04 | 7.40[b] | 14.4 ± 0.6 |
| 1.30 | 0.714 | 2.12 | 3.97 ± 0.04 | | |
| | | 2.30 | 6.39 ± 0.06 | | |

| | **2** | | | **3** | | |
|---|---|---|---|---|---|---|
| Reaction phase[c] | pH | $k_b$ or $k_cK^d$, $M^{-1}$ $s^{-1}$ | $k_a$ or $k_c{}^d$, $s^{-1}$ | pH | $k_b$ or $k_cK^d$, $M^{-1}$ $s^{-1}$ | $k_a$ or $k_c{}^d$, $s^{-1}$ |
| **1** | | 112 ± 10 | 0.53 ± 0.03 | | 39 ± 3 | 0.60 ± 0.01 |
| **2** | 7.25 | 18 ± 1 | 0.113 ± 0.004 | 6.80 | 18.1 ± 0.7 | 0.082 ± 0.002 |
| **3** | | 2.90 ± 0.07 | 0.020 ± 0.001 | | 4.1 ± 0.3 | 0.013 ± 0.001 |
| **1** | | 462 ± 36 | 1.0 ± 0.1 | | 107 ± 5 | 0.92 ± 0.02 |
| **2** | 7.90 | 58 ± 3 | 0.14 ± 0.01 | 7.63 | 34 ± 4 | 0.18 ± 0.01 |
| **3** | | 9.8 ± 0.6 | 0.020 ± 0.002 | | 8.8 ± 0.8 | 0.030 ± 0.003 |
| **1** | | 1338 ± 83 | 0.6 ± 0.3 | | 480 ± 18 | 0.89 ± 0.06 |
| **2** | 8.48 | 125 ± 3 | 0.18 ± 0.01 | 8.33 | 118 ± 6 | 0.20 ± 0.02 |
| **3** | | 20.3 ± 0.9 | 0.032 ± 0.003 | | 26.3 ± 0.4 | 0.039 ± 0.001 |
| **1** | | 8776 ± 148 | 59 ± 2 | | 2262 ± 72 | 10.9 ± 0.5 |
| **2** | 9.29[d] | 654 ± 34 | 3.9 ± 0.3 | 9.00[d] | 431 ± 21 | 1.86 ± 0.11 |
| **3** | | 109 ± 5 | 0.88 ± 0.09 | | 88 ± 4 | 0.60 ± 0.05 |
| **1** | | 23 460 ± 1110 | 183 ± 18 | | 7178 ± 465 | 38 ± 3 |
| **2** | 9.72[d] | 1694 ± 36 | 18 ± 1 | 9.60[d] | 1222 ± 10 | 7.5± 0.9 |
| **3** | | 291 ± 4 | 6.8 ± 0.5 | | 263 ± 14 | 3.0 ± 0.4 |

[a] Acetate buffer. [b] Gomorie buffer. [c] Reaction phase refers to the phase of the reaction controlled by $k_{obs1}$, $k_{obs2}$ and $k_{obs3}$, respectively. [d] Second-order rate constant $k_cK$, the initial slope of the non-linear concentration dependence, and limiting rate constant $k_c$.

and **3** as a possible reason for the observed intercepts. Thus, the non-zero values of $k_a$ point to the reversibility of the redox processes in systems **2** and **3** for solutions of a pH close to 7.

This means that Ru(II) complexes produced in these reactions are converted back to Ru(III) species. Since Ru(II) complexes are known to be oxygen sensitive, one of the possible oxidants could be $O_2$. Additional kinetic tests using the **2** – L-ascorbic reaction system carried out under a dioxygen saturated atmosphere, confirmed re-oxidation of the Ru(II) product, but on a much slower timescale. As mentioned above, the **3** – L-ascorbic acid system was investigated under argon atmosphere. Therefore, interference of dioxygen in the studied systems could be excluded.

Keeping in mind that the final product of L-ascorbic acid oxidation is dehydroascorbic acid/or dehydroascorbate, some kinetic tests were performed using a large excess of DHA. Again, the $k_{obs}$ values estimated for the observed oxidation of the Ru(II) species are much lower than those of the $k_a$ intercepts. Thus, re-oxidation of Ru(II) by DHA also did not contribute to the observed non-zero $k_a$ values.

In turn, in more alkaline media the conducted experiments revealed neither spectroscopic nor kinetic evidence for a back reaction in the systems involving complexes **2** and **3**. Taking into account that on one hand changes in $[AscH_2]_T$ and pH did not result in changes of the degree of conversion of **2** and **3**, and on the other hand the plots seen in Fig. 27c originate from (0,0), irreversibility of the electron transfer processes at higher pH can be concluded.

Kinetic experiments carried out as a function of pH gave one more piece of important mechanistic information. As noted above (see Scheme 18), L-ascorbic acid can exist in three protolytic forms within the standard pH scale. It follows from the given p$K_a$ values that the predominating protolytic forms under conditions applied in our studies, are: $AscH_2$ (pH 1.0–2.3, 99.9–98.4%) and $AscH^-$ (pH 5.0–7.4, 88.8–99.9%, pH 6.8–9.7, 99.8–97.4%). Nevertheless, values of all the second-order rate constants ($k$ and $k_b$ or $k_cK$) listed in Table 11 and dependences plotted in Fig. 28 clearly illustrate a very strong effect of pH on the kinetics of the electron transfer processes in all three studied systems. It must be related to the difference in the reducing abilities of two protolytic forms involved in the rate-determining step (Scheme 18, Table 10), *viz*. $AscH_2$ and $AscH^-$ in strongly acidic media (pH 1.0–2.3), and $AscH^-$ and $Asc^{2-}$ in less acidic, neutral and slightly alkaline solutions (pH 5.0–7.4 and 6.8–9.7).

A typical oxidation process of L-ascorbic acid by inert Ru(III) complexes occurs in two consecutive outer-sphere steps. The first step outlined in eqn (28a, 28b) or (29a, 29b), determines the reaction rate and leads to the generation of the ascorbyl radical and Ru(II) species. In the subsequent rapid, kinetically

 

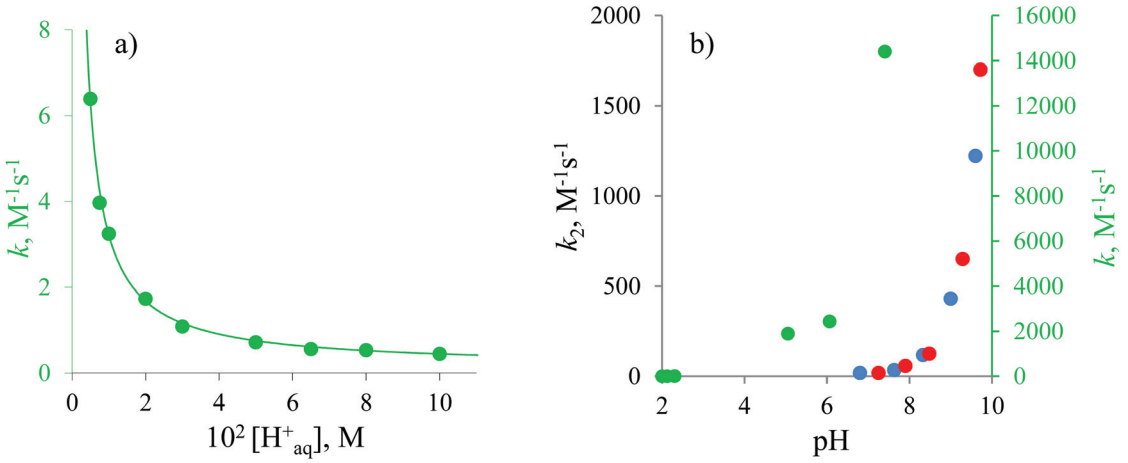


**Fig. 28** Dependence of the second-order rate constant $k$ on $[H^+_{aq}]$ for the reaction of **1** in the pH range 1.0–2.3; $I$ = 1 M ($NaClO_4$) (a) and pH dependence of the second-order rate constant $k$ for the reaction of **1** (●) and $k_2$ (≡ $k_b$ or $k_cK$) for the second phase of the reaction of **2** (●) and **3** (●) (see Table 11) with L-ascorbic acid at 25 °C (b).

indistinguishable step, $Asc^{\bullet-}$ reduces Ru(III) to Ru(II) and forms dehydroascorbic acid/or dehydroascorbate, DHA, whose protolytic forms have been omitted for clarity (eqn (30)).

$$AscH_2 + [Ru(III)] \xrightarrow{k_{AscH_2}} [Ru(II)] + Asc^{\bullet-} + 2\,H^+_{aq} \quad (28a)$$

$$H^+_{aq} \rightleftharpoons K_{a1}$$

$$AscH^- + [Ru(III)] \xrightarrow{k_{AscH^-}} [Ru(II)] + Asc^{\bullet-} \quad (28b)$$

$$AscH^- + [Ru(III)] \xrightarrow{k_{AscH^-}} [Ru(II)] + Asc^{\bullet-} + H^+_{aq} \quad (29a)$$

$$H^+_{aq} \rightleftharpoons K_{a2}$$

$$Asc^{2-} + [Ru(III)] \xrightarrow{k_{Asc^{2-}}} [Ru(II)] + Asc^{\bullet-} \quad (29b)$$

$$Asc^{\bullet-} + [Ru(III)] \rightarrow [Ru(II)] + DHA \quad (30)$$

Based on the mechanisms presented in eqn (28a, 28b) and (30) or (29a, 29b) and (30) (depending on the reaction conditions) the following expressions are derived for the second-order rate constant $k$ (Table 11) *vs.* $[H^+_{aq}]$ dependence (eqn (31) and (32)):

$$k = \frac{2k_{AscH_2}[H_{aq}^+] + 2k_{AscH^-}K_{a_1}}{K_{a_1} + [H_{aq}^+]} \quad (31)$$

$$k = \frac{2k_{AscH^-}[H_{aq}^+] + 2k_{Asc^{2-}}K_{a_2}}{K_{a_2} + [H_{aq}^+]} \quad (32)$$

where $k_{AscH_2}$, $k_{AscH^-}$, $k_{Asc^{2-}}$,$K_{a1}$ and $K_{a2}$ represent the second-order rate constants for the reduction of Ru(III) by $AscH_2$, $AscH^-$ and $Asc^{2-}$, and the acid-dissociation constants of $AscH_2$ and $AscH^-$, respectively. If $[H^+_{aq}] \gg K_{a1}$ and $[H^+_{aq}] \gg K_{a2}$ eqn (31) and (32) simplify to eqn (33) and (34), respectively.

$$k = 2k_{AscH_2} + \frac{2k_{AscH^-}K_{a1}}{[H_{aq}^+]} \quad (33)$$

$$k = 2k_{AscH^-} + \frac{2k_{Asc^{2-}}K_{a2}}{[H_{aq}^+]} \quad (34)$$

Reduction of **1** by L-ascorbic acid was studied over a wide acidity range. Therefore, the data collected within lower (1.0–2.3) and higher (5.0–7.4) pH ranges were fitted to eqn (33) and (34), respectively. The values of $k_{AscH_2}$ and $k_{AscH^-}$ calculated with the aid of the literature value for $K_{a1}$ are $(5 \pm 1) \times 10^{-2}$ and $194 \pm 4$ $M^{-1}$ $s^{-1}$ at 25 °C, respectively. The value of $k_{Asc^{2-}}$ calculated using the value obtained above for $k_{AscH^-}$ and the literature value for $K_{a2}$ equals $(5.6 \pm 0.6) \times 10^7$ $M^{-1}$ $s^{-1}$ at 25 °C. The two other systems (**2** and **3**) were investigated over a much higher pH range, *i.e.* 6.8–9.6 and 7.2–9.7, respectively. The values of $k_{AscH^-}$ and $k_{Asc^{2-}}$ (eqn (34)) for systems **2** and **3** are (11 ± 2) and $(326 \pm 2) \times 10^2$ $M^{-1}$ $s^{-1}$, and (25 ± 15) and $(300 \pm 15) \times 10^2$ $M^{-1}$ $s^{-1}$, respectively, at 25 °C. The results demonstrate drastic differences in the reactivities of the three protolytic forms of L-ascorbic acid. Based on the second-order rate constants, $AscH_2$ is less reactive than $AscH^-$, which in turn is less reactive than $Asc^{2-}$ towards **1** over three and nearly five orders of magnitude, respectively. In the case of **3** and **2**, $AscH^-$ is less reactive than $Asc^{2-}$ by three to four orders of magnitude. The results lead to the conclusion that $AscH^-$ is the actual reductant of **1** at pH 1.0–2.3 and $Asc^{2-}$ is the actual reductant of **1** at pH 5.0–7.4, **2** and **3** at pH 6.8–9.7. The two species present in solution at very low concentrations, *viz.* $AscH^-$ 0.1% at pH 1.0 and 1.6% at pH 2.3, and $Asc^{2-}$ $4.5 \times 10^{-5}$% at pH 5.0 and 2.6% at pH 9.7, control the rates of the overall reduction processes of the Ru(III) complexes. This can only be accounted for in terms of the much stronger reducing abilities of $AscH^-$ compared to $AscH_2$, and $Asc^{2-}$ compared to $AscH^-$ (Scheme 18, Table 10). It is worth to emphasize that the quantitative comparison of the reactivity, obtained for all three protolytic forms of L-ascorbic acid towards one oxidant is a unique case. As mentioned above, the huge qualitative increase in the reactivity of L-ascorbic acid towards metal com-

plexes, resulting from its deprotonation, is well known. However, quantitative data were reported only for either $AscH_2$ and $AscH^-$ or $AscH^-$ and $Asc^{2-}$ couples involved in a few systems.[57,204] The $AscH^-/AscH_2$ and $Asc^{2-}/AscH^-$ reactivity ratios provided in the literature are approximately $10^3$–$10^4$ and $10^4$–$10^7$, respectively, thus of the same order of magnitude as those found for the systems studied by us.

The two-step mechanism presented in eqn (28a, 28b) or (29a, 29b) and (30), accounts exactly for the simple kinetics found for system **1**, but does not account for the unexpected complex kinetic behaviour of systems **2** and **3**. A detailed investigation of the systems and in-depth analysis of the collected data based on the strong similarity of systems **2** and **3**, revealed that the observed differences must be related to the redox properties of the Ru(III) complexes. As stated above, **1** is a much stronger oxidant than **2** and **3**, which exhibit similar and very weak oxidising properties. Consequently, the thermodynamic driving force of the L-ascorbic acid – **1** system is much higher than that for systems **2** and **3**. As a result, the reduction of **2** and **3** is much slower than that of **1**. This in turn allowed (i) to study the electron transfer process in systems **2** and **3** over a much higher pH range (6.8–9.7) than in the case of system **1** (pH 1.0–7.4), and thereby (ii) to get closer to the reactivity of $Asc^{2-}$. This is unique because of the very high reactivity of this ion. Moreover, the reduction process of **1** displayed clean pseudo-first-order behaviour throughout the examined pH range with no evidence for the interference of a back reaction. In contrast, the reduction process of **2** and **3** exhibited the apparent three exponential behaviour and reversibility, within the lower applied pH range (6.8–8.5), evidenced by both the spectroscopic and kinetic data. We ascribe these mechanistic complications to redox equilibration involving re-oxidation of Ru(II) to Ru(III) by the $Asc^{\bullet-}$ radical, as shown in eqn (35). The equilibration arises from the low-driving force of systems **2** and **3**.

$$Asc^{\bullet-} + [Ru(II)] + H_{aq}^{+} \rightarrow [Ru(III)] + AscH^- \quad (35)$$

The thermodynamic driving force for the overall reduction of Ru(III) is the oxidation of the $Asc^{\bullet-}$ radical to DHA (eqn (30)). It stays approximately constant in acidic and neutral solutions and increases along with the pH > 8 as depicted in Table 12. Interestingly, at the same time, the thermodynamic driving force of the $Asc^{\bullet-}$ radical causes re-oxidation of the Ru(II) species generated in the systems, and decreases with increasing pH. Comparison of the values summarised in Table 12 points to the conclusion that in system **1** the $Asc^{\bullet-}$ radical is oxidised to DHA (eqn (30), Fig. 27a), whereas in systems **2** and **3** the oxidation and reduction of the $Asc^{\bullet-}$ radical (eqn (30) and (35)) are concurrent processes. This in turn leads to the reversible conversion of Ru(III) to Ru(II) (see Fig. 27b). An increase in pH favours oxidation of the $Asc^{\bullet-}$ radical and shifts the overall electron transfer process towards the Ru(II) species (eqn (30)). Therefore, in more alkaline media (pH 6.8–9.7), no evidence was found for the back reaction (see Fig. 27c). It is worth noting that to the best of our knowledge, there is no report on the re-oxidation of any metal complex by the $Asc^{\bullet-}$ radical as proposed in our studies.

In search for further support for the proposed reaction mechanism for low-driving force metal complex – L-ascorbic acid systems (eqn (28a), (28b), (29a), (29b)–(30) and (35)) and a unique role of the $Asc^{\bullet-}$ radical, V(II) was employed as a much stronger reducing agent. The $V(OH)^{2+}{}_{aq}/V^{2+}{}_{aq}$ couple is characterised by the redox potential $E^\circ = -0.082$ V at pH 3–3.5.[205] Hence, the thermodynamic driving force of the V(II) – **2** and V(II) – **3** systems equal to 0.11 and 0.13 V, respectively, is much higher than that of the analogous L-ascorbic acid systems. Furthermore, V(II) is a one-electron donor which is a further advantage in terms of the simplicity of the process (eqn (36)).

$$V_{aq}{}^{2+} + [Ru(III)] \rightarrow [Ru(II)] + V(OH)_{aq}{}^{2+} + H_{aq}{}^{+} \quad (36)$$

If the mechanistic complications, especially the observed three exponential kinetic behaviour found for systems **2** and **3**, are a consequence of the redox equilibration involving $Asc^{\bullet-}$ under low driving force conditions, then in systems with a high thermodynamic driving force the reduction of **2** and **3** should be a straightforward process. Thus, an electron is expected to be transferred from the very labile V(II) to Ru(III) *via* a simple inner-sphere mechanism.[206] Indeed, spectral changes accompanying the reduction of **2** and **3** by V(II), shown in Fig. 29, are characteristic for a simple first-order reaction with excellent fits of the kinetic traces to a single exponential function (see Fig. 29).

Table 12 Thermodynamic driving force and relevant equilibrium constant $K$ estimated for the reduction of 1, 2 and 3, and re-oxidation of their reduced analogues by the $Asc^{\bullet-}$ radical. DHA represents dehydroascorbic acid or its conjugate base at pH < 8 and pH > 8, respectively

| **1** | | | **2** | | | **3** | | |
|---|---|---|---|---|---|---|---|---|
| pH | Driving force, V | $K$ | pH | Driving force, V | $K$ | pH | Driving force, V | $K$ |
| **$Asc^{\bullet-}$ + [Ru(II)] → [Ru(II)] + DHA** | | | | | | | | |
| 1.0–7.4 | 0.49 | $2 \times 10^8$ | 7.0–8.0 | 0.19 | 1700 | 7.0–8.0 | 0.22 | $5 \times 10^3$ |
| | | | 9.7 | 0.22 | $5 \times 10^3$ | 9.6 | 0.31 | $2 \times 10^5$ |
| **$Asc^{\bullet-}$ + [Ru(II)] + $H_{aq}^{+}$ → [Ru(III)] + $AscH^-$** | | | | | | | | |
| 1.0 | 0.33 | $4 \times 10^5$ | 7.0 | 0.27 | $4 \times 10^4$ | 6.8 | 0.26 | $2.5 \times 10^4$ |
| 5.0 | 0.09 | 33 | 9.7 | 0.12 | 100 | 9.6 | 0.09 | 40 |
| 7.4 | −0.05 | 0.12 | | | | | | |

 

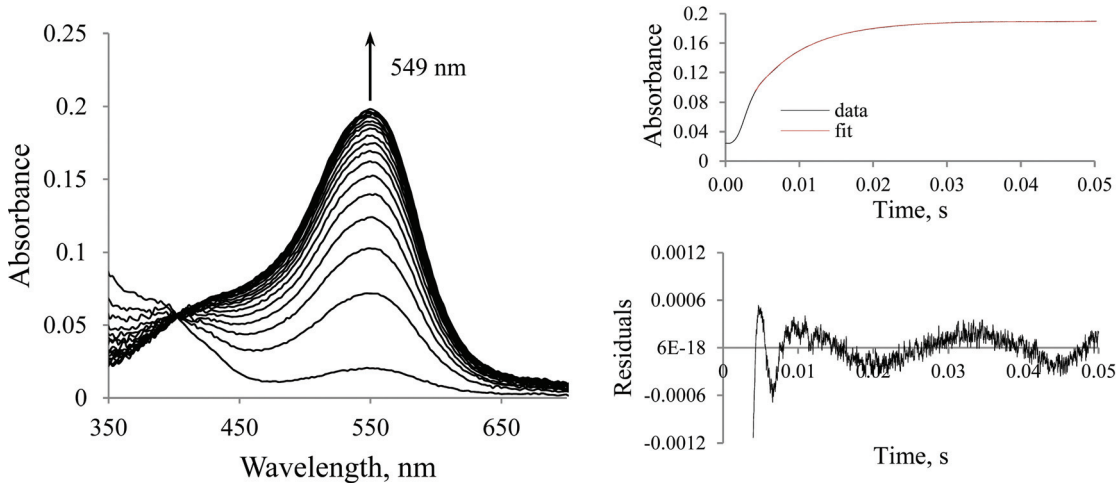


Fig. 29 Typical spectral changes and kinetic trace recorded during the reduction of 0.02 mM 3 by 0.1 mM V(II) at 2 °C, pH = 4.90 (acetate buffer), $I$ = 0.1 M ($NaClO_4$), scans taken every 5 ms. Inset: kinetic trace recorded at 549 nm (black) fitted to a single exponential function (red). The first part of the kinetic trace is affected by the dead time of the stopped-flow instrument which is 2–4 ms. The calculated rate constant for the reaction is 142.15 ± 0.04 $s^{-1}$. Note the expanded scale used for the reported residuals of the kinetic trace. Reprinted with permission from ref. 184. Copyright 2017 Wiley-VCH Verlag GmbH & Co. KGaA.

### 5.4 Conclusion

The results reported in this chapter clearly demonstrate that the mechanism of electron transfer processes in the L-ascorbic – Ru(III) systems can be strongly affected by their thermodynamic driving force. Under low driving force conditions, redox equilibration can lead to unexpected mechanistic complications reflected in unusual kinetic behaviour. We believe that the reported findings are of model character for other redox systems studied under similar conditions.

## 6. Ru(II) polypyridyl complexes and their application

### 6.1 Introduction

The systematic development of coordination chemistry began in 1798 when the French scientist B. M. Tassaert discovered solutions of cobalt chloride in the presence of ammonia, as the first known coordination compound. Particularly noteworthy are biological, physiological and pathophysiological properties of coordination compounds that enabled their widespread application, especially in medicine.[207] Studies on the application of metal complexes in medicine developed rapidly since the first successful application of cisplatin and its analogues as therapeutic agents. Although, cisplatin is characterised by a broad spectrum of activity, a serious problem exists with its cytotoxicity, resistance to the drug and many side effects accompanying human treatment.[208] Therefore, scientists are still working on the design of new transition metal compounds for therapeutic and diagnostic applications in cancer and other areas of medicine associated with lower side effects and drug resistance and higher biocompatibility than the compounds used so far. The major goal in the discovery of new drugs is to develop and implement innovative therapies with increased effectiveness and tolerability, with special emphasis on the targeting of metal complexes towards a wider range of tumour types and their biotransformation. So far, a significant number of transition metal complexes (*i.e.* Co(III), Fe(III), Pt(IV), Ru(III/II), Os(II), and Ir(III)) have been reported to exhibit promising biological and anticancer activity.[177,209] However, only a few have reached human clinical trials. Promising results have been reported for ruthenium polypyridyl complexes.[181,210–213] Ruthenium-based therapeutics are widely studied due to their unique properties (*i.e.* biological, photophysical, optical, electronic and catalytic properties) giving favourable therapeutic application possibilities. In contrast to platinum-based anticancer compounds, ruthenium complexes under physiological conditions can exist in three oxidation states, *viz.* Ru(II)/(III)/(IV).[181] In addition, due to their octahedral coordination geometry, ruthenium-based compounds coordinate a wide range of ligands of different electronic and steric properties, which allow the tuning of the rate of ligand exchange reactions and redox properties. These, in turn, are important in terms of the activation of drugs, since it is well known that anticancer metallo-therapeutics are pro-drugs activated *in vivo* by ligand exchange or redox processes.[181,214] Despite this great potential, knowledge about the application of ruthenium based drugs is still insufficient and requires further extensive research.

Structural diversity, chemical and redox properties of ruthenium compounds provide a unique opportunity for a design of new series of drugs and new therapies. Based on recent literature reports, ruthenium complexes may play an important role in the redox biology of cells. It was shown by Sadler and coworkers in a series of papers[215–219] that inert organometallic complexes of Ir(III), Ru(II/III), Rh(III), Os(II) and Fe(II) can react with NADH as a source of hydride ($H^-$) to form reactive oxygen

species (ROS), such as hydroperoxide, $O_2 + H^- \rightarrow HOO^-$, and cause oxidative stress. In these organometallic complexes, metal–carbon bonds labilise the metal centre and induce a high reactivity for the interaction with crucial species such as NADH to control the redox balance and inflammation in living cells. Oxidative stress is an effective method to kill cancer cells, since an increase in the level of ROS disturbs redox homeostasis inside cells and causes destruction. Furthermore, organometallic complexes of Ru(II) of the pseudo-octahedral type can in the presence of formate (as a hydride transfer agent) control the $[NAD^+]/[NADH]$ ratio and cause reductive stress. In this way, these complexes can catalytically reduce $NAD^+$ in cancer cells and cause reductive stress. Therefore, organometallic complexes are apparently unique in their ability to achieve redox modulation (oxidative *vs.* reductive stress) in living cells. In our most recent work we demonstrated that a similar effect can be reached with the application of usually more biocompatible non-organometallic Ru(II) complexes.[220]

In this chapter we report results of our studies on a range of Ru(II) polypyridyl complexes with diverse electronic properties (σ donor and π back-bonding) and steric hindrance provided by spectator ligands. Our work focused on the tuning of their reactivity in terms of monodentate ligand exchange reactions that could be of biological relevance.[221–223] We also discuss briefly the ability of one of the most promising non-organometallic Ru(II) complexes, recently examined by us, to catalyse the regio-selective transfer of hydride in terms of its possible application in redox biology.[220]

### 6.2 Substitution behaviour of polypyridyl Ru(II) complexes in water

A series of polypyridyl ruthenium complexes of the general formula [Ru(terpy)(N^N)Cl]Cl (terpy = 2,2′:6′,2″-terpyridine, N^N = bidentate N,N-donor ligand) was synthesized and fully characterized in the solid state by single crystal X-ray diffraction and elemental analysis, and in solution NMR, ESI-MS and UV-Vis spectroscopies.[221–223] The coordination sphere of these complexes consists of a tridentate π-acceptor terpyridine chelate, a bidentate ligand of various different electronic and steric properties, and a chlorido ligand. We obtained five complexes with the following bidentate spectator ligands: ethylenediamine (en), **1** with σ donor properties, 2-(aminomethyl)pyridine (ampy), **2** containing a σ-donor amine and a π-acceptor pyridine chelate, 2,2′-bipyridine (bipy), **3** and 1,10-phenantroline (phen), **4** typically π back-bonding, and *N*,*N*,*N*′,*N*′-tetramethylethylenediamine (tmen) **5** a bulky derivative of ethylenediamine with four methyl groups (see Fig. 30).

To tune the lability of the chlorido complexes,[221–223] the composition of the coordination sphere, selection of the bidentate spectator chelates based on the number of pyridine rings, and steric effects can be employed. We therefore compared the stability of the series of $[Ru^{II}(terpy)(N^N)Cl]^+$ complexes in aqueous solution, and chemical behaviour of their aquated derivatives, *i.e.* $[Ru^{II}(terpy)(N^N)(H_2O)]^{2+}$ ions, in terms of acidity and water substitution reactions. All reactions were followed using electronic absorption spectroscopy in the visible range under pseudo-first-order conditions, *i.e.* applying at least 10-fold excess of an entering ligand over Ru(II) concentration.

The stability and chemical behaviour of Ru(II) complexes in aqueous solution are particularly important for their potential biological application. Water in living matter plays a role as an inert solvent, a dispersing medium for colloidal solutions and as a nucleophile in numerous biological reactions. Furthermore, water transports drugs from their site of administration to the tumour where they undergo activation. It has been proposed that the common feature of many of the synthesised and tested Ru(II) complexes is their activation *via*

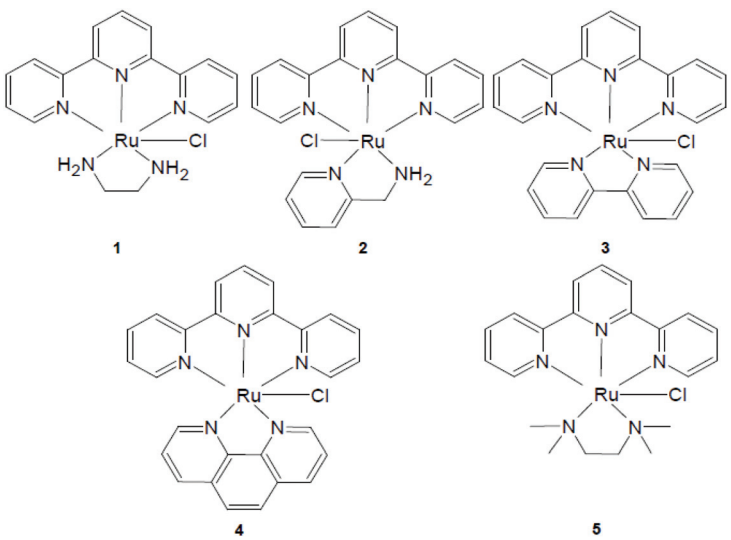


Fig. 30 Schematic structures of the studied $[Ru^{II}(terpy)(N^N)Cl]^+$ complexes.

 

aquation of the monodentate ligand.[181,214] This process allows the metal centre to coordinate to intracellular bio-molecules such as DNA, proteins and other biological targets. However, aquation of a Ru(II) species administered intravenously cannot be too fast under physiological conditions, since it needs to be selectively activated inside cancer cells without additional side effects before reaching its biological destination. Thus, intracellular hydrolysis has long been thought to be an important process for the activation of chlorido Ru(II) complexes and their drug action. Medicinal drugs are often administered in solution, such that their stability at room and body temperature are of primary importance. At 37 °C the spontaneous aquation reactions we studied, that is, those of phen, bipy, tmen, ampy and en complexes, are complete within 3.5 h, 2.4 h, 2.2 h, 30 min and 2 min, respectively, $k_{phen}$ = (2.82 ± 0.02) × $10^{-4}$ $s^{-1}$, $k_{bipy}$ = (4.01 ± 0.03) × $10^{-4}$ $s^{-1}$, $k_{tmen}$ = (4.33 ± 0.03) × $10^{-4}$ $s^{-1}$, $k_{ampy}$ = (1.89 ± 0.01) × $10^{-3}$ $s^{-1}$ and $k_{en}$ = (2.45 ± 0.04) × $10^{-2}$ $s^{-1}$. At 25 °C the aquation reactions are 4, 3.6, 3.6, 3 and 3.5 times slower, respectively. It follows that the stability of the Ru(II) chlorido complexes studied is strongly affected by both the electronic and steric factors. It increases with the increasing number of pyridine rings coordinated to the metal centre, *i.e.* with the π back-bonding abilities of the spectator chelate. Moreover, comparison of the data for the en and tmen complexes indicates a much higher stability of tmen due to the steric hindrance provided by the bulky tmen ligand: phen > bipy ≈ tmen > ampy > en.

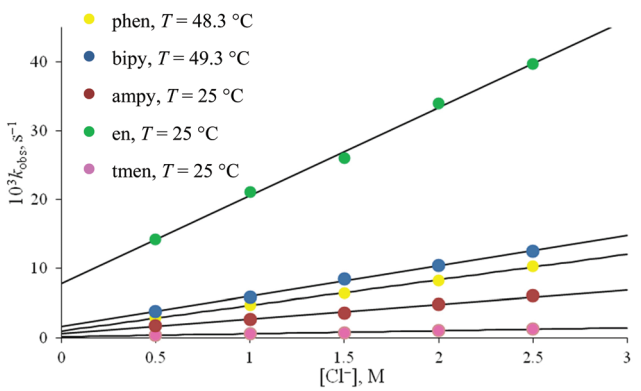


**Fig. 31** Plots of $k_{obs}$ *vs.* [$Cl^-$] for the reaction of [Ru(terpy)(N^N)($H_2O$)]$^{2+}$ with chloride; *I* = 2.5 M ($Na^+$, $NO_3^-$, $Cl^-$).

Aquation of the chlorido complexes studied can be fully reversed upon addition of an excess of chloride (eqn (37)). In general, the dependence of the aquation reaction on the chloride concentration may allow the ruthenium species to be selectively activated inside tumour cells without any or with limited interactions before reaching the biological target. We found that the observed rate constants for reformation of all parent complexes are linear functions of chloride concentration with significant intercepts that indicate reversibility of the examined reactions (see Fig. 31). The slopes of the linear dependence are the second-order rate constants for the anation of the aqua complexes by chloride, whereas the intercepts represent the first-order rate constants for the aquation of the chlorido complex as given by eqn (37)–(38).

$$[Ru^{II}(terpy)(N\hat{N})Cl]^+ + H_2O \underset{k_{-1}}{\overset{k_1}{\rightleftharpoons}} [Ru^{II}(terpy)(N\hat{N})(H_2O)]^{2+} + Cl^- \quad (37)$$

$$k_{obs} = k_1 + k_{-1}[Cl^-] \quad (38)$$

The calculated $k_1$, $k_{-1}$ and equilibrium constants *K* (= $k_1/k_{-1}$) for the reactions outlined in eqn (37) are reported in Table 13. Analysis of the collected data demonstrates that the rate constants $k_1$ and $k_{-1}$ are significantly larger for the en complex than for the other complexes. On the other hand, reactivity of the tmen complex is similar to that of the bipy and phen complexes for both the aquation and anation reactions. This again shows clearly that the steric hindrance has a significant impact on the lability of the Ru(II) complexes studied. Furthermore, the higher *K* value for the en complex suggests that it aquates to a higher degree than the other complexes. The values of *K* demonstrate that in aqueous solution with a water concentration of 55.5 M all complexes exist in their aqua forms and a high concentration of chloride is required to prevent spontaneous aquation of the starting complexes. Detailed parallel studies on spectral data as a function of chloride concentration confirmed that 2–4 M chloride is required to shift the equilibrium given in eqn (37) back for all considered complexes. Thus, the concentration of chloride ion

**Table 13** p$K_a$ values, rate and equilibrium constants, and thermal activation parameters for aquation and anation by $Cl^-$ of [Ru(terpy)(N^N)(Cl/$H_2O$)]$^{+/2+}$ at 25 °C [221–223]

| System | $10^3k_1$ [$s^{-1}$] | $10^3$ $k_{-1}$ [$M^{-1}$ $s^{-1}$] | *K* [M] | p$K_a$ (*I* = 0 M) | $\Delta H^{\ddagger}$ [kJ $mol^{-1}$] | $\Delta S^{\ddagger}$ [J $K^{-1}$ $mol^{-1}$] |
|---|---|---|---|---|---|---|
| [en-Cl] + $H_2O$ | 7.0 ± 0.1 | — | 0.62 ± 0.03 | | — | — |
| [en-$H_2O$] + $Cl^-$ | — | 12.8 ± 0.4 | | 10.83 ± 0.03 | — | — |
| [ampy-Cl] + $H_2O$ | 0.64 ± 0.03 | — | 0.31 ± 0.03 | | — | — |
| [ampy-$H_2O$] + $Cl^-$ | — | 2.09 ± 0.08 | | 10.36 ± 0.03 | 75 ± 3 | −44 ± 11 |
| [bipy-Cl] + $H_2O$ | 0.11 ± 0.01 | — | 0.26 ± 0.03 | | — | — |
| [bipy-$H_2O$] + $Cl^-$ | — | 0.42 ± 0.01 | | 9.83 ± 0.03 | 78 ± 2 | −46 ± 5 |
| [phen-Cl] + $H_2O$ | 0.072 ± 0.001 | — | 0.20 ± 0.01 | | — | — |
| [phen-$H_2O$] + $Cl^-$ | — | 0.36 ± 0.01 | | 9.59 ± 0.03 | 82 ± 2 | −37 ± 6 |
| [tmen-Cl] + $H_2O$ | 0.12 ± 0.01 | — | 0.28 ± 0.01 | | — | — |
| [tmen-$H_2O$] + $Cl^-$ | — | 0.43 ± 0.02 | | 10.03 ± 0.02 | 79 ± 2 | −44 ± 2 |

in the blood plasma (100 mM) is insufficient to prevent the spontaneous aquation of the Ru(II) complexes studied.[224]

If this is the case, in view of their potential bio-relevance, the acidity of the aqua complexes studied is of importance since hydroxo complexes are known to be less labile than the corresponding aqua complexes. The p$K_a$ values determined using spectrophotometric pH titrations, are included in Table 13. As can be seen, all $[Ru(terpy)(N^N)(H_2O)]^{2+}$ complexes are characterised by very high p$K_a$ values, varying from 9.59 to 10.83 with $[Ru(terpy)(phen)(H_2O)]^{2+}$ and $[Ru(terpy)(en)(H_2O)]^{2+}$ being the most and least acidic complexes, respectively. Accordingly, under physiological conditions all five examined $[Ru(terpy)(N^N)(H_2O)]^{2+}$ complexes exist in their more reactive aqua form.

Careful analysis of the data in Table 13 reveals that the observed differences in acidic properties of the studied complexes are consistent with the difference in lability of the starting chlorido complexes. For instance, the water molecule is bound stronger to the Ru(II) centre in the phen complex than in the en complex. Values of the equilibrium constant $K$ (eqn (37)) are controlled by the efficiency of the forward ($k_1$) and back ($k_{-1}$) reactions. On the other hand, the efficiency of the back reaction ($k_{-1}$) correlates with the p$K_a$ values, which in turn increase with the lability of the coordinated water molecule. This is well illustrated by plots of $\log k_1$ *vs.* $\log K$ and $\log k_{-1}$ *vs.* p$K_a$ presented in Fig. 32. The data collated in Table 13 indicate that both the reactivity and p$K_a$ values of the Ru(II) complexes can be tuned by a systematic variation of electronic and steric effects provided by the bidentate chelates. The increasing π back-bonding abilities of the bidentate ligands cause an increase in the electrophilicity of the Ru(II) centre and change its electronic nature more in the direction of inert Ru(III). As a consequence, the reactivity of the complexes increases in the order: phen ≤ bipy ≈ tmen < ampy < en.

Being stimulated by the above reported results, we carried out further studies aimed at expanding our knowledge on the substitution behaviour of the series of complexes. We examined their reactions with two bio-relevant nucleophiles of different nucleophilicity such as thiourea (TU) and its sterically hindered derivate, *N*,*N*′-dimethylthiourea (DMTU). The studied ligands differ from chloride not only in their charge but also in their nucleophilicity based on the $\eta^0_{Pt}$ scale: $Cl^-$ < DMTU < TU.[225] Both substitution reactions were followed as a function of the entering ligand concentration. Plots of $k_{obs}$ *vs.* thiourea concentration are linear with zero intercepts within the error limits (see Fig. 33a), demonstrating the irreversibility of the reactions:

$$k_{obs} = k_2[TU] \tag{39}$$

In contrast, values of $k_{obs}$ show a non-linear dependence on the *N*,*N*′-dimethylthiourea concentration and pass through the origin within error limits (see Fig. 33b). This kind of dependence can be explained by the general reaction mechanism that consists of a rapid precursor-formation step ($Q$) prior to a rate-limiting ligand exchange step ($k$), outlined in a simplified way in eqn (40):

$$\begin{array}{l} [Ru^{II}(terpy)(N^N)(H_2O)]^{2+} + DMTU \overset{Q}{\rightleftharpoons} \{[Ru^{II}(terpy)(N^N)(H_2O)]\cdot DMTU\}^{2+} \\ \qquad\qquad\qquad\qquad\qquad\qquad\qquad\qquad\qquad\qquad \downarrow k \\ \qquad\qquad\qquad\qquad\qquad\qquad\qquad\qquad\qquad\qquad [Ru^{II}(terpy)(N^N)(DMTU)]^{2+} + H_2O \end{array} \tag{40}$$

The corresponding rate expression is given in eqn (41):

$$k_{obs} = \frac{kQ[DMTU]}{1 + Q[DMTU]} \tag{41}$$

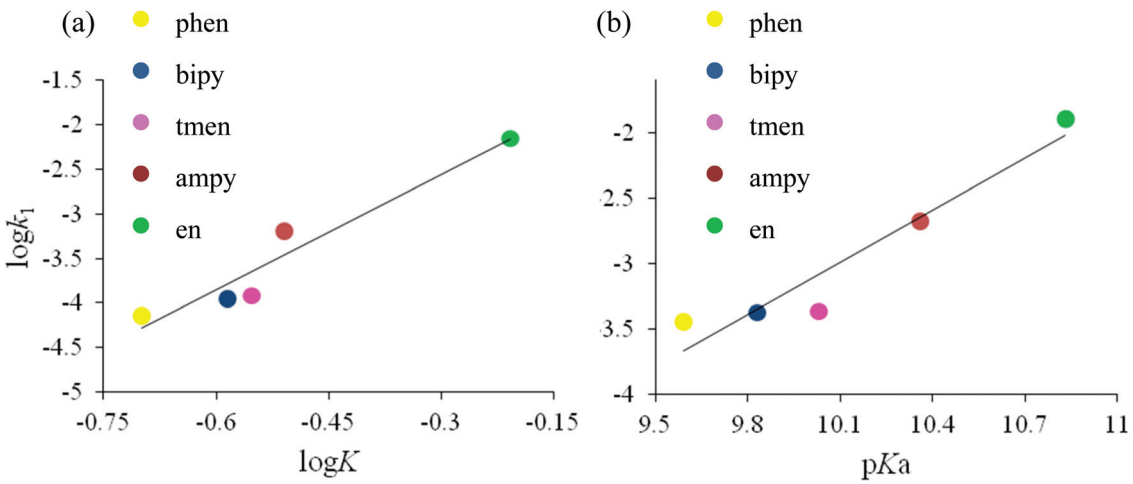


Fig. 32 Plots of $\log k_1$ *vs.* $\log K$ (a) and $\log k_{-1}$ *vs.* p$K_a$ (b) for the $[Ru(terpy)(N^N)(H_2O)]^{2+}$ complexes.

 

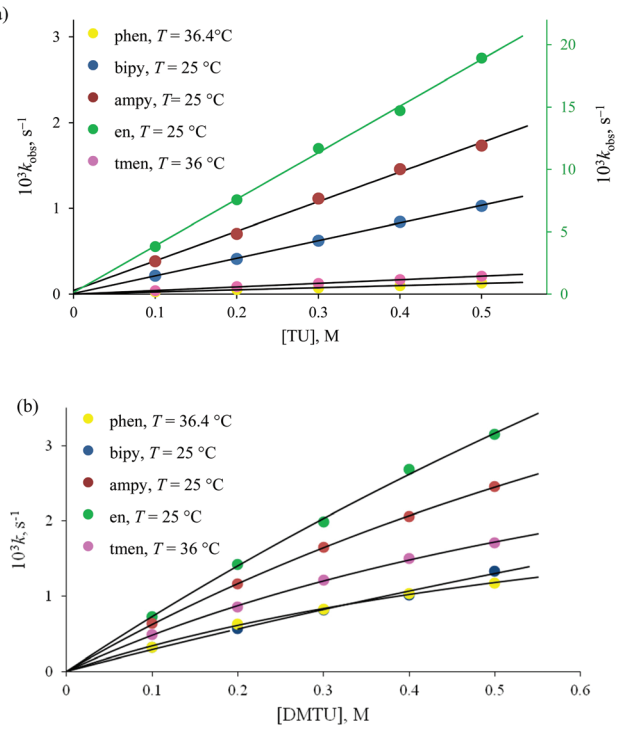


**Fig. 33** Plots of $k_{obs}$ *vs.* [nucleophile] for the reactions of the [Ru(terpy)(N^N)$(H_2O)]^{2+}$ complexes with (a) thiourea and (b) *N*,*N*′-dimethylthiourea; $I$ = 0.1 M ($NaNO_3$).

Comparison of the reaction rates with thiourea and *N*,*N*′-dimethylthiourea may be drawn by using the second-order rate constant $k_2$ and the initial slope of the plot in Fig. 33b that presents the overall second-order rate constant $k_3 = kQ$ derived from eqn (41). Values of the second-order rate constants summarised in Table 14 show that the majority of the reactions with DMTU are faster than with TU. The only exception is the $[Ru^{II}(terpy)(en)(H_2O)]^{2+}$ complex for which the $k_3$ value is lower than that of $k_2$ (see Table 14). At present we do not have a plausible reason for the higher reactivity of the complexes towards DMTU. It could be that the precursor formation step accelerates the efficiency of the ligand exchange reaction in terms of an interchange mechanism, in spite of the steric hindrance provided by DMTU and its lower nucleophilicity compared to TU.[222,223]

Aqua substitution reactions from the [Ru(terpy)(N^N)$(H_2O)]^{2+}$ complexes by chloride and thiourea were also followed as a function of temperature. The temperature dependence was determined under the following experimental conditions. Anation by chloride was examined at a high chloride concentration of 2.5 M to prevent the spontaneous aquation of the generated [Ru(terpy)(N^N)Cl]$^+$ (see eqn (37)). Under these conditions contribution of the intercept towards the rate expression given in eqn (38) can be ignored, such that $k_{obs} \approx k_{-1}[Cl^-]$. Substitution by thiourea was in turn studied in the presence of 0.3 M TU based on the linear dependence presented in Fig. 33a. The results obtained are given in Tables 13 and 14. The negative values of the activation entropies support an associative interchange ($I_a$) mechanism of the water displacement in all the [Ru(terpy)(N^N)$(H_2O)]^{2+}$ complexes. The $I_a$ activation mode is typical for substitution reactions of Ru(II).[206,226]

To sum up, our studies showed that the reactivity and p$K_a$ values of the [Ru(terpy)(N^N)$(Cl/H_2O)]^{+/2+}$ type complexes can be tuned systematically by the nature of the bidentate spectator ligand. Introduction of π-acceptors into the coordination sphere causes a decrease in electron density on the Ru(II) centre and results in stronger coordination of a leaving monodentate ligand. This in turn reflects in the higher acidity of coordinated water as well as in the lower substitution reactivity of the complex. The p$K_a$ values decrease with increasing number of pyridine rings surrounding the Ru(II) centre: en < ampy < bipy < phen. By way of example, the phen complex is by factors of 100 and 40–60 less labile than the en complex, for aquation and water substitution reactions at 25 °C, respectively. Furthermore, the results described demonstrate that the reactivity and p$K_a$ values of the Ru(II) complexes can be tuned not only by electronic, but also by steric effects of the spectator bidentate ligands. The presence of four methyl groups attached to nitrogen atoms of the tmen ligand, leads to significant deceleration of all substitution reactions of the tmen complex. Compared to the most labile en complex, the tmen complex is more inert towards aquation and water substitution reactions at 25 °C by factors of 50 and 30–45, respectively. In such a way, the reactivity of the tmen and bipy complexes towards all entering ligands is very similar. As to be expected, also the acidity of these complexes is comparable. In general, rates of both the spontaneous aquation of the [$Ru^{II}$(terpy)(N^N)Cl]$^+$ complexes and substitution of the coordinated water

**Table 14** Rate constants and activation parameters for substitution of the [Ru(terpy)(N^N)$(H_2O)]^{2+}$ complexes by TU and DMTU

| Complex | Incoming ligand | $T$ [°C] | $10^3k_2$ [$M^{-1}$ $s^{-1}$] | $10^3k_2$ [$M^{-1}$ $s^{-1}$] | $\Delta H^{\ddagger}$ [kJ $mol^{-1}$] | $\Delta S^{\ddagger}$ [J $K^{-1}$ $mol^{-1}$] |
|---|---|---|---|---|---|---|
| [en-$H_2O$] | TU | 25 | 37.4 ± 0.1 | | 65 ± 2 | −55 ± 6 |
| | DMTU | | | 28.0 ± 0.2 | — | — |
| [ampy-$H_2O$] | TU | 25 | 3.57 ± 0.05 | | 79 ± 1 | −27 ± 4 |
| | DMTU | | | 6.64 ± 0.09 | — | — |
| [bipy-$H_2O$] | TU | 25 | 0.58 ± 0.02 | | 83 ± 1 | −29 ± 2 |
| | DMTU | | | 1.08 ± 0.03 | — | — |
| [phen-$H_2O$] | TU | 36.4 | 1.71 ± 0.04 | | 79 ± 2 | −43 ± 7 |
| | DMTU | | | 3.72 ± 0.04 | — | — |
| [tmen-$H_2O$] | TU | 36 | 2.89 ± 0.06 | | 70 ± 2 | −72 ± 7 |
| | DMTU | | | 5.39 ± 0.06 | — | — |

molecule in $[Ru^{II}(terpy)(N^N)(H_2O)]^{2+}$ by chloride, thiourea and *N*,*N*′-dimethylthiourea, increases in the following order: $[Ru^{II}(terpy)(phen)X]^{+/2+} < [Ru^{II}(terpy)(bipy)X]^{+/2+} \approx [Ru^{II}(terpy)(tmen)X]^{+/2+} < [Ru^{II}(terpy)(ampy)X]^{+/2+} < [Ru^{II}(terpy)(en)X]^{+/2+}$.

### 6.3 Application of the Ru(II) polypyridyl amine catalyst for hydride transfer to coenzyme $NAD^+$ in the presence of formate

As a follow-up to the studies described in section 6.2, we investigated the regio-selective reduction of $NAD^+$ using the most promising candidate of the described complexes, *i.e.* the most labile $[Ru^{II}(terpy)(en)(H_2O)]^{2+}$ complex, the first non-organometallic complex as a catalyst for hydride transfer reactions. Herein, we report the highlights of our most recent work.[220]

The Sadler group studied in detail the regio-selective reduction of $NAD^+$ to 1,4-NADH catalysed by neutral pseudo-octahedral organometallic Ru(II) complexes using formate as a source of hydride.[215–219] Based on our preliminary results,[220] we have experimental evidence that non-organometallic complexes of the type $[Ru^{II}(terpy)(N^N)(H_2O)]^{2+}$ can control the redox biology of cells involving reactions with $NAD^+$ in the presence of formate as source of hydride. In these complexes terpy instead of the arene is now responsible for the labilisation of coordinated water *via* π-acceptor properties. The advantage of non-organometallic coordination compounds is their bio-compatible nature that is known for many related systems presently used in anti-cancer treatment, which in general is not always the case for organometallic complexes. So far we found that the $[Ru(terpy)(en)(H_2O)]^{2+}$ complex in the presence of an excess of sodium formate can be rapidly converted into the formato complex. In the presence of $NAD^+$, a subsequent slow reaction transfers hydride to $NAD^+$ to form NADH with a characteristic band at 340 nm. The latter reaction shows typical saturation kinetics as a function of formate concentration, but on a much slower time scale. The catalytic conversion of $NAD^+$ to 1,4-NADH was studied in the presence of a small and large excess of formate. The observed spectral changes associated with the formation of NADH at the lower formate concentration indicate that the reaction follows first-order kinetics (Fig. 34a), whereas at the higher formate concentration typical zero-order kinetics with a characteristic dead-end were observed (Fig. 34b). These observations suggest that the mechanism of the hydride transfer process at high formate concentration must involve a totally different rate-determining step. This may be related to a rearrangement of coordinated formate to enable the release of $CO_2$ and hydride, where the latter rapidly reacts with $NAD^+$ to form NADH.

## 7. Relevant physicochemical properties and reaction mechanisms in ionic liquids

### 7.1 Introduction

Many chemical reactions in solution are sensitive to the nature of the solvent, ranging from extreme variation of reaction rates, particularly for some organic reactions, and some organometallic reactions; for example, *tert*-BuCl solvolysis has a rate constant range of $10^6$ for four solvents (water, methanol acetic acid and ethanol).[225,227–229] Other reactions are relatively indifferent to solvent variation in that the rate constant varies little or not at all. For example, the dissociation of the $[Rh\{P(OMe)_3\}_5]^+$ cation has the same rate constant in five different solvents.[230] It is incumbent upon kinetics and mechanism investigators to endeavour to understand these variations in terms of solvation differences between the initial state and transition state, together with analysis of activation parameters acquired from temperature variation studies ($\Delta H^{\ddagger}$ and $\Delta S^{\ddagger}$), and where practicable, the volume of activation, $\Delta V^{\ddagger}$, acquired from the relationship between the rate constant and applied hydrostatic pressure. The volume of activation may have two contributing components, intrinsic and solvation whose

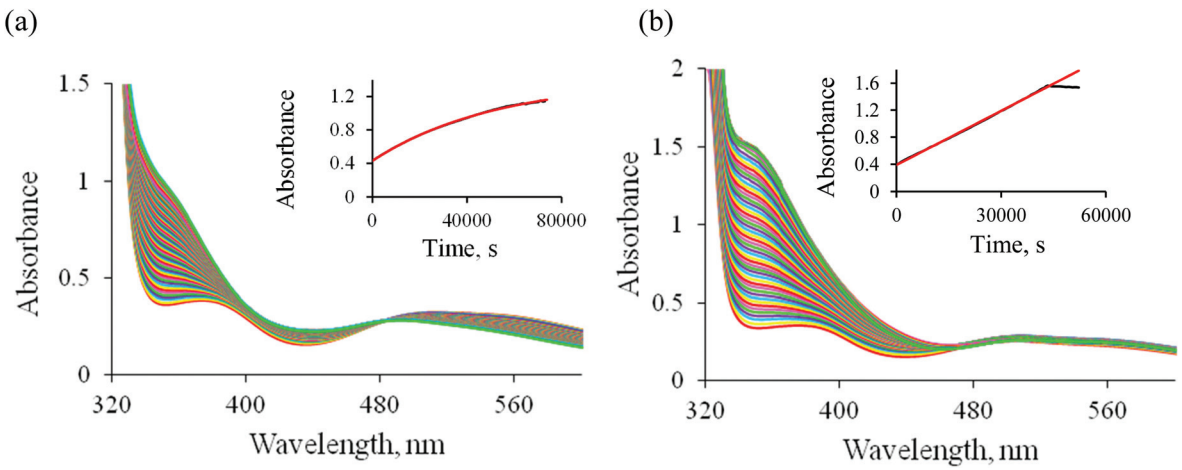


Fig. 34 Spectral changes observed during the catalysed reduction of $NAD^+$ to 1,4-NADH in the presence of formate. Experimental conditions: (a) $[HCOO^-]$ = 0.0011 M, (b) $[HCOO^-]$ = 0.0145 M; [Ru(II)] = $5.3 \times 10^{-5}$ M, $[NAD^+] = 3.1 \times 10^{-4}$ M, $T$ = 36.8 °C, 1 : 9 v/v $H_2O$/EtOH, spectra recorded every 900 s.

values may be additive or neutralising each other, wholly or partially.[1,4,231–233]

The history of development of empirical correlations for reaction rates in different solvents can be accessed from early prominent publications and traced through later developments.[225,234–237] One widely applied method in organic chemistry can be attributed to Grunwald and Winstein.[229] They were able to distinguish between $S_N1$ and $S_N2$ mechanisms for substitution at organic halides by using a solvent parameter derived from a reference value, and correlating this to logarithmic values of the rate constants; the correlation differed for the two mechanisms. In principle their method could be applied to some inorganic reactions, and analyses have been reported for M(III)-chloride hydrolysis (M = Co or Ru)[238] and for isomerisation of halo-alkyne and halo-alkene complexes of platinum.[239–242] Other solvent properties that have traditionally been used to provide correlation with kinetic parameters include ionic strength (the Brønsted–Bjerrum equation),[243–247] a dielectric constant $\varepsilon$ function $(\varepsilon - 1)/(\varepsilon + 2)$[248] and the Reichardt spectroscopically based $E_T$ parameter used in a kinetics study of the oxidative addition of methyl iodide, dihydrogen and dioxygen to Vaska's compound, *trans*-[IrCl(CO)($PPh_3$)$_2$].[249–251] For solubility and other reasons many inorganic reactions, particularly those of transition metal complexes have been conducted in aqueous medium or other solvents of suitable dielectric constant, whether the reactions are complex formation, ligand substitution, electron transfer or catalytic reactions.

Hereafter this introduction, perforce from the title, the only solvents under consideration will be individual ionic liquids, except where comparison with other solvents is required. A brief digression: mixed solvents have been used for some reactions, and a variety of solvent structure effects as well as marked solvation effect changes and other thermodynamic features can emerge from the analysis of the experimental data.[252] For example Caldin *et al.*, explored the kinetics of formation of metal complexes notably of Ni(II) in water with added mole fractions of methanol, or ethanol or *tert*-butyl alcohol. For formation of Ni(II)(2.2′-bipyridine), the thermally derived activation parameters correlated with the mole fraction of the added alcohol where the added co-solvent exerted a maximum structural effect upon the mixed solvent.[253–257] The compositions of maximum structuredness of specific aqueous solvent mixtures had been established from a variety of spectroscopic and thermodynamic data.[258] In another example, the kinetics of reduction of hexachloroiridate(IV) by iodide ion in mixed solvents could be analysed using transfer chemical potentials, either obtained directly from solubility measurements for the reactants, or by modelling the transfer chemical potentials from solubility measurements on the Ir(III) species, as the transition state model.[259] The volume of activation for the base hydrolysis of the $[Fe(gmi)_3]^{2+}$ cation, where gmi = MeN=CHCH=NMe, in water is significantly positive reflecting extensive hydroxide desolvation upon reaching the transition state. Upon addition of alcohols the volume of activation decreases markedly, consistent with a reduced solvational contribution, and reduces further at co-solvent mole fraction levels where a structural contribution in the mixed solvent is maximal. In the absence of a solvation component the intrinsic value of $\Delta V^{\ddagger}$ would be expected to be a negative value.[260]

A treatment derived originally by Savage and Wood for equilibrium properties in organic chemistry, involves addition of inert co-solutes/co-solvents to reactions in aqueous solution, and has been extended to the kinetics of inorganic reactions for which the mechanism in aqueous solution has been established.[261] In specific examples, the kinetics of base hydrolysis of some iron(II)-di-imine complexes were studied in the presence of varying concentrations of stereo-isomeric carbohydrates. The data (rate constants at different molalities of co-solute/co-solvent) are treated to yield a parameter that represents the difference sum of pair-wise Gibbs energy interaction parameters describing the interaction of the particular co-solute or co-solvent with the reactant and activated complex. Significant differences between the values of the parameter for different added co-solutes/co-solvents can be interpreted further.[262,263]

### 7.2 Ionic liquids

Organic solvents traditionally used in a vast range of industrial and academic chemistry applications began to become under increased scrutiny some time ago, as has been noted many times. Their properties, for example, flammability, volatility, toxicity, together with their undesirable environmental consequences, such as issues regarding disposal, led to searches for alternative solvent media whose properties are less disadvantageous. Frequently, science publications, such as Chemistry World (RSC) or Chemical and Engineering News (ACS), report that certain solvents are banned by regulatory agencies.

Searches for alternative solvents had limited success, until the full realisation of the value of ionic liquids, ILs, (*vide infra*). However, just one prior example is now cited. Some sixty years ago the solvent sulfolane, (tetrahydrothiophene-1,1-dioxide) produced in the petrochemical industry, became available and held promise for some applications.

It is a liquid at temperatures just above ambient, has low vapour pressure, boils at 285 °C, and is miscible both with water and some organic solvents. It has been exploited in industrial processes, but has seen less application in academic research. Sulfolane is toxic, and its combustion will yield $SO_2$. It is available commercially, and is cited with additional information in publications such as the Merck Index. Properties of sulfolane, "a versatile dipolar aprotic solvent" have been highlighted, quite recently.[264] Thus, although sulfolane has some favourable characteristic it has obvious drawbacks.

**7.2.1 Background to the growth of ionic liquids as solvents: applications in chemistry.** Although solvents comprised of cations and anions (ILs), have been known for a considerable time, very few were available and perhaps their full potential was not optimally recognised until two or three decades ago. However, that situation is now reversed and there has been an exponential growth in published research on the use and application of ILs, in synthesis, catalysis, electrochemistry

and other areas. In addition, there is a massive challenge to develop an insight into the liquid organisation and physicochemical properties of ILs beyond their measurable macroscopic properties. There have been some cautionary accounts regarding the validity of ILs as green and sustainable "wonder"/designer solvents. One needs to assemble a complete profile of energy and materials used in their preparation and manufacture, and that includes a full assessment of recycling or disposal issues as well as toxicity, beside economic factors, to claim the plaudits. It is beyond the scope of this article to describe or summarise the voluminous literature on various aspects of chemistry associated with ILs. However, several authoritative reviews are available; clearly this is a selection and the contributions of for example, the Seddon,[265–267] Welton[268–272] and Wasserscheid[273,274] groups, and the chemical review of MacFarlane and colleagues,[275] and many others are noteworthy.[276–278] Our emphasis in the van Eldik group, has been on understanding inorganic reaction mechanisms in ILs and we will present below a summary of the findings from investigations of an eclectic set of reactions mostly from the last decade. Our interest in reaction mechanisms in ionic liquids began almost twenty years ago.[279–281] Furthermore, beside the emphasis on a kinetics approach, we will present our endeavours to provide a systematic scale of properties of a component of several ILs, *viz*, a donor number related to the Gutmann scale, and acceptor values. From an experimental aspect, few earlier kinetics studies in ILs published before those reported by our group had used special fast reaction techniques, stopped-flow spectrometry or laser flash photolysis spectrometry, for example, or reactions at high hydrostatic pressures with ILs as solvents. A report from our group, earlier than some of those reported herein[279] had applied the stopped-flow method; however, different ILs from that used in that study, can possess different magnitudes of properties, for example viscosity. Our other early investigations in the IL research field are presented in other reports.[280,281] Therefore an additional challenge was to determine whether our experimental designs for future investigations would be amenable and compatible with other selected ILs as solvents.

We authored a brief tutorial review on reactions in ionic liquids as well as on general properties of ILs and this may serve as a starting point for newcomers to the field.[9] However, in-depth coverage should be accessed from the specialist literature.[265–278]

#### 7.2.2 Pt(II) chemistry in ionic liquids

*Kinetics of substitution reactions of a Pt(II) complex in an IL.*[282] The nucleophiles, thiourea (TU) and iodide ion, were reacted with $[Pt^{II}(apa)Cl]^+$ in [bmim][bta], in methanol and in water: apa is 2,6-bis(aminomethyl)pyridine and [bmim][bta] is 1-butyl-3-methylimidazoliumbis(tri-fluoromethylsulfonyl) amide (see Schemes 19 and 20).

The kinetics were monitored spectrophotometrically, as a function of temperature and pressure. The second-order rate constant, $k_2$, is greater for the reaction in water, compared

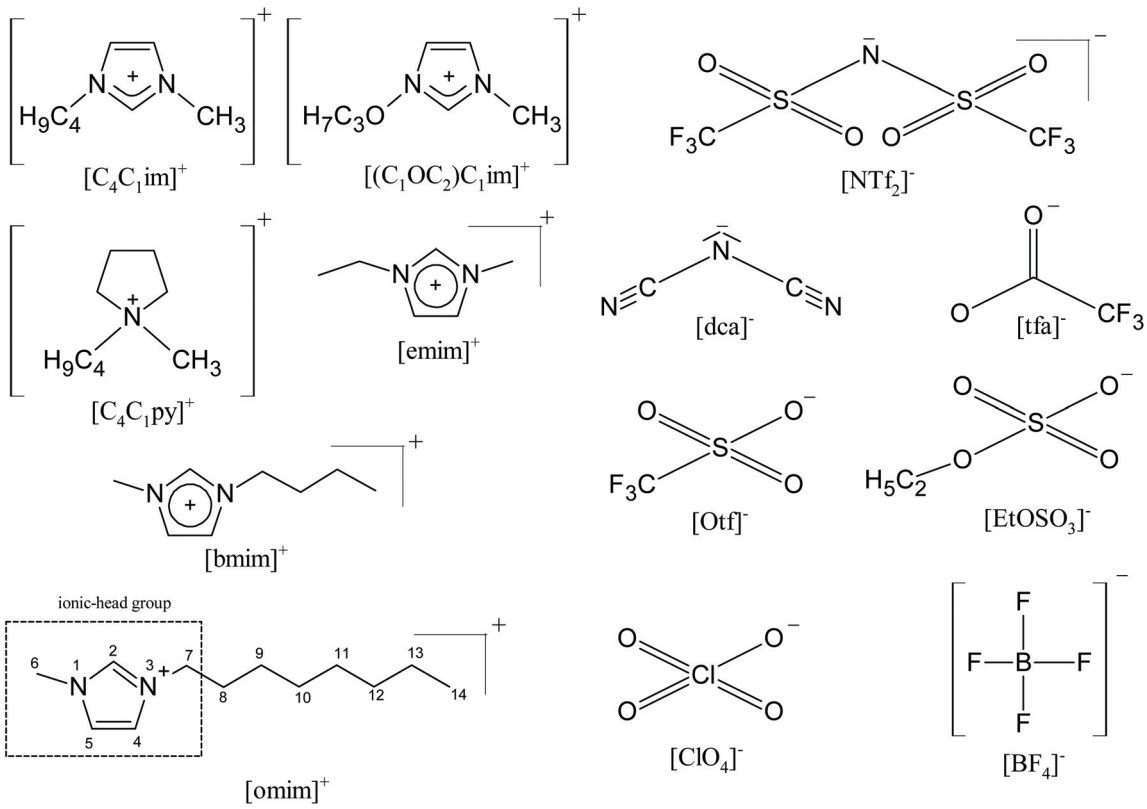


Scheme 19 Summary of abbreviations used for the cationic (left) and anionic (right) components of the ionic liquids.

 

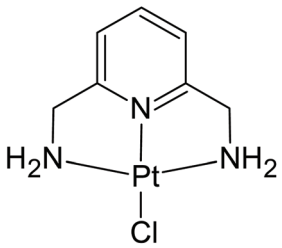


[Pt(apa)Cl]$^+$

**Scheme 20** Schematic presentation of the [Pt(apa)Cl]$^+$ complex ion.



with those of similar magnitude of $k_2$ for reaction in methanol and in the IL. The polarity of the latter is regarded as close to that of ethanol. To ascertain whether adventitious water in the IL might play a role, the substitution reactions was carried out in the presence of small added increments of water. The rate constants were essentially constant, indicating very little or no influence of the presence of minor quantities of water in the IL. The expectation from earlier work was that the mechanism would follow an associative character; this was borne out by the sign and magnitude of the entropies and of the volumes of activation. DFT calculations indicated that the mechanism could be an associative interchange mechanism. The entropies of activation were in the range of −40 to −90 J mol$^{-1}$ K$^{-1}$ (TU), and −50 to −60 J mol$^{-1}$ K$^{-1}$ (I$^-$), and the $\Delta V^{\ddagger}$ values were in the range −7 to −14 cm$^3$ mol$^{-1}$ (TU), and −7 to −14 cm$^3$ mol$^{-1}$ (I$^-$). The fact that the values of $\Delta V^{\ddagger}$ for reaction in the IL of both TU and I$^-$ are essentially identical, led to the notion that the IL is not sensitive to charge difference as the transition state is reached. Overall, the kinetics results and their analysis support the premise that the reactions in IL are parallel to those in conventional solvents. However, a more detailed discussion of the activation parameter differences for the different solvents and the two entering nucleophiles, and the subtleties involved in the analysis are accessible in the publication. It was noteworthy that this publication was believed to be the first in which a volume of activation had been determined and reported for reaction in an IL.

*Mechanistic studies on fast ligand substitution reactions of Pt (II) in IL.*[283] Having reported in the previous section upon the comparative reaction kinetics of a Pt(II) complex in an IL relative to "standard" solvents, it was incumbent upon us to choose a well-characterised reaction, as indicated in the previous sub-section title, and determine the reaction kinetics of substitution, in a range of ILs. It had become increasingly clear that acquisition of not only comparative kinetic data was desirable, but some of the properties of the individual ILs needed to be established. These are not just the obvious macroscopic properties, but those such as polarity of ILs and obtained as a function of temperature and of pressure, since variations of the latter, if found, could be valuable in understanding thermal and pressure-derived activation parameters. Further an assessment is required of the ability, or not, of a component of an IL to bond to a reactant, for example, the anion of an IL with a positively charged reactant or product. These considerations were addressed.[283]

The temperature dependence of the polarity of [emim][tfa], [emim][NTf$_2$] and [emim][dca] (Scheme 19), as well as for THF and methanol, was studied in the 10–50 °C temperature range on the basis of solvatochromic shifts using the Reichardt dye method and the phenol blue method. A small incremental decrease occurred with increase in temperature for the ILs, consistent with a trend for THF but with the latter possessing a much lower polarity level. The values for methanol are close to those of the ILs although the decrements of $E_T$ with temperature in methanol and in acetone are slightly larger. The kinetics of the substitution reaction of [Pt$^{II}$(terpy)Cl]$^+$ (terpy is 2,2′:6′,2″-terpyridine) by thiourea in four ILs were determined. The results for the reaction in methanol and water were reported earlier.[284] The ILs are [emim][NTf$_2$], [emim][dca], [emim][EtSO$_4$] and [emim][OTf]. The structures of the latter are shown in Scheme 19. The kinetics were followed as a function of excess TU concentration, and as a function of temperature. The derived second-order rate constants at 25 °C show a wide variation: the reaction in water was close to 3 × 10$^3$ M$^{-1}$ s$^{-1}$, while that for reaction in methanol is less than half of that value. In ILs the rate constants all in M$^{-1}$ s$^{-1}$ were significantly reduced; in [emim][NTf$_2$] 500, in [emim][dca] 153, in [emim][EtSO$_4$] 17.6, and in [emim][OTf] 11.8. The temperature dependence of the rate constants yielded markedly negative entropies of activation in all media, reflecting an associative character of the mechanism. It may be concluded that the reduction in reaction rate in ILs is a reflection of the interaction of the anionic component of the IL with the positive reactant Pt(II) complex. It appears that the electronic interaction of the anion and the Pt centre, where the electron density of the anion can shield the vacant $p_z$ orbital of the Pt centre and hinder nucleophilic attack by TU. There is an element of reinforcement of this effect by the high electrophilicity of the metal centre from the π-acceptor property of the terpyridine chelate. Computations indicate that the [EtSO$_4$] and [OTf] anions have a stronger ability than the [dca] and [NTf] anions for interaction with the Pt centre, findings that are consistent with the rate constant variations. Further calculations support this by showing the positions of anions relative to the Pt centre.

Some aspects of the results were considered in terms of the Kamlet–Taft (K–T) parameters; specifically the rate constants in ILs correlated with the $\beta$ parameter of the K–T relationship: $\beta$ is a measure of hydrogen bonding accepting basicity.[285] Results obtained from prudently chosen $^1$H and $^{13}$C NMR experiments provided support for the analysis. In addition, computations of the stabilisation energies of interaction between components of ILs were reported.

*Fast Substitution reactions of Pt(II) in ILs.*[286] In a study with some parallels to the report discussed above, the kinetics of substitution of the same terpyridine complex by the SCN$^-$ nucleophile have been investigated in the IL solvents possessing a common imidazolium cation, ([emim]), and with the

anionic components [$NTf_2$], [dca], [OTf], [$EtOSO_3$] as partners, and in methanol. Here an assessment can be made of the potential effect of changes to reaction kinetics upon using an anionic nucleophile, rather than a neutral one. This will be of value in understanding further the influence or not of varying ILs on reaction rates and derived properties. Using an excess of $SCN^-$, the kinetics for the reactions in the ILs [emim][OTf], [emim][dca] and [emim][$EtOSO_3$] yielded profiles that are fit by a single exponential. For the reaction in [emim][$NTf_2$] and $CH_3OH$, a second slower reaction was observed; that is a two-exponential fit of the data. The second step did not interfere with the characterisation of the former step. It is believed that the former step is the substitution of Cl, as is the case for those ILs in which a single step is observed, while the slower step may be the incipient dechelation of one terminal pyridine by $SCN^-$. The latter proposition has support from computational methods. Decreases in the derived second-order rate constant are accompanied by an increase in both $\Delta H^{\ddagger}$ and $\Delta S^{\ddagger}$. The second-order rate constants vary over three orders of magnitude, and the fastest substitution (in [emim][$NTf_2$]) is an order of magnitude slower than is the reaction in methanol. The biggest difference in reactivity from the results for reaction of the nucleophile TU is for the reaction of $SCN^-$ in [emim][$EtOSO_3$], a factor of 1300 times slower. The deceleration is expected upon changing from a neutral to a negatively charged nucleophile. The transition state for substitution is neutral for reaction with $SCN^-$ and thus less favoured in a solvent of high ionic strength. Thus the transition state is destabilised and the ground state stabilised accounting for deceleration for substitution by $SCN^-$ relative to that by TU. The question of why the substitution was 3 orders of magnitude faster in [emim][$NTf_2$] than in [emim][$EtOSO_3$] was addressed by examining the K–T β factor for the ILs. The latter solvent has an increased value over that for the former – resulting in a higher $\Delta H^{\ddagger}$ and a reduction of the reaction rate. The results suggest that among the solvent anions, those possessing an oxygen donor atom, for example $[EtOSO_3]^-$, may be part of the reason that they bind more strongly to solute species and decelerate the reaction. This seems to be the case for both charged and neutral nucleophile substitution moieties.

*An old reaction in new media.*[279] This contribution to the issue focuses on reports from our group, but it would be remiss if we did not include a contemporary publication regarding substitution of a Pt(II) complex in ILs from other investigators. Accordingly the paper of Correia and Welton is presented in summary, but readers are encouraged to view the paper itself for its in-depth analysis of results.[287] The kinetics of substitution of $[Pt(dpma)Cl]^+$ (see Scheme 21) by thioacetate, where dpma = di(2-picolyl)amine, were studied in water, methanol, DMSO and four ILs; [$C_4C_1$im][$NTf_2$]. [$C_4C_1$py][$NTf_2$], [$C_4C_1$py][OTf] and [$(C_3O)C_1$im][$NTf_2$]. The IL structures are in Scheme 19.

Other ILs were tested for their suitability as solvents for the reaction, but for technical reasons could not be employed. The derived second-order rate constants, $k_2$, were in the order: reaction in water > ILs ≈ DMSO > methanol. The solvent effect was examined using a linear solvation energy relationship based on the K–T solvent scale of parameters, $\alpha$, $\beta$ and $\pi^*$. The value of $k_2$ increases with H-bond donor ability and dipolar/polarizability of the solvent. This was established from an in-depth evaluation of the K–T parameters.

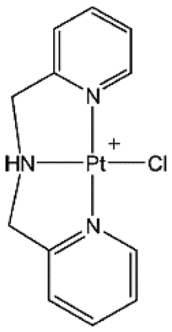


**Scheme 21** Schematic presentation of the $[Pt(dpma)Cl]^+$ cationic complex.

As in common with other substitution reactions of Pt(II) complexes (*vide supra*), the mechanism was common to all solvents, including ILs, as associative in nature. Confirmation of this was evident from the $\Delta H^{\ddagger}/\Delta S^{\ddagger}$ iso-kinetic plot, with an excellent correlation factor, and led the authors to conclude that an associative mechanism operates. In this case there was no special effect brought about by ILs as solvents.

### 7.2.3 Nitric oxide chemistry in ionic liquids

*The interaction of $Fe^{III}$(TMPS) with dissolved NO in an IL.*[288] Previously we have studied the reaction between different modified water soluble $Fe^{III}$(porphyrin) complexes and dissolved nitric oxide as a model system for ferrihaem proteins with a view of providing insight into mechanisms that may prevail in natural systems. It became of interest to extend our knowledge from an aqueous system to that of an IL solvent. Thereby the interaction of *meso*-[tetra-(3-sulfonatomesityl) porphin]-iron(III), ($Fe^{III}$(TMPS), see Scheme 22) with dissolved NO in 1-ethyl-3-methylimidazoliumbis-triflouromethyl-sulfonylamide ([emim][$NTf_2$]), was examined.

In water, $Fe^{III}$(TMPS), depending upon pH, exists as hexacoordinate diaqua [(TMPS)$Fe^{III}(H_2O)_2$], or as a penta-coordinate monohydoxo species [(TMPS)$Fe^{III}$(OH)], with a $pK_a$ of 6.9.

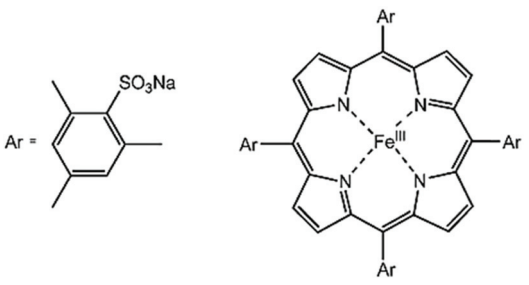


**Scheme 22** Schematic presentation of $Fe^{III}$(TMPS). Reprinted with permission from ref. 288. Copyright 2009 American Chemical Society.

 

Despite there being negatively charged substituents on $Fe^{III}$(TMPS) it can react not only with NO but also with nitrite ion. The latter can be present as an impurity or experiments can be conducted with nitrite ion deliberately added to the medium. Another revelation, unearthed from scrupulous, exhaustive inspection of relevant UV-Vis spectra, was that a minor quantity of *N*-methylimidazole (MeIm) could be present in the IL, as an impurity. The consequences can have a profound impact on the reaction at issue. Accordingly, a thorough purification of the IL samples was undertaken, and control experiments with deliberately added quantities of MeIm were conducted to resolve this issue. A comprehensive, creative regime design of experiments involving NMR and UV-Vis spectroscopies, the stopped-flow technique, with pressure and temperature dependencies of parameters determined, permitted the extraction of kinetic and activation parameters for the binding of NO and nitrite ion to $Fe^{III}$(TMPS) and of equilibrium parameters for the binding of nitrite. The presence of MeIm leads to the generation of hexa-coordinate (TMPS) $Fe^{III}$(OH)(MeIm). The reaction with NO occurs initially by the departure of MeIm, followed by the binding of NO yielding the species which may be written formally as the diamagnetic (TMPS)$Fe^{II}$(OH)($NO^+$), in the IL.

The reaction in the presence of MeIm is limiting dissociative in mechanism, (dissociation of MeIm), supported by the positive sign and magnitude of the entropy and of the volume of activation, +86 J $mol^{-1}$ $K^{-1}$ and +24 $cm^3$ $mol^{-1}$, respectively.

$$[(TMPS)Fe^{III}(OH)MeIm] \rightleftharpoons [(TMPS)Fe^{III}(OH)] + MeIm \quad (42)$$

$$[(TMPS)Fe^{III}(OH) + NO \rightarrow [(TMPS)Fe^{II}(OH)(NO^+)] \quad (43)$$

In marked contrast, in the absence of MeIm, the formation of the NO complex in the IL is accompanied by significantly negative activation parameters, the entropy and volume of activation were −53 J $mol^{-1}$ $K^{-1}$ and −20 $cm^3$ $mol^{-1}$, respectively, decisively indicative of an associative mechanism.

$$[(TMPS)Fe^{III}(OH) + NO \rightleftharpoons [(TNPS)Fe^{II}(OH)(NO^+)] \quad (44)$$

Repeating the extensive experimental data of the actual publication, and discussing the findings of the interaction of $NO_2^-$ with the (TMPS)$Fe^{III}$ complex are beyond the space available. Consultation of the original paper itself is highly recommended.

Beyond the significance of the results and the conclusions, it is clear that extraneous impurities in ionic liquids can have potentially serious consequences for investigators. In the study referred to above, the MeIm impurity was at a level of 6 μM as determined by ion chromatography. Although this may sound to be very low, in our case the (TMPS)$Fe^{III}$ complex was used at a concentration level of 2 μM, which accounts for the huge effect of the impurity! In addition to the issue of purity of ILs, the components of ILs may, in certain circumstances interact with solutes, and the interactions may not be readily detected, thus causing further complications.

*Kinetics, mechanism and spectroscopy of the reversible binding of NO to Fe(II) in an IL.*[289] Nitric oxide is a very important molecule in bioinorganic chemistry, and its binding to metal centres such as iron is the basis of the classic "brown-ring" reaction. The reaction has been thoroughly characterised in aqueous medium; therefore it was of considerable interest to endeavour to characterise the reaction in an ionic liquid. The ionic liquid selected, in part, because of its suitable properties as a solvent was [emim][dca] (see Scheme 19). It prevailed after a thorough examination of various properties that the iron(II) species that is generated in the IL and actually undergoes the reaction with NO is monomeric $[Fe(dca)_5Cl]^{4-}$ (see Scheme 23).

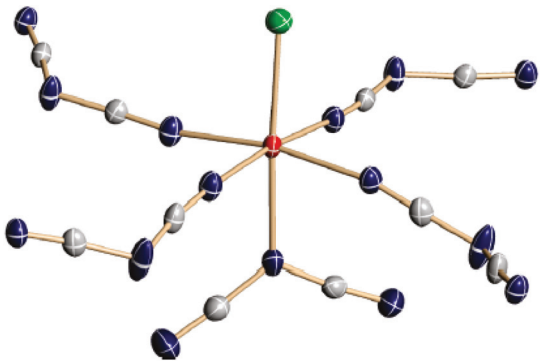

**Scheme 23** Schematic presentation of the $[Fe(dca)_5Cl]^{4-}$ complex anion in which four dca anions are coordinated in an end-on and the fifth one in the side-on mode. Reprinted with permission from ref. 289. Copyright 2011 American Chemical Society.

The equilibrium constant ($K_{eq}$) for reaction (45)

$$[Fe(dca)_5Cl]^{4-} + NO \rightleftharpoons [Fe(dca)_5(NO)]^{3-} + Cl^- \quad (45)$$

was determined to be 170 ± 20 at 25 °C. This value is a factor of six smaller than $K_{eq}$ in water. The accompanying thermodynamic parameters were established as follows: $\Delta H^\circ$ = +37 ± 1 kJ $mol^{-1}$, $\Delta S^\circ$ = −81 ± 4 J $K^{-1}$ $mol^{-1}$ and $\Delta V^\circ$ = −7.5 ± 0.2 $cm^3$ $mol^{-1}$, indicating among other factors that the products have a lower partial molar volume than the reactants.

A laser flash photolysis method was used to study the kinetics of the 'on' and 'off' reactions, a first for this method to be used for both ambient and elevated pressure measurements in an ionic liquid. The activation parameters are summarized in Table 15.

The mechanism in aqueous solution is a dissociative interchange ($I_d$) ligand substitution mechanism. The entropies and volumes of activation for the equivalent reaction in

**Table 15** Summary of the activation parameters for the reaction of Fe(II) with NO in the IL and water as solvent

| | $\Delta H^\ddagger$ [kJ $mol^{-1}$] | $\Delta S^\ddagger$ [J $mol^{-1}$ $K^{-1}$] | $\Delta V^\ddagger$ [$cm^3$ $mol^{-1}$] |
|---|---|---|---|
| **'On' reaction** | | | |
| IL | 27 ± 4 | −14 ± 12 | +14.3 ± 0.5 |
| $H_2O$ | 37.1 ± 0.5 | −3 ± 2 | +6.1 ± 0.4 |
| **'Off' reaction** | | | |
| IL | 66 ± 3 | −73 ± 9 | +25 ± 2 |
| $H_2O$ | 48 ± 1 | −15 ± 5 | −1.3 ± 0.2 |

[emim][dca] are clearly very different and point to a limiting dissociative (*D*), ligand substitution mechanism in both the 'on' and 'off' reactions, indicating the presence of an IL brings about that change. The difference arises from the participation of the IL anion. This is supported by the finding that in the solid state $[Fe(dca)_5Cl]_x[emim]_{2x}$ polymeric chains are formed, as verified by X-ray crystallography. The monomeric reaction product, $[Fe(dca)_5NO]^{3-}$ formed in the IL, was characterised thoroughly by IR, Mössbauer and EPR spectroscopies. The resemblance of the product to other nitrosyl complexes was discussed.

**7.2.4 Coordination of terpyridine to $Li^+$ in two ionic liquids.** This investigation follows for comparative or contrasting purposes with one in which the ligand used was 2,2′-bipyridine.[290–292] Lithium ions feature in many technical applications. It is of interest to discover the mode of interaction of components of ionic liquids, with respect to their donor or acceptor properties, regarding their coordination to lithium ions or other metal ions. In this study two ILs were selected, in part, because of their low donicity values and low coordination abilities. They were $[emim][NTf_2]$ and $[emim][ClO_4]$, the former somewhat hydrophobic while the latter is more hydrophilic in character. Complex formation of terpyridine with $Li^+$ was monitored by the shift in the $^7Li$ NMR signal as a function of the added ligand. Various, different equilibria can be formed between the IL solvent components, the ligand and the metal ion; these were to be established from the NMR measurements. It was further proposed to obtain the coordination arrangements in the solid state on the basis of X-ray diffraction measurements, and also from density functional theory computations. $Li^+$ ions dissolved in $[emim][NTf_2]$ exhibit a solvent shell of two $NTf_2$ anions coordinated as chelate ligands *via* sulfonyl oxygen atoms thus generating a tetrahedral coordination geometry at the lithium centre. Thus upon titration with terpyridine a successive displacement of bidentate $NTf_2$ anion ligands by terpy occurs. Thus it was concluded that the coordination sphere of $Li^+$ is saturated by two terpy ligands, a conclusion supported by computations. It was noted that there was a significant increase in stability of $[Li(terpy)_2]^+$ compared with $[Li(bipy)_2]^+$ studied previously in ILs. The smaller perchlorate anion, less sterically demanding led to higher competition between terpy and $ClO_4^-$ for interaction with $Li^+$. Therefore, the bis-terpy complex in $[emim][ClO_4]$ is of lower complex stability than it is in $[emim][NTf_2]$. The standard reaction parameters, $\Delta H^\circ$ and $\Delta S^\circ$ for complex formation provided a distinct difference: complex formation of $[Li(terpy)_2]^+$ in $[emim][NTf_2]$ was enthalpy driven, whereas formation in $[emim][ClO_4]$ was entropy driven. Previously the formation of $[Li(terpy)_2]^+$ in the non-ionic solvent nitromethane had been characterised thermodynamically; the stability constants were much in excess of the values for the terpy complexes in the two ILs reflecting the weaker solute–solvent interaction of the non-ionic solvent and suggesting a stronger chelating contribution to the stability. A similar trend was noted for the relative stabilities of $[Li(bipy)_2]^+$ in the three solvents at issue.

The preparation of solid state samples suitable for X-ray studies did not yield complexes of the same stoichiometry as in solution. The crystal structure obtained from the perchlorate-containing IL shows a dimeric lithium species $[Li(terpy)(ClO_4)]_2$. By contrast the composition of the solid species emerging from the $[emim][NTf_2]$ solvent is polymeric, $[Li(terpy)(NTf_2)]_x$. The geometries and organisations of the species are illustrated with colourful, artistic skill in the original publication. The detailed geometry of the solid species suggests that the crystallisation process may be controlled by charge neutralisation and π–π-stacking interactions.

**7.2.5 Gutmann donor and acceptor numbers for ionic liquids.**[293] In order to understand further the physicochemical properties of ionic liquids, it is necessary, as noted earlier, to proceed beyond bulk macroscopic properties. Beyond the intrinsic value of the knowledge of donor and acceptor properties of ILs, investigators can use the knowledge to select an IL for a required purpose; this could include, for example, in chemical synthesis or even to phase transfer catalysis as highlighted in a recent report.[294] Other reports have cited values of such properties, according to various references or definitions, and with a range of experimental methods; thus the current work will be set in context of other notable developments, somewhat later in this section.

Herein the objective was to determine a quantitative set of values for ILs, in which in many cases the cationic component will be common, as an imidazolium species, $[emim]^+$, varied in some cases by change of the alkyl substituent, while the anionic partners will be a broad range of species, ranging from those somewhat familiar in the IL community to less well known or even rare anionic species. There is scope to modify the anion of the IL in order to fine tune a donor or acceptor value, in the sense that the interaction of solute substrates can be ascertained, and adapted as needed. For example, electron rich nucleophiles could react with metal centres. The properties of ILs can then be compared or contrasted with those of molecular solvents. An advantage is that the methods used to obtain each donor or acceptor value will be the same for each IL.

Donor numbers (DNs) were obtained by $^{23}Na$ NMR spectroscopy, and showed a pronounced dependence on the anionic component. This method had been applied earlier[295] for solvents for which the calorimetric methods of Gutmann[296] were not feasible. One principal reason to use this approach was to ensure comparability of our results with those reported earlier. The DN values for 26 different ionic liquids were obtained and listed (see Table 16); the values covered a wide range and were thoroughly analysed.

Other work, as reported by Linert *et al.*[297] used a solvatochromic indicator method for measuring DNs (see correlation shown in Fig. 35). It was shown by Marcus[298] that the $\beta$ parameter (hydrogen bond acceptor parameter) of the K–T relationship correlated with the Gutmann DN values. Although probably of more value as a qualitative measure of DNs, the HSAB concept of Pearson[299] was included in the discussion on the subject of several contributions. Another concept within the

 

Table 16 NMR spectroscopy data and DNs for the investigated ILs. All measurements were carried out at 298 K (exceptions are given in brackets). Reprinted with permission from ref. 293. Copyright 2012 WILEY-VCH Verlag GmbH & Co. KGaA, Weinheim

| IL | Chemical shift of $^{23}$Na [ppm] | Donor number [kcal mol$^{-1}$] | IL | Chemical shift of $^{23}$Na [ppm] | Donor number [kcal mol$^{-1}$] |
|---|---|---|---|---|---|
| [emim][FAP] | −21.378 | −12.3 | [emim][B(CN)$_4$] (328 K) | −5.646 | 20.8 |
| [emim][PF$_6$] | −18.509 | −6.2 | [emim][NO$_3$] | −5.010 | 22.2 |
| [emim][SbF$_6$] | −13.326 | 4.7 | [emim][EtOSO$_3$] | −4.966 | 22.3 |
| [C$_{12}$mim][NTf$_2$] | −12.356 | 6.7 | [emim][HexOSO$_3$] | −3.146 | 26.1 |
| [emim][Pf$_2$N] | −12.145 | 7.2 | [emim][TCM] | −3.131 | 26.1 |
| [emim][BF$_4$] | −12.086 | 7.3 | [emim][BuOSO$_3$] | −2.954 | 26.5 |
| [C$_{10}$mim][NTf$_2$] | −12.000 | 7.5 | [emim][(EtO)$_2$PO$_2$] | −0.683 | 31.3 |
| [emim][ClO$_4$] | −11.951 | 7.6 | [emim][DCA] | 2.389 | 37.8 |
| [C$_8$mim][NTf$_2$] | −11.622 | 8.3 | [emim][NO$_2$] (348 K) | 2.946 | 38.9 |
| [C$_6$mim][NTf$_2$] | −11.497 | 8.5 | [emim][SnCl$_3$] | 3.166 | 39.4 |
| [C$_4$mim][NTf$_2$] | −10.696 | 10.2 | [emim][Ac] | 5.030 | 43.3 |
| [emim][NTf$_2$] | −10.220 | 11.2 | [emim][SCN] | 6.257 | 45.9 |
| [C$_8$mim][OTf] | −6.712 | 18.6 | [emim][MeOAc] | 7.610 | 48.8 |
| [emim][B(CN)$_4$] | −5.895 | 20.3 | [omim][I] | 12.605 | 59.3 |
| [emim][OTf] | −5.840 | 20.4 | [C$_{10}$mim][Cl] (328 K) | 16.030 | 66.5 |
| [emim][PO(EtHex)$_2$] | −5.828 | 20.5 | [omim][Cl] | 17.327 | 69.2 |
| [C$_4$mim][OTf] | −5.826 | 20.5 | [emim][Cl] (358 K) | 18.981 | 72.7 |
| [emim][OctOSO$_3$] | −5.761 | 20.6 | [emim][Br] (358 K) | 20.858 | 76.7 |

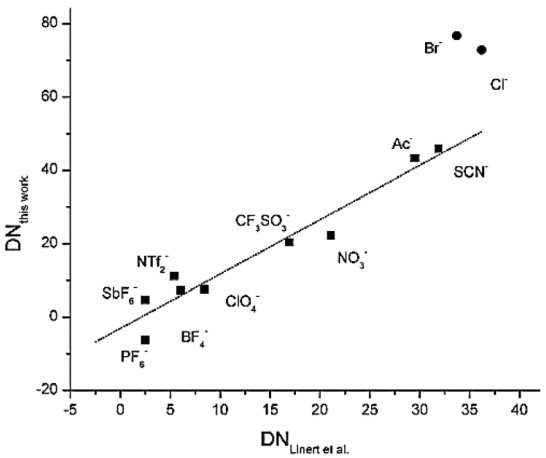


Fig. 35 Correlation between DNs for anions determined by Linert *et al.*,[297] and those for the corresponding [emim]-based ILs. Reprinted with permission from ref. 293. Copyright 2012 WILEY-VCH Verlag GmbH & Co. KGaA, Weinheim.

Table 17 The $^{31}$P chemical shifts and ANs for the ILs under investigation. Reprinted with permission from ref. 293. Copyright 2012 WILEY-VCH Verlag GmbH & Co. KGaA, Weinheim

| Solvent | $^{31}$P NMR $\delta_\infty$ [ppm] | AN |
|---|---|---|
| [emim][EtOSO$_3$] | −9.067 | 25.0 |
| [C$_{12}$mim][NTf$_2$] | −9.081 | 25.0 |
| [C$_8$mim][NTf$_2$] | −9.322 | 25.6 |
| [emim][NTf$_2$] | −10.107 | 27.4 |
| [emim][FAP] | −10.904 | 29.3 |
| [emim][TCM] | −10.943 | 29.4 |
| [emim][dca] | −11.939 | 31.7 |
| [emim][SCN] | −12.211 | 32.4 |
| [emim][BF$_4$] | −12.688 | 33.5 |
| [emim][OTf] | −14.218 | 37.1 |
| [emim][ClO$_4$] | −21.458 | 54.0 |
| [emim][SnCl$_3$] | −30.593 | 75.4 |

subject of DNs, is that of "ionicity" as described by Watanabe *et al.*[300] In their report they showed the change in ionicity was proportional to, and decreases markedly, with elongation of the alkyl chain of the imidazolium moiety, although the changes in corresponding DN vales are relatively small. Steinrück *et al.*[301] used X-ray photoelectron spectroscopy to provide insight into DN values. In our work we determined bonding energies between the separate components of the ILs and their conformation as adjacent partners from DFT calculations. The bonding energies thus calculated could be analysed in terms of the composition and structure of the respective cations and anions.

Acceptor numbers (ANs). These were obtained by application of $^{31}$P NMR spectroscopy, and revealed a variation as a function of the cationic and anionic components of the IL (see Table 17). The method of processing the NMR data was modified from the procedure originally used by Gutmann.[296] AN values obtained were close to the acceptor values of aliphatic alcohols as the electrophilic properties are similar, but in most cases the range of variation was very much smaller than for DNs. Small differences were noted in ANs for imidazolium cations containing longer alkyl chain moieties. This is consistent qualitatively with the case for DNs. It may be suggested that longer alkyl residues give rise to increasing steric hindrance of cation-anion interaction, and aggregation of long chain imidazolium cations *via* van der Waals forces, thus impeding solvent–solute interactions. In general the values obtained from our measurements are in agreement with those reported by others.

Photoelectron emission spectroscopy (PEES) was used by Katoh *et al.* on ILs containing the $BF_4^-$ and $NTf_2^-$ anions paired with imidazolium based cations to determine their AN values.[302] Their data were compared with the PEES results of Watanabe and the assigned values, close to 25, were compar-

able to our results. A report by Kimura *et al.*[303] described the application of Raman spectroscopy using diphenylcyclopropanone as a probe to determine AN values for [bmim][$BF_4$] and [bmim][$NTf_2$]; again our results were consistent with those reported.[293]

It should be noted that some very high values of AN have been found for ILs containing metal chloride moieties as anion partners with typically [emim] or [omim] cations. The IL that recorded the highest AN value in our study was [emim][$SnCl_2$] (a 1 : 1 mixture of [emim][Cl] and $SnCl_2$). The higher acceptor property originates from the high Lewis acidity of $SnCl_2$, rendering this IL as a strongly electrophilic medium. This finding is consistent with the results of Seddon *et al.*[304] whose values of AN showed variation according to the composition of "melts" using $InCl_3$, $GaCl_3$ and $AlCl_3$ as Lewis acids. This aspect of high ANs in this context had been addressed earlier by Osteryoung.[305]

In summary, in this section we have described the methods used to obtain respectively DN and AN values for a large number of ILs, composed of imidazolium based cations, with a wide variety of composition and structure among the partnering anions. In one sense this section also forms a review of many earlier contributions, as referenced, and they were used as a context background for our investigations.

After the appearance of the publication "Gutmann donor and acceptor numbers in ionic liquids", Gal and Laurence queried the reliability of the $^{23}$Na NMR experimental method for generating authentic Gutmann scale DNs for ILs.[306] They were echoing mostly misgivings in earlier publications on the subject.[307,308] However, there was acknowledgement that our publication provided a valuable source of DN parameters for a considerable number of ILs. In an ensuing communication[309] the DNs were cited to be perhaps more appropriately termed Popov-Gutmann DN values in order to acknowledge that their values could be recognised as being developed from the method of Erlich and Popov.[295] Seddon has hinted that the differences determined for DN and AN numbers may well reflect differences in the methods used to obtain them or differences of the properties of probe molecules.[304]

**7.2.6 Studies of the reaction of iron(II) with NO in a non-coordinating ionic liquid.**[310] Earlier the reaction of an Fe(II) species with NO in an IL containing a strongly coordinating solvent component, the dca anion was described. We were curious regarding the outcome of a parallel investigation using an IL with the same cationic component as in the earlier study but employing an anionic component of weakly coordinating ability. The ion selected to partner the $[emim]^+$ species was $OTf^-$ where $OTf^-$ is the trifluoromethylsulfonate ion. Not surprisingly there were marked differences in several aspects. The solubility of $FeCl_2$ in [emim][OTf] is limited; this limitation could be addressed by the addition of chloride ions and/or water. Formation parameters for the reaction of the iron species present in [emim][OTf] with NO were determined. Of particular note was the standard entropy of formation which was distinctly positive which reflects the fact, also from other observations, that $OTf^-$ is not coordinated to the iron centre, which is only coordinated by $Cl^-$ or $H_2O$ ligands. As noted above, the corresponding reaction in [emim][dca] is characterised by a significant decrease in entropy where the Fe centre is coordinated to five $dca^-$ ligands well incorporated in bulk solvent. In [emim][OTf] the reaction may be described as in eqn (46):

$$[emim]_2[FeCl_4] + NO \rightleftharpoons [emim][FeCl_3NO] + [emim][Cl] \quad (46)$$

The composition of the reactant species, containing the tetrachloridoferrate complex ion, was established from an X-ray crystallographic study. The UV-Vis spectrum of the product resembles that formed in water and in [emim][dca]. However, the $\{Fe–NO\}^7$ species has $Fe^{II}–NO^{\bullet}$ character, in contrast to $Fe^{III}–NO^-$ species formed in other solvents. A comprehensive experimental study employing Mössbauer spectroscopy showed a dissimilarity between the iron-containing product in [emim][OTf] from that in water and [emim][dca], confirming the presence of an iron(II) species in solution and the absence of an iron(III) species, revealing that indeed oxidation does not occur in this case upon binding of NO. The nature of the product in the equation above was confirmed by EPR and IR spectroscopy experiments and analysis of the results. In summary, it is clear that in studying transition metal ions in ILs the anion component of the IL can give rise to very different product outcomes.

**7.2.7 Insertion mechanism of $CO_2$ in a ruthenium complex.** This perspective article incorporates many of the features and analyses in the earlier sections of this component of the journey within our group. It thus represents, in part, a review of the need to be cognisant of the donor and acceptor properties of the ILs, and incorporates the relevance to the reactions described therein.[311]

However, one section of the perspective has not been presented hitherto, and yet the chemistry involved has the potential to address a well-known environmental issue: the removal of excess carbon dioxide from the atmosphere. One potential method described involves activation of $CO_2$ by a hydride transfer reaction in which $CO_2$ is reduced to formic acid, and thence further reduction. A ruthenium complex, [Ru(bipy)(terpy)H]$^+$ (Scheme 24) abbreviated Ru–H, reacts to permit


**Scheme 24** Schematic presentation of the structure of [Ru(bipy)(terpy)H]$^+$. Reprinted with permission from ref. 312. Copyright 2012 American Chemical Society.

 

insertion of $CO_2$ to form the formate complex, [Ru(bipy)(terpy)(OCHO)]$^+$ as shown in reaction (47).[312]

$$[Ru(bipy)(terpy)H]^+ + CO_2 \rightarrow [Ru(bipy)(terpy)(OCHO)]^+ \quad (47)$$

The reactivity of the hydride complex depends upon the acceptor properties of the solvents employed. Thus depending on the ability of a solvent to accept electron density, the hydridic character of Ru–H can vary as an effect of stabilisation or of destabilisation. A corollary of a solvent acceptor property range is that employment of an IL as solvent permits an investigation of the influence of the acceptor property of the IL. Furthermore, there may be an advantage if $CO_2$(g) has a higher saturation level in the IL, with respect to other solvents. Another aspect may be that kinetics studies are experimentally more straightforward in an IL, because the insertion reaction of $CO_2$ into Ru–H in aqueous solution is bedevilled by the consequence of the autoprotolysis of water, the formation of bicarbonate ion. However, the experimental difficulty of the latter could be circumvented by use of suitable buffer media, judicious choice of pH and employment of the pH-jump stopped-flow method. The kinetics of the insertion reactions were studied in aqueous solution, as a reinvestigation in methanol and ethanol, and in the ionic liquid [emim][$NTf_2$]. The IL was selected as it exhibited suitable properties of high optical purity, low viscosity and a moderate AN value.

In all cases under the reaction conditions applied, the kinetics followed a single exponential profile and $CO_2$ insertion is an irreversible reaction. The kinetic data and activation parameters derived from them for reaction in each solvent were tabulated. Of particular interest to us were the volumes of activation, and since there is no leaving group in the insertion reaction, on that basis alone, in the absence of changes in solvation, the value of $\Delta V^{\ddagger}$ should be negative and by a quantity reflective of the partial molar volume of $CO_2$. It prevails that changes in solvation upon reaching the transition state should be minimal as there is no overall change in charge proceeding through the transition state. In methanol and in ethanol $\Delta V^{\ddagger}$ was −36 and −39 cm$^3$ mol$^{-1}$, respectively, values thought to be consistent with the decrease in volume arising from insertion of $CO_2$. The values in water and in [emim][$NTf_2$] were considerably less negative, −14.4 cm$^3$ mol$^{-1}$ in [emim][$NTf_2$], but since the partial molar volume of $CO_2$ in the IL is not known with any certainty, a commitment to interpretation cannot be made. The insertion reaction in water is characterised by an even more modest negative value of $\Delta V^{\ddagger}$ = −5.9 cm$^3$ mol$^{-1}$. This was hypothesized to result from rearrangement of the solvation shell through formation and cleavage of hydrogen bonds. Such changes in the solvent shell account for the positive entropy of activation value in water whereas this parameter is markedly negative in the other solvents. The hydridic character of Ru–H markedly depends on the ability of surrounding solvent molecules to accept electron density. A relationship between the rate constant (logarithmic value) for insertion and the solvent AN has been noted by Konno *et al.*[313] Although ethanol has a higher AN value than that of [emim][$NTf_2$], the relevant rate constants are within the same order of magnitude.

### 7.3 Conclusions

In the Introduction selected aspects of the importance of solvation by traditional solvents with respect to kinetics and mechanism investigations, in the period prior to the widespread emergence of ionic liquids as solvents, were described. Clearly such history requires elaboration by consulting the original reports provided. Our interest, while not unaware of the broad range of research involving ILs in, for example, synthesis, catalysis, or electrochemistry, is an emphasis on detailed mechanistic studies of inorganic reactions in different ILs. This has necessitated employing various spectroscopic and kinetics techniques, and, where appropriate, providing support of experimental results from computations principally using DFT methods. As may be seen from the contents of this section, a diverse set of reactions has been selected for inclusion, involving ligand substitution, complex formation or insertion reactions. The properties of ILs and their components are an integral part of the intimate mechanisms in some cases; that is an anionic component of an IL can become part of the solute reactant. This behoved us to derive a scale of physicochemical properties for a large range of ILs, particularly of a wide range of anionic partners. There were methods already established for this purpose for some solvents, and our findings were described in comparison, in the context of the literature. Many fascinating chemistry insights have been obtained from the diverse chemical reactions we have described, and many more remain to be discovered.[294]

## 8. Mechanistic insight from computational chemistry

### 8.1 Introduction

As an experimental group interested in IRM, it is clear that we did not have the expertise to be involved in computational work. However, we were fortunate in Erlangen to be able to collaborate with our colleagues from the Computer-Chemistry-Centre that extended our mechanistic insight through the application of DFT methods. It is important to note that in most cases we had experimental results at hand, such as activation enthalpy and activation entropy data that required further mechanistic clarification. Personally, the corresponding author finds it difficult to accept computational studies in the absence of any kinetic data such as rate constants and activation parameters due to uncertainty in DFT calculations using a range of 'favoured' basis sets (see further Discussion).

### 8.2 Ligand exchange processes on solvated lithium cations

In a series of papers[290,314–318] a systematic study on ligand exchange reactions of solvated lithium cations was undertaken. Water exchange reactions on $Li^+$ are extremely fast and

on the basis of complex-formation data was predicted to be *ca.* $10^9$ $s^{-1}$ at 25 °C.[319,320] The application of B3LYP/6-311+G** was used to calculate the energy profiles for water and $NH_3$ exchange around the lithium cation as shown in Fig. 36. Water exchange proceeds through a trigonal bipyramidal five-coordinate intermediate $[Li(H_2O)_5]^+$ that is reached *via* a late transition state. In the case of $NH_3$ exchange, the fifth $NH_3$ from the second coordination sphere is weakly bound through a hydrogen bridging bond to two $NH_3$ ligands in the first coordination sphere. It follows from the energy profiles that the water exchange reaction favours a limiting associative (A) mechanism, whereas $NH_3$ exchange favours an associative interchange ($I_a$) mechanism.

In a subsequent study,[316] $^7$Li NMR spectroscopy was used to study complex-formation reactions of the lithium cation in DMSO/γ-butyrolacetone and water/DMSO mixtures. Addition of DMSO to γ-butyrolacetone as solvent evidenced the formation of a 1 : 4 complex between Li and DMSO. In the case of the water/DMSO mixed solvent, no selective solvation was detected, indicating that on increasing the water content of the solvent mixture, DMSO is gradually displaced by water in the coordination sphere of $Li^+$. The ligand-exchange mechanism of $Li^+$ solvated by DMSO and water/DMSO mixtures was studied using DFT calculations. The energy profiles shown in Fig. 37 demonstrate that DMSO exchange follows an associative mechanism characterized by a five-coordinate intermediate, whereas the substitution of water by DMSO proceeds through an associative interchange mechanism. No stable five-coordinate intermediate could be found, despite extensive searches.

In another study,[317] we used $^7$Li NMR chemical shifts to indicate that the $Li^+$ cation is coordinated by four acetonitrile molecules in nitromethane as solvent. In the water/acetonitrile (ACN) mixture, we found that water coordinates more strongly to $Li^+$ than acetonitrile, such that addition of water leads to the formation of $[Li(H_2O)_4]^+$. The solvent exchange mechanisms for $[Li(ACN)_4]^+$ and $[Li(HCN)_4]^+$ were studied by DFT calculations (RB3LYP/6-311+G**) and found to follow limiting associative mechanisms involving the formation of relatively stable five-coordinate intermediates.

In two further studies,[315,318] the coordination of $Li^+$ by different cryptands (see Scheme 25) in γ-butyrolacetone and acetone as solvent, was investigated using $^7$Li NMR spectroscopy as a function of temperature and high pressure (up to 150 MPa). In the case of γ-butyrolacetone as solvent,[315] the kinetic experiments indicated that the rate of the exchange reaction increased not only with increasing cavity size of the cryptand, but also with increasing concentration of the

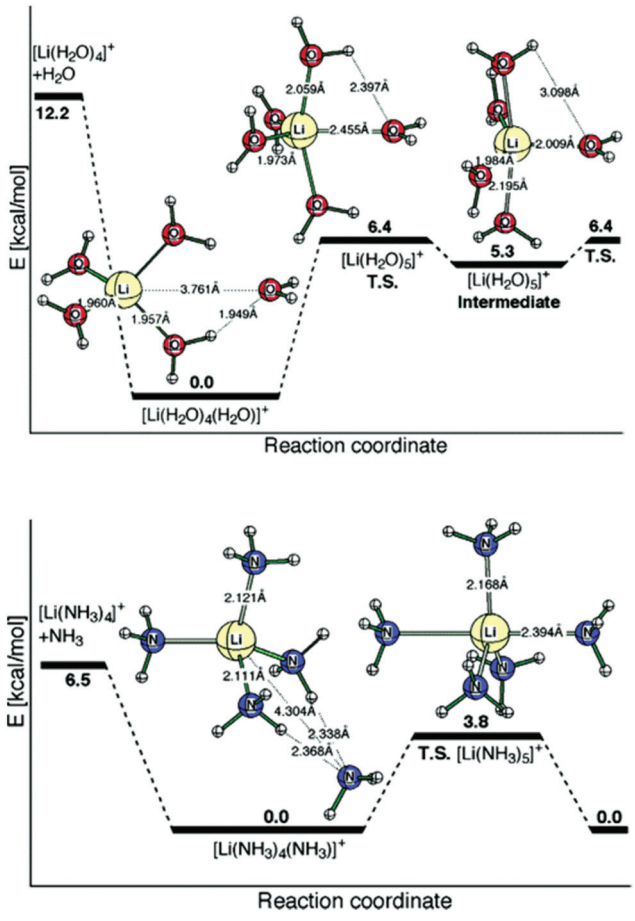


Fig. 36 Energy profiles for water (top) and $NH_3$ (bottom) exchange around the solvated $Li^+$ cation (relative energies: B3LYP/6-311+G**). Reprinted with permission from ref. 314. Copyright 2004 American Chemical Society.

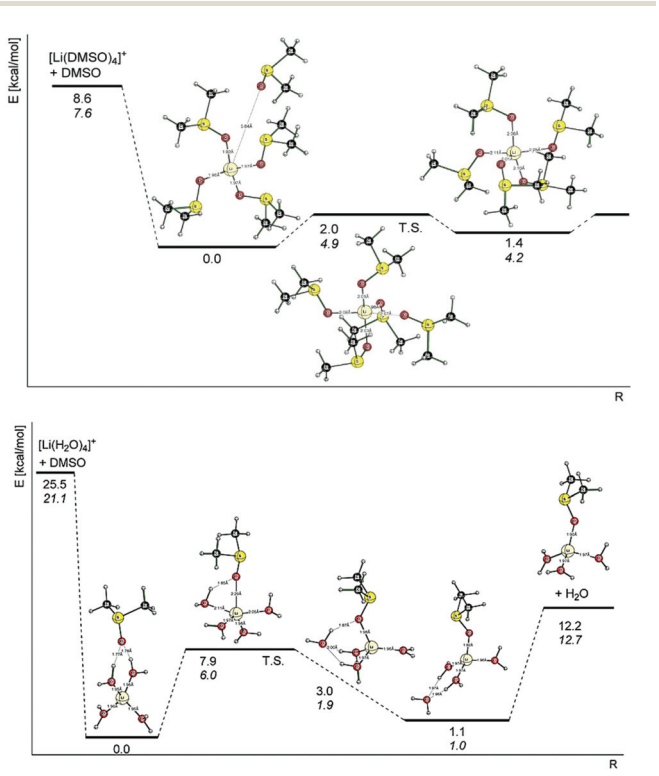


Fig. 37 Energy profiles for DMSO exchange on $[Li(DMSO)_4]^+$ (top) and $[Li(H_2O)_4]^+$ (bottom). Reprinted with permission from ref. 318. Copyright 2007 WILEY-VCH Verlag GmbH & Co. KGaA.

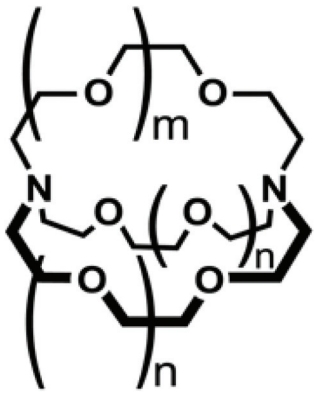

Scheme 25 Structure of the cryptands used in the reported studies: C211: $m = 0$, $n = 1$; C221: $m = 1$, $n = 0$; C222: $m = 1$, $n = 1$.[315,318]

Table 18 Values of $k_{obs}$ calculated from the NMR line shape for $Li^+$ exchange between solvated and chelated sites at 25 °C [315]

| Mole ratio C221 : $Li^+$ | $k_{obs}$, $s^{-1}$ | Mole ratio C221 : $Li^+$ | $k_{obs}$, $s^{-1}$ |
|---|---|---|---|
| 0.4 | 2.68 ± 0.05 | 0.35 | 654 ± 13 |
| 0.5 | 4.3 ± 0.1 | 0.45 | 851 ± 25 |
| 0.65 | 6.9 ± 0.3 | 0.55 | 1282 ± 51 |
| 0.8 | 9.6 ± 0.5 | 0.65 | 1352 ± 68 |

chelate, as can be seen from the values of $k_{obs}$ in Table 18. The activation entropy for the exchange process is significantly negative and points to the operation of an associative interchange ($I_a$) mechanism.

The effect of pressure on the exchange reaction was found to be very small, such that the rate constants calculated for each pressure were very similar within the experimental error limits and resulted in $\Delta V^{\ddagger} \approx 0$. This points to an interchange mechanism where bond formation and bond cleavage occur in a concerted fashion without the formation of a distinct intermediate of higher or lower coordination number. This conclusion was supported by DFT calculations.[315]

In the case of acetone as solvent,[318] a very similar reaction behaviour was found and detailed $^7$Li NMR line broadening experiments as a function of temperature and pressure were performed. The reported activation parameters favour an associative exchange process in line with the reported DFT calculations. In this case $\Delta V^{\ddagger}$ was also found to be close to zero.

In a more recent study,[290] $^7$Li NMR spectroscopy was used to study the complexation of $Li^+$ by the chelates shown in Scheme 26. In a weakly coordinating solvent such as nitromethane, the $^7$Li NMR data revealed evidence for the formation of tetrahedral 1 : 2 complexes of $Li^+$ with both bipy and phen. DFT (B3LYP/LANL2DZp) structures of both complexes were calculated. In the case of biox, a ligand that is of catalytic importance, we used γ-butyrolactone as solvent because of the poor solubility of biox in nitromethane. The experimental results revealed that the $^7$Li signal is shifted to higher field on stepwise addition of biox, but the shift represents only a small

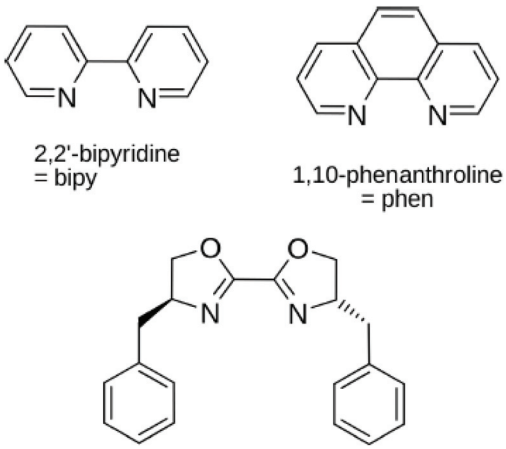


Scheme 26 The chelates used in this study.[290]

effect, indicating that coordination of biox to $Li^+$ is not favourable at all. Thus, determination of the coordination number is not possible using $^7$Li NMR techniques. This is in agreement with the DFT (B3LYP/LANL2DZp) calculations, which clearly indicate that the non-favoured coordination of biox is not caused by steric effects but rather by the different electronic nature of the heterocyclic systems.[290]

### 8.3 Ligand exchange processes on solvated beryllium cations

Despite the high toxicity of beryllium and its compounds, beryllium plays an important role in the modern world. This element attracted our attention in its cationic form and the way it interacts with solvent molecules and ligands. Earlier work by Merbach *et al.* focussed on the mechanistic clarification of solvent exchange reactions through the application of high pressure $^{17}$O NMR techniques.[321] The reported activation volumes varied from −13.6 ($H_2O$), −2.5 (DMSO) and −3.1 (DMF) to +10.5 (tetramethylurea) and +10.3 (dimethylpropyleneurea) $cm^3\ mol^{-1}$, covering the whole range of limiting A to D mechanisms. Our DFT calculations focussed on the exchange of small solvent molecules such as $H_2O$, $NH_3$, $CO_2$, $H_2CO$, MeOH, $Me_2O$, HCN, $N_2$ and CO on $Be^{2+}$. In all cases $Be^{2+}$ forms a tetrahedral complex of the type $[Be(sol)_4]^{2+}$ for which the calculations favoured a transition state typical for an associative interchange ($I_a$) mechanism as shown for the water exchange reaction in Fig. 38. The more bulky solvent molecules as studied by Merbach *et al.* will cause steric hindrance on the $Be^{2+}$ centre and prevent an associative attack by the entering solvent molecule, thereby favouring an $I_d$ or $D$ mechanism. In a later study,[322] the effect of water clusters and the selected DFT levels were studied in more detail for the water exchange reaction on $[Be(H_2O)_4]^{2+}$. The lowest barrier of 8.3 kcal $mol^{-1}$ for the water exchange process in terms of an $I_a$ mechanism, was obtained by optimizing the precursor and transition states within the PCM- and CPCM-solvent models.

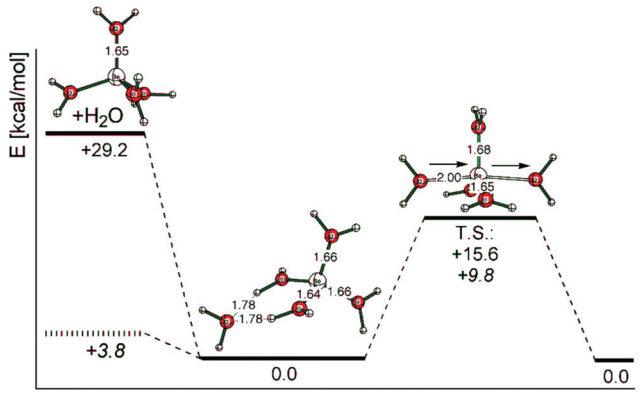


Fig. 38 Energy profile for the exchange of $H_2O$ around $Be^{2+}$. Distances in Å, energies in kcal $mol^{-1}$. Calculated at the B3LYP/6-311+G** and B3LYP(IPCM)/6-311+G** levels (energy value in italics). Reprinted with permission from ref. 322. Copyright 2005 Verlag Helvetica Chimica Acta AG, Zürich, Switzerland.

In a subsequent study,[323] DFT calculations at the B3LYP/6-311+G** level were used to optimize the structure of $[BeCl(12\text{-crown-4})]^+$ and $[Be(solvent)(12\text{-crown-4})]^{2+}$ which are quadratic pyramidal complexes. In the case of the chlorido complex, the X-ray structure is known[324] and compares well with the computed structure shown in Fig. 39 (left). The water exchange reaction of the five-coordinate $[Be(H_2O)(12\text{-crown-4})]^{2+}$ complex ion follows an $I_a$ mechanism as can be seen from the energy profile reported in Fig. 39 (right).

Finally, we would like to mention two contributions in which more mechanistic information on water exchange reactions of $Be^{2+}$ metal complexes was obtained. In the one case,[325] protonation of the 1*H*-imidazole-4,5-dicarboxylate chelate in the $[Be(H_2O)_2(1H\text{-imidazole-4,5-dicarboxylate})]$ complex reduced the activation barrier for the $I_a$ water exchange process from 16.6 to 13.8 kcal $mol^{-1}$, which is the same as that found for water exchange on $[Be(H_2O)_4]^{2+}$. In the other case,[326] it was found that the displacement of one coordinated water molecule by ligands such as $H^-$, $F^-$, $Cl^-$, $Br^-$, $OH^-$, $CN^-$ and $NCNCN^-$, had practically no influence on the rate of the water exchange reaction in $[Be(X)(H_2O)_3]^+$.

### 8.4 Host–guest complexes: prediction of ion selectivity by quantum chemical calculations

The well-known cryptand [2.2.2] and its derivatives, first prepared in 1969, were immediately recognized to have an outstanding potential to selectively bind guest metal ions, in particular alkaline- and alkaline-earth metal ions. In our first paper on the rational design of cation hosts, we started our theoretical work with the prediction of cation stability by quantum chemical calculations.[327] Different computational methods such as MNDO, AM1, PM3, PM3/SPASS and PM5 were employed to calculate the stability of host–guest interactions. The results show that structures of $[M{\subset}2.2.2]^{n+}$ evaluated against X-ray and DFT (B3LYPP/LANL2DZp) geometries agree very well, followed by PM3/SPASS. Furthermore, the ion selectivity calculated with DFT and PM3/SPASS for simple reactions, agrees quite well with complex formation constants, $\log K_S$.[327]

In the subsequent series of papers,[328–336] many different host molecules were systematically studied for the selective binding of alkaline- and alkaline-earth metal ions. A few typical examples will be presented here. In the first case,[331] the selectivity of the cryptands [2.2.bpy] and [2.bpy.bpy] (see Scheme 27) for the endohedral complexation of alkali, alkaline-earth and earth metal ions, was predicted with the help of DFT (B3LYP/LANL2DZp) calculated structures and complex-formation energies. The results showed that the cavity size in both cryptands was between that for [2.2.2] and [bpy.bpy.bpy], such that the complexation of $K^+$, $Sr^{2+}$ and $Tl^{3+}$ was favourable.

The calculated complexation energies for the reaction outlined in Scheme 28 are summarised in Fig. 40 for both the

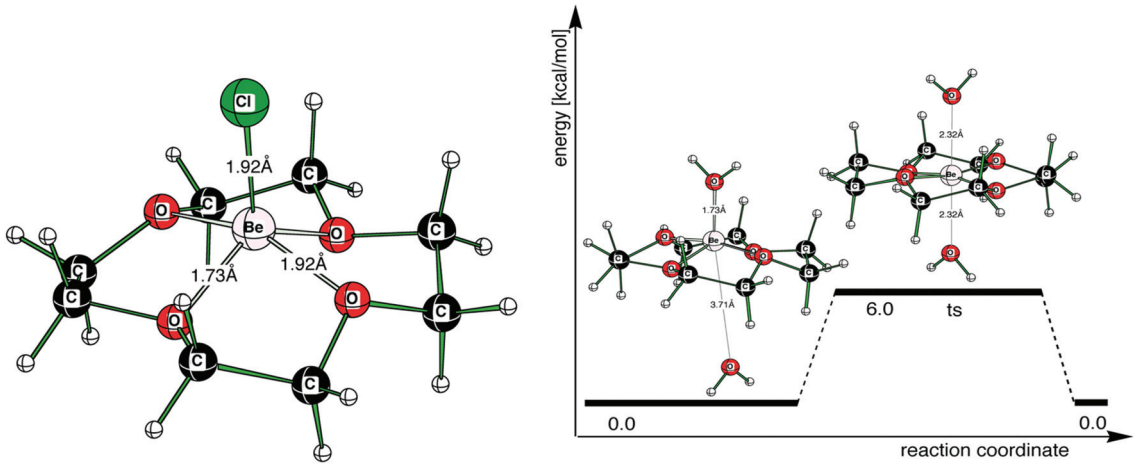


Fig. 39 Calculated (B3LYP/6-311_G**) structure of $[BeCl(12\text{-crown-4})]^+$ (left) and energy profile for water exchange on $[Be(H_2O)(12\text{-crown-4})]^{2+}$ (right).[323]

 

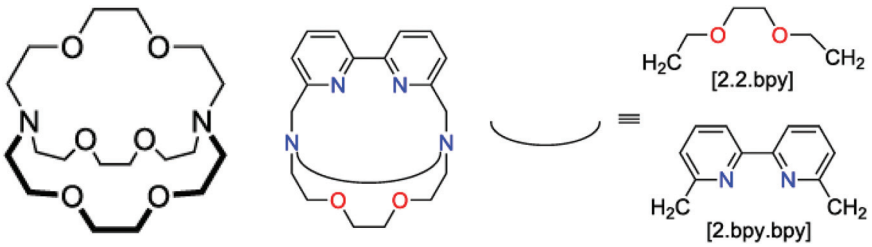


**Scheme 27** Structures of [2.2.2] (left) and [2.2.bpy] and [2.bpy.bpy] (right). Reprinted with permission from ref. 331. Copyright 2013 Beilstein-Institut zur Förderung der Chemischen Wissenschaften.

$$[M(H_2O)_6]^{m+} + \text{cryptand} \rightarrow [M \quad \text{cryptand}]^{m+} + 6H_2O \qquad (48)$$

**Scheme 28** Model reaction for the cryptands: [2.2.bpy] and [2.bpy.bpy].

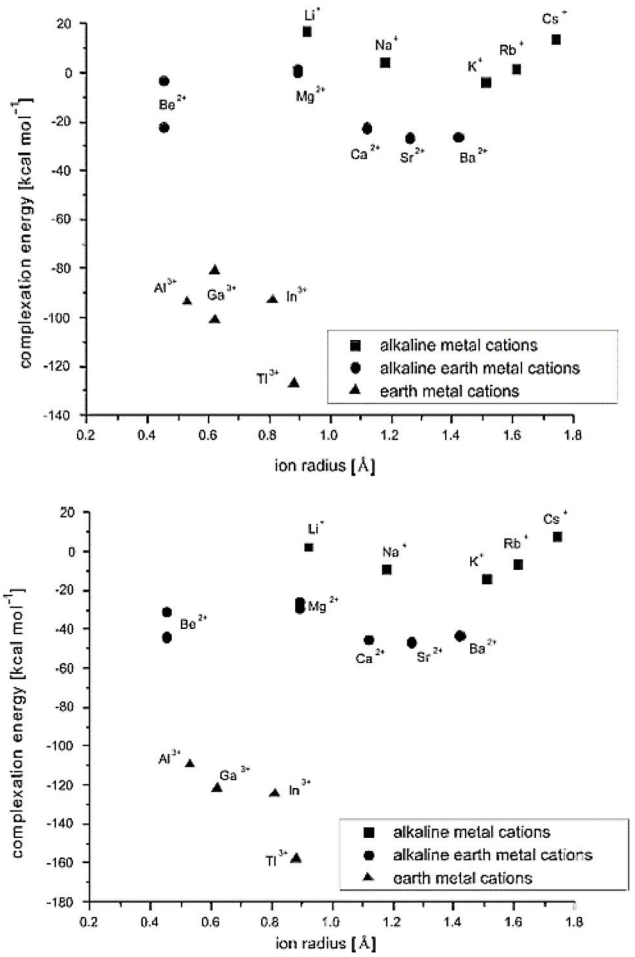


**Fig. 40** Complexation energies for the reaction outlined in Scheme 28 for the cryptands [2.2.bpy] (top) and [2.bpy.bpy] (bottom) as a function of ionic radius. Reprinted with permission of ref. 331. Copyright 2013 Beilstein-Institut zur Förderung der Chemischen Wissenschaften.

cryptands [2.2.bpy] and [2.bpy.bpy]. The results in Fig. 40 show that the ability of the metal cations to fit into the cryptands is very similar in both cases.

Another interesting example is the ability of the Saalfrank-type $\{Fe_2L_3\}$ cryptand to form host–guest complexes.[337] DFT calculations (B3LYP/LANL2DZp) showed that the cryptand can accommodate $K^+$, $Sr^{2+}$ and $Ba^{2+}$, but not the other cations shown in the pictorial presentation in Fig. 41.

In the final and most recent example, the ability of the recently synthesized bis-triazacyclononane trispyridyl N9-aza-cryptand (Beer-Can) to accommodate alkaline- and alkaline-earth metal cations ($Li^+$–$Cs^+$ and $Be^{2+}$–$Ba^{2+}$), was investigated using DFT (B3LYP/LANL2DZp) calculations. A schematic presentation of the Beer-Can cryptand is presented in Scheme 29.[336] The calculations show that the host can bind the alkali cation $K^+$ best, followed by the alkaline-earth cations $Ca^{2+}$ and $Sr^{2+}$, and by $Na^+$ and $Ba^{2+}$.

### 8.5 Be aware of pitfalls in DFT calculations

The application of DFT calculations has become extremely popular for mechanistic studies in inorganic (and organic) chemistry, where it has reached the stage that when we talk about reaction mechanisms it is in general understood as application of DFT methods. This cannot take away the fact that such calculations are performed in the gas phase at 0 K and need to be extrapolated to the solution phase usually at around room temperature. This is not always as easy as one

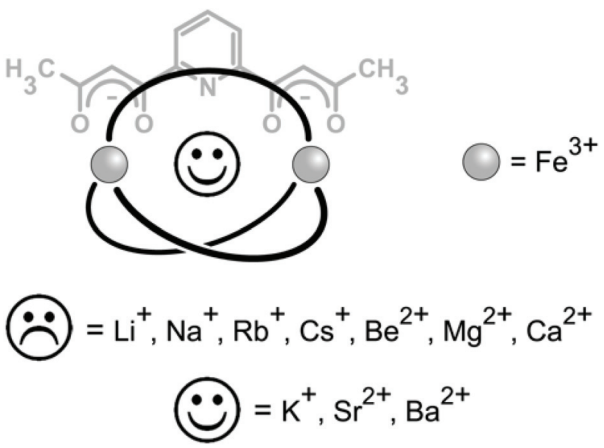


**Fig. 41** Pictorial presentation of the outcome of the DFT calculations on the Saalfrank-type cryptand.[337]

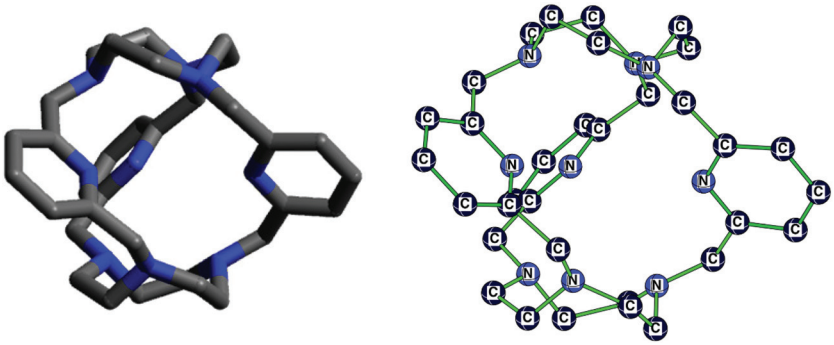

Scheme 29 Schematic presentation of the Beer-Can cryptand.[336]



would think it is. In a recent report, de Visser and co-workers[338] have performed a detailed DFT study using not less than 10 different methods and basis sets to determine the activation enthalpy and activation entropy for the *para*-substituted thioanisole sulfoxidation by a nonheme iron(IV)-oxo complex (see Table 19). Only in one particular case could the activation enthalpy be correctly estimated, but the activation entropy was 50% more negative in all cases. Admittedly, the theoretical estimation of the activation entropy is indeed quite complex. On the other hand, who would go through such an effort to estimate the enthalpy barrier for the transition state which varies between 0.5 and 21.5 kcal $mol^{-1}$ for the different methods and basis sets used?

Table 19 DFT calculated transition states for the reaction of $[Fe^{IV}(O)(N4Py)]^{2+}$ with *para*-H thioanisole. The enthalpy and entropy of activation are reported in kcal $mol^{-1}$ and cal $mol^{-1}$ $K^{-1}$, respectively[338]

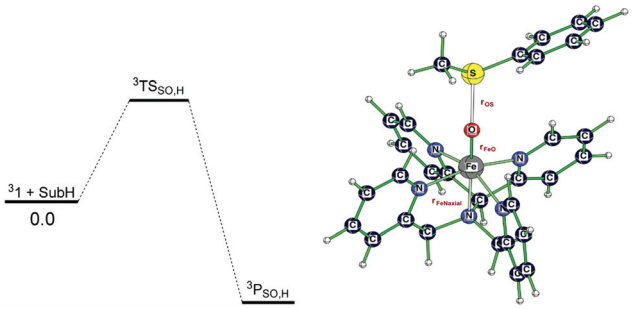


| Method | $r_{FeO}$ | $r_{OS}$ | $r_{FeNaxial}$ | Imag freq | $\Delta H^{\ddagger}$ | $\Delta S^{\ddagger}$ |
|---|---|---|---|---|---|---|
| B3LYP/BS1 | 1.702 | 2.079 | 2.124 | i352 | 0.5 | −29.9 |
| B3LYP/BS1 + PCM | 1.694 | 2.104 | 2.121 | i284 | 16.7 | −31.4 |
| B3LYP/BS1 + SMD | 1.712 | 2.066 | 2.099 | i433 | 17.8 | −31.0 |
| B3LYP-D3/BS1 + PCM | 1.709 | 2.012 | 2.097 | i577 | 5.3 | −37.5 |
| BP86/BS1 + PCM | 1.817 | 1.892 | 2.181 | i495 | 21.5 | −35.5 |
| BPE0/BS1 + PCM | 1.690 | 2.043 | 2.087 | i423 | 12.4 | −31.0 |
| B3LYP/BS2 + PCM | 1.717 | 2.069 | 2.115 | i424 | 16.3 | −30.2 |
| B3LYP-D3/BS2 + PCM | 1.725 | 2.013 | 2.100 | i582 | 5.9 | −36.2 |
| B3LYP/BS3 + PCM | 1.723 | 2.060 | 2.129 | i391 | 20.4 | −37.6 |
| B3LYP-D3/BS3 + PCM | 1.739 | 1.978 | 2.099 | i680 | 9.1 | −36.0 |
| Experimental | | | | | 12.4 | −19.2 |

## 9. Overall conclusions

The clarification of IRM as outlined in this personal journey, leads to the detailed clarification of the underlying reaction mechanisms that advanced our understanding of inorganic chemistry in solution. This in turn enabled the extrapolation of the gained mechanistic insight to the systematic development of more efficient biomimetic models and homogeneous catalysts required to solve energy related problems. During the journey we worked in different areas, starting with the activation of NO, turning to the activation of peroxides, looking at the wonder-world of Ru(edta) chemistry, followed more recently by HNO chemistry, the redox chemistry of Ru(III) complexes, reactivity tuning and application of Ru(II) polypyridyl complexes, and using ionic liquids to study their influence on IRM.

It has been a long journey! We were always highly motivated to solve the next intriguing mechanistic question or apparent discrepancy. All in all, it was a very successful and productive time ..... and we had a lot of fun too!!!

## Conflicts of interest

There are no conflicts to declare.

## Acknowledgements

First of all, I would like to acknowledge the numerous PhD students, post-doctoral co-workers and visiting scientists that performed the experimental and theoretical work that lead to many clarifications of IRM, their names are on the papers cited from our work. Secondly, a special word of thanks to the authors of this review for their enthusiastic participation and team work under a limited time schedule. You have all done a great job! I am particularly indebted to Dr Achim Zahl in Erlangen for his outstanding expertise in ambient and high pressure NMR over the past twenty-five years. We have greatly benefitted from our collaborations with Ralph Puchta, Tim Clark and Nico von Eikema-Hommes (Computer-Chemistry-

 

Centre in Erlangen) for their computational studies. I have also been supported by very capable crystallographers in Erlangen and Torun that helped us to solve some important crystal structures mentioned in the review. Furthermore, I would like to acknowledge the very productive collaboration with Grazyna Stochel of the Jagiellonian University in Krakow for over more than 35 years, and still ongoing. In addition, a special word of thanks goes to Colin Hubbard for his help with the Introduction and linguistics of some of the sections of this review, and his enormous help as Co-Editor of not less than 6 volumes (54, 61, 65, 68, 70 and 74) of Advances in Inorganic Chemistry (Academic Press). On a personal note, CDH wishes to thank John Burgess for his help with literature searches.

I am indebted to several funding agencies that supported our work over so many years: Deutsche Forschungsgemeinschaft (DFG) in the form of individual projects, SFB and SPP actions; Fonds der Chemischen Industrie; Volkswagen Foundation; and several COST Actions. MO, JP, MC and RvE acknowledge financial support from the National Science Centre in Poland, Grant No. 2016/23/D/ST4/00303, 2016/21/N/ST4/00178, 2019/33/N/ST4/00700 and 2015/16/W/ST5/00005, respectively.



## References

1 R. van Eldik and C. D. Hubbard, in *High Pressure Chemistry. Synthetic, Mechanistic, and Supercritical Applications*, ed. R. van Eldik and F.-G. Klärner, Wiley-VCH, 2002, ch. 1.
2 R. van Eldik and C. D. Hubbard, in *Chemistry at Extreme Conditions*, ed. M. Riad Manaa, Elsevier, 2005, ch. 4.
3 C. D. Hubbard and R. van Eldik, High pressure chemistry, principles, technology and applications, in *Kirk-Othmer Encycl. Chem. Technol*, 2005, vol. 13, pp. 402–455.
4 C. D. Hubbard and R. van Eldik, in *Physical Inorganic Chemistry. Principles, Methods and Models*, ed. A. Bakac, Wiley, 2010, ch. 7.
5 A. Zahl, R. van Eldik, M. Matsumoto and T. W. Swaddle, *Inorg. Chem.*, 2003, **42**, 3718–3722.
6 A. V. Davis, D. Fiedler, G. Seeber, A. Zahl, R. van Eldik and K. N. Raymond, *J. Am. Chem. Soc.*, 2006, **128**, 1324–1333.
7 J. S. Mugridge, A. Zahl, R. van Eldik, R. G. Bergman and K. N. Raymond, *J. Am. Chem. Soc.*, 2013, **135**, 4299–4306.
8 B. Petrović, S. Jovanović, R. Puchta and R. van Eldik, *Inorg. Chim. Acta*, 2019, **495**, 118953.
9 C. D. Hubbard, P. Illner and R. van Eldik, *Chem. Soc. Rev.*, 2011, **40**, 272–290.
10 T. Schneppensieper, S. Finkler, A. Czap, R. van Eldik, M. Heus, P. Nieuwenhuizen, C. Wreesmann and W. Abma, *Eur. J. Inorg. Chem.*, 2001, 491–501.
11 T. Schneppensieper, A. Wanat, G. Stochel, S. Goldstein, D. Meyerstein and R. van Eldik, *Eur. J. Inorg. Chem.*, 2001, 2317–2325.
12 T. Schneppensieper, A. Wanat, G. Stochel and R. van Eldik, *Inorg. Chem.*, 2002, **41**, 2565–2573.
13 J. Maigut, R. Meier, A. Zahl and R. van Eldik, *Inorg. Chem.*, 2007, **46**, 5361–5371.
14 J. Maigut, R. Meier, A. Zahl and R. van Eldik, *Inorg. Chem.*, 2008, **47**, 5702–5719.
15 A. Wanat, T. Schneppensieper, G. Stochel, R. van Eldik, E. Bill and K. Wieghardt, *Inorg. Chem.*, 2002, **41**, 4–10.
16 C. A. Brown, M. A. Pavlosky, T. E. Westre, Y. Zhang, B. Hedman, K. O. Hodgson and E. I. Solomon, *J. Am. Chem. Soc.*, 1995, **117**, 715–732.
17 G. Monsch and P. Klüfers, *Angew. Chem., Int. Ed.*, 2019, **58**, 8566–8571.
18 A. Drljaca, A. Zahl and R. van Eldik, *Inorg. Chem.*, 1998, **37**, 3948–3953.
19 C. Kupper, J. A. Rees, S. Dechert, S. DeBeer and F. Meyer, *J. Am. Chem. Soc.*, 2016, **138**, 7888–7898.
20 M. J. Chalkley and J. C. Peters, *Angew. Chem., Int. Ed.*, 2016, **55**, 11995–11998.
21 M. Wolf, B. M. Aas and P. Klüfers, *Eur. J. Inorg. Chem.*, 2017, 2301–2312.
22 B. M. Aas and P. Klüfers, *Eur. J. Inorg. Chem.*, 2017, 2313–2320.
23 J. J. Yan, M. A. Gonzales, P. K. Mascharak, B. Hedman, K. O. Hodgson and E. I. Solomon, *J. Am. Chem. Soc.*, 2017, **139**, 1215–1225.
24 T. Schneppensieper, A. Zahl and R. van Eldik, *Angew. Chem., Int. Ed.*, 2001, **40**, 1678–1680.
25 M. Wolak and R. van Eldik, *J. Am. Chem. Soc.*, 2005, **127**, 13312–13315.
26 J.-E. Jee, M. Wolak, D. Balbinot, N. Jux, A. Zahl and R. van Eldik, *Inorg. Chem.*, 2006, **45**, 1326–1337.
27 J.-E. Jee, S. Eigler, F. Hampel, N. Jux, M. Wolak, A. Zahl, G. Stochel and R. van Eldik, *Inorg. Chem.*, 2005, **44**, 7717–7731.
28 J.-E. Jee, S. Eigler, N. Jux, A. Zahl and R. van Eldik, *Inorg. Chem.*, 2007, **46**, 3336–3352.
29 J.-E. Jee and R. van Eldik, *Inorg. Chem.*, 2006, **45**, 6523–6534.
30 A. Franke, G. Stochel, C. Jung and R. van Eldik, *J. Am. Chem. Soc.*, 2004, **126**, 4181–4191.
31 A. Franke, N. Hessenauer-Ilicheva, D. Meyer, G. Stochel, W.-D. Woggon and R. van Eldik, *J. Am. Chem. Soc.*, 2006, **128**, 13611–13624.
32 M. Wolak, G. Stochel, M. Hamza and R. van Eldik, *Inorg. Chem.*, 2000, **39**, 2018–2019.
33 L. G. Rochelle, S. J. Morana, H. Kruszyna, M. A. Russell, D. E. Wilcox and R. P. Smith, *J. Pharmacol. Exp. Ther.*, 1995, **275**, 48–52.
34 M. Brouwer, W. Chamulitrat, G. Ferruzzi, D. L. Sauls and J. B. Weinberg, *Blood*, 1996, **88**, 1857–1864.
35 S. S. Greenberg, J. Xie, J. M. Zatarain, D. R. Kapusta and M. J. Miller, *J. Pharmacol. Exp. Ther.*, 1995, **273**, 257–265.
36 R. A. Firth, H. A. O. Hill, J. M. Pratt, R. G. Thorp and R. J. P. Williams, *J. Chem. Soc. A*, 1969, 381–386.
37 F. Roncaroli, T. E. Shubina, T. Clark and R. van Eldik, *Inorg. Chem.*, 2006, **45**, 7869–7876.
38 M. Wolak, A. Zahl, T. Schneppensieper, G. Stochel and R. van Eldik, *J. Am. Chem. Soc.*, 2001, **123**, 9780–9791.

39 C. Selcuki, R. van Eldik and T. Clark, *Inorg. Chem.*, 2004, **43**, 2828–2833.
40 L. Hannibal, C. A. Smith, D. W. Jacobsen and N. E. Brasch, *Angew. Chem., Int. Ed.*, 2007, **46**, 5140–5143.
41 H. A. Hassanin, L. Hannibal, D. W. Jacobsen, K. L. Brown, H. M. Marques and N. E. Brasch, *Dalton Trans.*, 2009, **3**, 424–433.
42 J. Polaczek, L. Orzel, G. Stochel and R. van Eldik, *J. Biol. Inorg. Chem.*, 2015, **20**, 1069–1078.
43 J. Polaczek, Ł. Orzeł, G. Stochel and R. van Eldik, *J. Biol. Inorg. Chem.*, 2018, **23**, 377–383.
44 J. Polaczek, Ł. Orzeł, G. Stochel and R. van Eldik, *J. Biol. Inorg. Chem.*, 2019, **24**, 311–313.
45 M. Wolak and R. van Eldik, *Coord. Chem. Rev.*, 2002, **230**, 263–282.
46 A. Wanat, M. Wolak, Ł. Orzeł, M. Brindell, R. van Eldik and G. Stochel, *Coord. Chem. Rev.*, 2002, **229**, 37–49.
47 A. Franke, F. Roncaroli and R. van Eldik, *Eur. J. Inorg. Chem.*, 2007, 773–798.
48 A. Franke and R. van Eldik, *Eur. J. Inorg. Chem.*, 2013, 460–480.
49 F. Roncaroli, J. A. Olabe and R. van Eldik, *Inorg. Chem.*, 2002, **41**, 5417–5425.
50 F. Roncaroli, J. A. Olabe and R. van Eldik, *Inorg. Chem.*, 2003, **42**, 4179–4189.
51 F. Roncaroli, R. van Eldik and J. A. Olabe, *Inorg. Chem.*, 2005, **44**, 2781–2790.
52 D. T. Walker, R. S. Dassanayake, K. A. Garcia, R. Mukherjee and N. E. Brasch, *Eur. J. Inorg. Chem.*, 2013, 1–12.
53 A. Katafias, O. Impert, P. Kita, J. Fenska, S. Koter, A. Kaczmarek-Kędziera, H. Różycki, A. Bajek, M. Uzarska and R. van Eldik, *Eur. J. Inorg. Chem.*, 2014, 2529–2535.
54 B. Bänsch, R. van Eldik and P. Martinez, *Inorg. Chim. Acta*, 1992, **201**, 75–82.
55 P. Martinez, J. Zuluaga, J. Kraft and R. van Eldik, *Inorg. Chim. Acta*, 1988, **146**, 9–12.
56 P. Martinez, J. Zuluaga, P. Noheda and R. van Eldik, *Inorg. Chim. Acta*, 1992, **195**, 249–253.
57 P. Martinez, J. Zuluaga, D. Uribe and R. van Eldik, *Inorg. Chim. Acta*, 1987, **136**, 11–16.
58 A. Wanat, R. van Eldik and G. Stochel, *J. Chem. Soc., Dalton Trans.*, 1998, **15**, 2497–2502.
59 H. A. Hassanin, L. Hannibal, D. W. Jacobsen, M. F. El-Shahat, M. S. A. Hamza and N. E. Brasch, *Angew. Chem., Int. Ed.*, 2009, **48**, 8909–8913.
60 H. Subedi and N. E. Brasch, *Eur. J. Inorg. Chem.*, 2015, 3825–3834.
61 H. Subedi and N. E. Brasch, *Dalton Trans.*, 2016, **45**, 352–360.
62 H. Subedi, H. A. Hassanin and N. E. Brasch, *Inorg. Chem.*, 2014, **53**, 1570–1577.
63 J. Polaczek, H. Subedi, L. Lisboa, R. B. Cink, G. Stochel, N. E. Brasch and R. van Eldik, in preparation.
64 J. P. Collman and S. E. Groh, *J. Am. Chem. Soc.*, 1982, **104**, 1391–1403.
65 M. M. Palcic, R. Rutter, T. Araiso, L. P. Hager and H. B. Dunford, *Biochem. Biophys. Res. Commun.*, 1980, **94**, 1123–1127.
66 J. E. Roberts, B. M. Hoffman, R. Rutter and L. P. Hager, *J. Biol. Chem.*, 1981, **256**, 2118–2121.
67 M. Oszajca, A. Franke, M. Brindell, G. Stochel and R. van Eldik, *Coord. Chem. Rev.*, 2016, **306**, 483–509.
68 J. Rittle and M. T. Green, *Science*, 2010, **330**, 933–937.
69 V. Schünemann, C. Jung, J. Terner, A. X. Trautwein and R. Weiss, *J. Inorg. Biochem.*, 2002, **91**, 586–596.
70 C. M. Krest, E. L. Onderko, T. H. Yosca, J. C. Calixto, R. F. Karp, J. Livada, J. Rittle and M. T. Green, *J. Biol. Chem.*, 2013, **288**, 17074–17081.
71 J. Rittle, J. M. Younker and M. T. Green, *Inorg. Chem.*, 2010, **49**, 3610–3617.
72 M. J. Cryle and J. J. De Voss, *Angew. Chem., Int. Ed.*, 2006, **45**, 8221–8223.
73 C. Li, L. Zhang, C. Zhang, H. Hirao, W. Wu and S. Shaik, *Angew. Chem., Int. Ed.*, 2007, **46**, 8168–8170.
74 M. J. Park, J. Lee, Y. Suh, J. Kim and W. Nam, *J. Am. Chem. Soc.*, 2006, **128**, 2630–2634.
75 M. S. Seo, T. Kamachi, T. Kouno, K. Murata, M. J. Park, K. Yoshizawa and W. Nam, *Angew. Chem., Int. Ed.*, 2007, **46**, 2291–2294.
76 W. Nam, H. J. Choi, H. J. Han, S. H. Cho, H. J. Lee and S.-Y. Han, *Chem. Commun.*, 1999, 387–388.
77 S. J. Yang and W. Nam, *Inorg. Chem.*, 1998, **37**, 606–607.
78 T. G. Traylor, C. Kim, J. L. Richards, F. Xu and C. L. Perrin, *J. Am. Chem. Soc.*, 1995, **117**, 3468–3474.
79 O. Almarsson and T. C. Bruice, *J. Am. Chem. Soc.*, 1995, **117**, 4533–4544.
80 T. C. Bruice, P. N. Balasubramanian, R. W. Lee and J. R. L. Smith, *J. Am. Chem. Soc.*, 1988, **110**, 7890–7892.
81 J. R. L. Smith, P. N. Balasubramanian and T. C. Bruice, *J. Am. Chem. Soc.*, 1988, **110**, 7411–7418.
82 Y. J. Lee, Y. M. Goh, S.-Y. Han, C. Kim and W. Nam, *Chem. Lett.*, 1998, **27**, 837–838.
83 J. F. Bartoli, P. Battioni, W. R. De Foor and D. Mansuy, *J. Chem. Soc., Chem. Commun.*, 1994, 23–24.
84 M. Wolak and R. van Eldik, *Chem. – Eur. J.*, 2007, **13**, 4873–4883.
85 M. Liu and Y. O. Su, *J. Electroanal. Chem.*, 1998, **452**, 113–125.
86 A. Franke, M. Wolak and R. van Eldik, *Chem. – Eur. J.*, 2009, **15**, 10182–10198.
87 M. Oszajca, A. Franke, A. Drzewiecka-Matuszek, M. Brindell, G. Stochel and R. van Eldik, *Inorg. Chem.*, 2014, **53**, 2848–2857.
88 A. Takahashi, T. Kurahashi and H. Fujii, *Inorg. Chem.*, 2007, **46**, 6227–6229.
89 W. J. Song, Y. O. Ryu, R. Song and W. Nam, *J. Biol. Inorg. Chem.*, 2005, **10**, 294–304.
90 R. Gupta, X.-X. Li, K.-B. Cho, M. Guo, Y.-M. Lee, Y. Wang, S. Fukuzumi and W. Nam, *J. Phys. Chem. Lett.*, 2017, **8**, 1557–1561.
91 C. Fertinger, A. Franke and R. van Eldik, *J. Biol. Inorg. Chem.*, 2012, **17**, 27–36.

 

92 W. Nam, M. H. Lim, H. J. Lee and C. Kim, *J. Am. Chem. Soc.*, 2000, **122**, 6641–6647.
93 W. Nam, S. W. Jin, M. H. Lim, J. Y. Ryu and C. Kim, *Inorg. Chem.*, 2002, **41**, 3647–3652.
94 W. Nam, Y. O. Ryu and W. J. Song, *J. Biol. Inorg. Chem.*, 2004, **9**, 654–660.
95 J. P. Collman, A. S. Chien, T. A. Eberspacher and J. I. Brauman, *J. Am. Chem. Soc.*, 2000, **122**, 11098–11100.
96 J. P. Collman, L. Zeng and R. A. Decréau, *Chem. Commun.*, 2003, 2974–2975.
97 P. R. Ortiz de Montellano and J. J. De Voss, *Nat. Prod. Rep.*, 2002, **19**, 477–493.
98 A. Franke, C. Fertinger and R. van Eldik, *Angew. Chem., Int. Ed.*, 2008, **47**, 5238–5242.
99 C. Fertinger, N. Hessenauer-Ilicheva, A. Franke and R. van Eldik, *Chem. – Eur. J.*, 2009, **15**, 13435–13440.
100 K. Tajima, S. Oka, T. Edo, S. Miyake, H. Mano, K. Mukai, H. Sakurai and K. Ishizu, *J. Chem. Soc., Chem. Commun.*, 1995, 1507–1508.
101 K. Tajima, M. Shigematsu, J. Jinno, K. Ishizu and H. Ohya-Nishiguchi, *J. Chem. Soc., Chem. Commun.*, 1990, 144–145.
102 M. Rivera, G. A. Caignan, A. V. Astashkin, A. M. Raitsimring, T. K. Shokhireva and F. A. Walker, *J. Am. Chem. Soc.*, 2002, **124**, 6077–6089.
103 J.-G. Liu, Y. Shimizu, T. Ohta and Y. Naruta, *J. Am. Chem. Soc.*, 2010, **132**, 3672–3673.
104 J.-G. Liu, T. Ohta, S. Yamaguchi, T. Ogura, S. Sakamoto, Y. Maeda and Y. Naruta, *Angew. Chem., Int. Ed.*, 2009, **48**, 9262–9267.
105 S. P. de Visser, J. S. Valentine and W. Nam, *Angew. Chem., Int. Ed.*, 2010, **49**, 2099–2101.
106 A. Franke, C. Fertinger and R. van Eldik, *Chem. – Eur. J.*, 2012, **18**, 6935–6949.
107 M. Selke, M. F. Sisemore and J. S. Valentine, *J. Am. Chem. Soc.*, 1996, **118**, 2008–2012.
108 M. Selke and J. S. Valentine, *J. Am. Chem. Soc.*, 1998, **120**, 2652–2653.
109 M. Oszajca, A. Drzewiecka-Matuszek, A. Franke, D. Rutkowska-Zbik, M. Brindell, M. Witko, G. Stochel and R. van Eldik, *Chem. – Eur. J.*, 2014, **20**, 2328–2343.
110 Z. Gross and S. Nimri, *Inorg. Chem.*, 1994, **33**, 1731–1732.
111 Z. Gross, S. Nimri, C. M. Barzilay and L. Simkhovich, *J. Biol. Inorg. Chem.*, 1997, **2**, 492–506.
112 Z. Gross, S. Nimri and L. Simkhovich, *J. Mol. Catal. A: Chem.*, 1996, **113**, 231–238.
113 A. Takahashi, T. Kurahashi and H. Fujii, *Inorg. Chem.*, 2009, **48**, 2614–2625.
114 D. Kumar, R. Latifi, S. Kumar, E. V. Rybak-Akimova, M. A. Sainna and S. P. de Visser, *Inorg. Chem.*, 2013, **52**, 7968–7979.
115 L. Ji, A. Franke, M. Brindell, M. Oszajca, A. Zahl and R. van Eldik, *Chem. – Eur. J.*, 2014, **20**, 14437–14450.
116 J. H. Dawson, *Science*, 1988, **240**, 433–439.
117 S. C. Tang, S. Koch, G. C. Papaefthymiou, S. Foner, R. B. Frankel, J. A. Ibers and R. H. Holm, *J. Am. Chem. Soc.*, 1976, **98**, 2414–2434.
118 T. G. Traylor, T. C. Mincey and A. P. Berzinis, *J. Am. Chem. Soc.*, 1981, **103**, 7084–7089.
119 M. P. Roach, A. E. Pond, M. R. Thomas, S. G. Boxer and J. H. Dawson, *J. Am. Chem. Soc.*, 1999, **121**, 12088–12093.
120 F. Ogliaro, S. Cohen, S. P. de Visser and S. Shaik, *J. Am. Chem. Soc.*, 2000, **122**, 12892–12893.
121 T. Higuchi, S. Uzu and M. Hirobe, *J. Am. Chem. Soc.*, 1990, **112**, 7051–7053.
122 S. Kozuch, T. Leifels, D. Meyer, L. Sbaragli, S. Shaik and W.-D. Woggon, *Synlett*, 2005, 675–684.
123 D. Meyer, T. Leifels, L. Sbaragli and W.-D. Woggon, *Biochem. Biophys. Res. Commun.*, 2005, **338**, 372–377.
124 L. Sbaragli and W.-D. Woggon, *Synthesis*, 2005, 1538–1542.
125 N. Suzuki, T. Higuchi and T. Nagano, *J. Am. Chem. Soc.*, 2002, **124**, 9622–9628.
126 N. Hessenauer-Ilicheva, A. Franke, M. Wolak, T. Higuchi and R. van Eldik, *Chem. – Eur. J.*, 2009, **15**, 12447–12459.
127 N. Hessenauer-Ilicheva, A. Franke, D. Meyer, W.-D. Woggon and R. van Eldik, *J. Am. Chem. Soc.*, 2007, **129**, 12473–12479.
128 N. Hessenauer-Ilicheva, A. Franke, D. Meyer, W.-D. Woggon and R. van Eldik, *Chem. – Eur. J.*, 2009, **15**, 2941–2959.
129 A. Franke, E. Hartmann, I. Schlichting and R. van Eldik, *J. Biol. Inorg. Chem.*, 2012, **17**, 447–463.
130 A. Franke and R. van Eldik, *Chem. – Eur. J.*, 2015, **21**, 15201–15210.
131 D. Chatterjee, A. Mitra and G. S. De, *Platinum Met. Rev.*, 2006, **50**, 2–12.
132 T. Matsubara and C. Creutz, *Inorg. Chem.*, 1979, **18**, 1956–1966.
133 H. C. Bajaj and R. van Eldik, *Inorg. Chem.*, 1988, **27**, 4052–4055.
134 Y. Yoshino, T. Uehiro and M. Saito, *Bull. Chem. Soc. Jpn.*, 1979, **52**, 1060–1062.
135 D. Chatterjee, H. C. Bajaj and A. Das, *J. Chem. Soc., Dalton Trans.*, 1995, 2497–2501.
136 D. Chatterjee and H. C. Bajaj, *J. Coord. Chem.*, 1996, **39**, 117–122.
137 M. M. T. Khan, D. Chatterjee, R. R. Merchant, P. Paul, S. H. R. Abdi, D. Srinivas, M. R. H. Siddiqui, M. A. Moiz, M. M. Bhadbhade and K. Venkatasubramanian, *Inorg. Chem.*, 1992, **31**, 2711–2718.
138 D. Chatterjee, *Coord. Chem. Rev.*, 1998, **168**, 273–293.
139 M. M. T. Khan, H. C. Bajaj, Z. Shirin and K. Venkatasubraminan, *Indian J. Chem.*, 1992, **31**, 303–308.
140 D. Chatterjee, A. Mitra, M. S. A. Hamza and R. van Eldik, *J. Chem. Soc., Dalton Trans.*, 2002, 962–965.
141 D. Chatterjee, M. S. A. Hamza, M. M. Shoukry, A. Mitra, S. Deshmukh and R. van Eldik, *Dalton Trans.*, 2003, 203–209.
142 D. Chatterjee, A. Mitra, A. Levina and P. A. Lay, *Chem. Commun.*, 2008, 2864–2866.
143 D. Chatterjee, *J. Chem. Soc., Dalton Trans.*, 1996, 4389–4392.

144 D. Chatterjee, A. Mitra and R. van Eldik, *Dalton Trans.*, 2007, 943–948.
145 D. Chatterjee, E. Ember, U. Pal, S. Ghosh and R. van Eldik, *Dalton Trans.*, 2011, **40**, 10473–10480.
146 D. Chatterjee, A. Sikdar, V. R. Patnam, A. Theodoridis and R. van Eldik, *Dalton Trans.*, 2008, 3851–3856.
147 J. Belej, *J. Electroanal. Chem. Interfacial Electrochem.*, 1986, **214**, 481–483.
148 D. Chatterjee, N. Jaiswal, A. Franke and R. van Eldik, *Chem. Commun.*, 2014, **50**, 14562–14565.
149 A. Ghosh, D. A. Mitchell, A. Chanda, A. D. Ryabov, D. L. Popescu, E. C. Upham, G. J. Collins and T. J. Collins, *J. Am. Chem. Soc.*, 2008, **130**, 15116–15126.
150 V. G. Povse and J. A. Olabe, *Transition Met. Chem.*, 1998, **23**, 657–662.
151 D. Chatterjee, U. Pal, S. Ghosh and R. van Eldik, *Dalton Trans.*, 2011, **40**, 1302–1306.
152 C. E. Paulsen and K. S. Carroll, *Chem. Rev.*, 2013, **113**, 4633–4679.
153 D. Chatterjee, E. Ember, U. Pal, S. Ghosh and R. van Eldik, *Dalton Trans.*, 2011, **40**, 10997–11004.
154 P. Sarkar, A. Saha and D. Chatterjee, *J. Coord. Chem.*, 2016, **69**, 3417–3423.
155 G. Lente, J. Kalmár, Z. Baranyai, A. Kun, I. Kék, D. Bajusz, M. Takács, L. Veres and I. Fábián, *Inorg. Chem.*, 2009, **48**, 1763–1773.
156 L. Asher and E. Deutsch, *Inorg. Chem.*, 1972, **11**, 2927–2933.
157 I. K. Adzamli and E. Deutsch, *Inorg. Chem.*, 1980, **19**, 1366–1373.
158 D. Chatterjee, S. Rothbart and R. van Eldik, *Dalton Trans.*, 2013, **42**, 4725–4729.
159 D. Chatterjee, B. Paul and R. Mukherjee, *Dalton Trans.*, 2013, **42**, 10056–10060.
160 D. Chatterjee, S. Shome, N. Jaiswal and S. C. Moi, *J. Mol. Catal. A: Chem.*, 2014, **386**, 1–4.
161 A. Wanat, T. Schneppensieper, A. Karocki, G. Stochel and R. van Eldik, *J. Chem. Soc., Dalton Trans.*, 2002, 941–950.
162 D. Chatterjee, S. Ghosh and U. Pal, *Dalton Trans.*, 2011, **40**, 683–685.
163 D. Chatterjee, A. Franke, M. Oszajca and R. van Eldik, *Dalton Trans.*, 2014, **43**, 3087–3094.
164 A. G. Tennyson and S. J. Lippard, *Chem. Biol.*, 2011, **18**, 1211–1220.
165 M. Knipp and C. He, *IUBMB Life*, 2011, **63**, 304–312.
166 D. Chatterjee, S. Shome, N. Jaiswal and P. Banerjee, *Dalton Trans.*, 2014, **43**, 13596–13600.
167 D. Chatterjee, N. Jaiswal, M. Schmeisser and R. van Eldik, *Dalton Trans.*, 2014, **43**, 18042–18046.
168 A. Weichsel, E. M. Maes, J. F. Andersen, J. G. Valenzuela, T. K. Shokhireva, F. A. Walker and W. R. Montfort, *Proc. Natl. Acad. Sci. U. S. A.*, 2005, **102**, 594–599.
169 M. Bueno, J. Wang, A. L. Mora and M. T. Gladwin, *Antioxid. Redox Signal.*, 2012, **18**, 1797–1809.
170 R. Wang, *Physiol. Rev.*, 2012, **92**, 791–896.
171 M. Eberhardt, M. Dux, B. Namer, J. Miljkovic, N. Cordasic, C. Will, T. I. Kichko, J. de la Roche, M. Fischer, S. A. Suárez, D. Bikiel, K. Dorsch, A. Leffler, A. Babes, A. Lampert, J. K. Lennerz, J. Jacobi, M. A. Martí, F. Doctorovich, E. D. Högestätt, P. M. Zygmunt, I. Ivanovic-Burmazovic, K. Messlinger, P. Reeh and M. R. Filipovic, *Nat. Commun.*, 2014, **5**, 4381.
172 R. Wedmann, S. Bertlein, I. Macinkovic, S. Boltz, J. L. Miljkovic, L. E. Munoz, M. Herrmann and M. R. Filipovic, *Nitric Oxide*, 2014, **41**, 85–96.
173 J. L. Miljkovic, I. Kenkel, I. Ivanović-Burmazović and M. R. Filipovic, *Angew. Chem., Int. Ed.*, 2013, **52**, 12061–12064.
174 D. Chatterjee, P. Sarkar, M. Oszajca and R. van Eldik, *Inorg. Chem.*, 2016, **55**, 5037–5040.
175 D. Chatterjee, C. Chowdhury, A. Datta and R. van Eldik, *New J. Chem.*, 2019, **43**, 15311–15315.
176 S. W. Chang, A. R. Lewis, K. E. Prosser, J. R. Thompson, M. Gladkikh, M. B. Bally, J. J. Warren and C. J. Walsby, *Inorg. Chem.*, 2016, **55**, 4850–4863.
177 P. Zhang and P. J. Sadler, *Eur. J. Inorg. Chem.*, 2017, 1541–1548.
178 P. J. Sadler, *Adv. Inorg. Chem.*, 1991, **36**, 1–48.
179 K. Lin, Z.-Z. Zhao, H.-B. Bo, X.-J. Hao and J.-Q. Wang, *Front. Pharmacol.*, 2018, **9**, 1323.
180 E. Alessio, *Eur. J. Inorg. Chem.*, 2017, 1549–1560.
181 M. Mital and Z. Ziora, *Coord. Chem. Rev.*, 2018, **375**, 434–458.
182 B. H. J. Bielski, A. O. Allen and H. A. Schwarz, *J. Am. Chem. Soc.*, 1981, **103**, 3516–3518.
183 O. Impert, A. Katafias, J. Fenska, M. Chrzanowska, S. Koter, C. Dücker-Benfer and R. van Eldik, *Eur. J. Inorg. Chem.*, 2016, 5380–5386.
184 O. Impert, A. Katafias, M. Chrzanowska, T. Muzioł, G. Wrzeszcz and R. van Eldik, *Eur. J. Inorg. Chem.*, 2017, 3275–3284.
185 N. H. Williams and J. K. Yandell, *Aust. J. Chem.*, 1983, **36**, 2377–2386.
186 M. J. Akhtar and A. Haim, *Inorg. Chem.*, 1988, **27**, 1608–1610.
187 D. Chatterjee, A. Sengupta, A. Mitra and S. Basak, *Inorg. Chem. Commun.*, 2006, **9**, 1219–1222.
188 P. Schluga, C. G. Hartinger, A. Egger, E. Reisner, M. Galanski, M. A. Jakupec and B. K. Keppler, *Dalton Trans.*, 2006, 1796–1802.
189 M. Brindell, D. Piotrowska, A. A. Shoukry, G. Stochel and R. van Eldik, *J. Biol. Inorg. Chem.*, 2007, **12**, 809–818.
190 Y.-N. Wang, K.-C. Lau, W. W. Y. Lam, W.-L. Man, C.-F. Leung and T.-C. Lau, *Inorg. Chem.*, 2009, **48**, 400–406.
191 M. A. W. Lawrence, P. T. Maragh and T. P. Dasgupta, *Transition Met. Chem.*, 2012, **37**, 505–517.
192 P. J. Lakshmi, K. C. Mallu, K. C. Rajanna and P. K. Saiprakash, *J. Mol. Catal. A: Chem.*, 1996, **108**, 63–76.
193 H. D. Moya and N. Coichev, *J. Braz. Chem. Soc.*, 2006, **17**, 364–368.

 

194 B. Żurowska and A. Kochel, *J. Mol. Struct.*, 2008, **877**, 100–104.
195 R. A. Anderson, *Diabetes Metab.*, 2000, **26**, 22–27.
196 K. F. Kingry, A. C. Royer and J. B. Vincent, *J. Inorg. Biochem.*, 1998, **72**, 79–88.
197 R. S. Slesinski, J. J. Clarke, R. H. C. San and R. Gudi, *Mutat. Res. Toxicol. Environ. Mutagen.*, 2005, **585**, 86–95.
198 G. W. Evans and E. C. Johnson, *J. Nutr.*, 1981, **111**, 68–75.
199 N. Ghatak, J. Chakravarty and S. Bhattacharya, *Polyhedron*, 1995, **14**, 3591–3597.
200 O. Impert, A. Katafias, P. Kita, G. Wrzeszcz, J. Fenska, G. Lente and I. Fábián, *Transition Met. Chem.*, 2011, **36**, 761.
201 O. Impert, A. Katafias, G. Wrzeszcz, T. Muzioł, K. Hrynkiewicz, N. Olejnik, M. Chrzanowska and R. van Eldik, *J. Coord. Chem.*, 2016, **69**, 2107–2120.
202 O. Impert, A. Katafias, J. Fenska and P. Kita, *Transition Met. Chem.*, 2012, **37**, 7–16.
203 M. C. Barral, R. Jiménez-Aparicio, E. C. Royer, M. J. Saucedo, F. A. Urbanos, E. Gutiérrez-Puebla and C. Ruíz-valero, *J. Chem. Soc., Dalton Trans.*, 1991, 1609–1613.
204 M. Kimura, M. Yamamoto (née Tsuruta) and S. Yamabe, *J. Chem. Soc., Dalton Trans.,*, 1982, 423–427.
205 P. Atkins, T. Overton, J. Rourke, M. Weller and F. Armstrong, *Shriver and Atkins Inorganic Chemistry*, Oxford University Press, Oxford, 5th edn, 2010.
206 L. Helm and A. E. Merbach, *Chem. Rev.*, 2005, **105**, 1923–1960.
207 T. Jurca, E. Marian, L. G. Vicaș, M. E. Mureșan and L. Fritea, in *Spectroscopic Analyses – Developments and Applications*, ed. E. Sharmin and F. Zafar, InTech, 2017, ch. 7, pp. 123–142.
208 R. J. Browning, P. J. T. Reardon, M. Parhizkar, R. B. Pedley, M. Edirisinghe, J. C. Knowles and E. Stride, *ACS Nano*, 2017, **11**, 8560–8578.
209 U. Ndagi, N. Mhlongo and M. E. Soliman, *Drug Des. Devel. Ther.*, 2017, **11**, 599–616.
210 S. Thota, D. A. Rodrigues, D. C. Crans and E. J. Barreiro, *J. Med. Chem.*, 2018, **61**, 5805–5821.
211 P. C. J. Coverdale, T. Laroiya-McCarron and I. Romero-Canelón, *Inorganics*, 2019, **7**, 31–46.
212 F. E. Poynton, S. A. Bright, S. Blasco, D. C. Williams, J. M. Kelly and T. Gunnlaugsson, *Chem. Soc. Rev.*, 2017, **46**, 7706–7756.
213 A. Notaro and G. Gasser, *Chem. Soc. Rev.*, 2017, **46**, 7317–7337.
214 I. Romero-Canelón and P. J. Sadler, *Inorg. Chem.*, 2013, **52**, 12276–12291.
215 A. Betanzos-Lara, S. Habtemariam and P. J. Sadler, *J. Mex. Chem. Soc.*, 2013, **57**, 160–168.
216 Z. Liu, I. Romero-Canelón, B. Qamar, J. M. Hearn, A. Habtemariam, N. P. E. Barry, A. M. Pizarro, G. J. Clarkson and P. J. Sadler, *Angew. Chem., Int. Ed.*, 2014, **53**, 3941–3946.
217 J. J. Soldevila-Barreda, I. Romero-Canelón, A. Habtemariam and P. J. Sadler, *Nat. Commun.*, 2015, **6**, 6582.
218 F. Chen, J. J. Soldevila-Barreda, I. Romero-Canelón, J. P. C. Coverdale, J.-I. Song, G. J. Clarkson, J. Kasparkova, A. Habtemariam, V. Brabec, J. A. Wolny, V. Schünemann and P. J. Sadler, *Dalton Trans.*, 2018, **47**, 7178–7189.
219 F. Chen, I. Romero-Canelón, J. J. Soldevila-Barreda, J.-I. Song, J. P. C. Coverdale, G. J. Clarkson, J. Kasparkova, A. Habtemariam, M. Wills, V. Brabec and P. J. Sadler, *Organometallics*, 2018, **37**, 1555–1566.
220 M. Chrzanowska, A. Katafias, R. van Eldik, *Inorg. Chem.*, to be submitted.
221 M. Chrzanowska, A. Katafias, O. Impert, A. Kozakiewicz, A. Surdykowski, P. Brzozowska, A. Franke, A. Zahl, R. Puchta and R. van Eldik, *Dalton Trans.*, 2017, **46**, 10264–10280.
222 M. Chrzanowska, A. Katafias, A. Kozakiewicz, R. Puchta and R. van Eldik, *J. Coord. Chem.*, 2018, **71**, 1761–1777.
223 M. Chrzanowska, A. Katafias and R. van Eldik, *Inorg. Chim. Acta*, 2020, **504**, 119449.
224 H. Huang, P. Zhang, Y. Chen, K. Qiu, C. Jin, L. Ji and H. Chao, *Dalton Trans.*, 2016, **45**, 13135–13145.
225 M. L. Tobe and J. Burgess, *Inorganic Reaction Mechanisms*, Addison-Wesley Longman, Harlow, England, 1999.
226 P. A. Adcock, F. R. Keene, R. S. Smythe and M. R. Snow, *Inorg. Chem.*, 1984, **23**, 2336–2343.
227 J. Burgess and E. Pelizzetti, *Gazz. Chim. Ital.*, 1988, **118**, 101–103.
228 J. Burgess and E. Pelizzetti, *Prog. React. Kinet.*, 1992, **17**, 1–170.
229 E. Grunwald and S. Winstein, *J. Am. Chem. Soc.*, 1948, **70**, 846–854.
230 A. D. English, P. Meakin and J. P. Jesson, *J. Am. Chem. Soc.*, 1976, **98**, 7590–7598.
231 R. van Eldik, *Inorganic High Pressure Chemistry. Kinetics and Mechanisms*, Elsevier, 1986.
232 *Mechanisms of Inorganic and Organometallic Reactions*, ed. M. V. Twigg, Plenum, 1985–1993, vol. 3–8.
233 A. Drljaca, C. D. Hubbard, R. van Eldik, T. Asano, M. V. Basilevsky and W. J. le Noble, *Chem. Rev.*, 1998, **98**, 2167–2290.
234 K. J. Laidler, *Chemical Kinetics*, McGraw-Hill, 2nd edn, 1963.
235 J. E. Leffler and E. Grunwald, *Rates and Equilibria of Organic Reactions*, Wiley, 1963.
236 J. W. Moore and R. G. Pearson, *Kinetics and Mechanism*, Wiley-Interscience, 3rd edn, 1981.
237 R. G. Wilkins, *Kinetics and Mechanism of Transition Metal Complexes*, VCH, 2nd edn, 1991.
238 L. A. P. Kane-Maguire and G. Thomas, *J. Chem. Soc., Dalton Trans.*, 1975, 1324–1329.
239 W. J. Bland, J. Burgess and R. D. W. Kemmitt, *J. Organomet. Chem.*, 1968, **15**, 217–223.
240 W. J. Bland, J. Burgess and R. D. W. Kemmitt, *J. Organomet. Chem.*, 1969, **18**, 199–202.

241 J. Burgess, M. M. Hunt and R. D. W. Kemmitt, *J. Organomet. Chem.*, 1977, **134**, 131–137.
242 J. Burgess, M. E. Howden, R. D. W. Kemmitt and N. S. Sridhara, *J. Chem. Soc., Dalton Trans.*, 1978, 1577–1581.
243 J. N. Brönsted, *Z. Phys. Chem.*, 1922, **102**, 169–207.
244 J. N. Brönsted, *Z. Phys. Chem.*, 1923, **115**, 337–364.
245 N. Bjerrum, *Z. Phys. Chem.*, 1924, **108**, 82–100.
246 N. Bjerrum, *Z. Phys. Chem.*, 1925, **118**, 251–254.
247 V. K. La Mer, *Chem. Rev.*, 1932, **10**, 179–212.
248 K. J. Laidler and H. Eyring, *Ann. N. Y. Acad. Sci.*, 1939, **39**, 303–340.
249 H. Stieger and H. Kelm, *J. Phys. Chem.*, 1973, **77**, 290–294.
250 R. Schmidt, M. Geis and H. Kelm, *Z. Phys. Chem.*, 1974, **92**, 223–234.
251 C. Reichardt, *Chem. Rev.*, 1994, **94**, 2319–2358.
252 M. J. Blandamer and J. Burgess, *Chem. Soc. Rev.*, 1975, **4**, 55–75.
253 H. P. Bennetto and E. F. Caldin, *J. Chem. Soc. A*, 1971, 2191–2198.
254 H. P. Bennetto and E. F. Caldin, *J. Chem. Soc. A*, 1971, 2198–2207.
255 H. P. Bennetto and E. F. Caldin, *J. Chem. Soc. A*, 1971, 2207–2210.
256 H. P. Bennetto, *J. Chem. Soc. A*, 1971, 2211–2213.
257 E. F. Caldin and P. Godfrey, *J. Chem. Soc., Faraday Trans. 1*, 1974, **70**, 2260–2266.
258 F. Franks and D. J. G. Ives, *Q. Rev., Chem. Soc.*, 1966, **20**, 1–15.
259 M. J. Blandamer, J. Burgess, S. J. Hamshere, C. White, R. I. Haines and A. McAuley, *Can. J. Chem.*, 1983, **61**, 1361–1370.
260 M. J. Blandamer, J. Burgess, J. Fawcett, P. Guardado, C. D. Hubbard, S. Nuttall, L. J. S. Prouse, S. Radulovic and D. R. Russell, *Inorg. Chem.*, 1992, **31**, 1383–1389.
261 J. J. Savage and R. H. Wood, *J. Solution Chem.*, 1976, **5**, 733–750.
262 M. J. Blandamer, J. Burgess, H. J. Cowles, A. J. De Young, J. B. F. N. Engberts, S. A. Galema, S. J. Hill and I. M. Horn, *J. Chem. Soc., Chem. Commun.*, 1988, 1141–1142.
263 S. P. Milde, M. J. Blandamer, J. Burgess, J. B. F. N. Engberts, S. A. Galema and C. D. Hubbard, *J. Phys. Org. Chem.*, 1999, **12**, 227–232.
264 U. Tilstam, *Org. Process Res. Dev.*, 2012, **16**, 1273–1278.
265 K. R. Seddon, *J. Chem. Technol. Biotechnol.*, 1997, **68**, 351–356.
266 M. Petkovic, K. R. Seddon, L. P. N. Rebelo and C. Silva Pereira, *Chem. Soc. Rev.*, 2011, **40**, 1383–1403.
267 N. V. Plechkova and K. R. Seddon, *Chem. Soc. Rev.*, 2008, **37**, 123–150.
268 T. Welton, *Chem. Rev.*, 1999, **99**, 2071–2084.
269 T. Welton, *Coord. Chem. Rev.*, 2004, **248**, 2459–2477.
270 J. S. Wilkes, P. Wasserscheid and T. Welton, *Ionic Liq. Synth.*, 2007, 1–6.
271 J. P. Hallett and T. Welton, *Chem. Rev.*, 2011, **111**, 3508–3576.
272 T. Welton, *Biophys. Rev.*, 2018, **10**, 691–706.
273 P. Wasserscheid and T. Welton, in *Ionic Liquids in Synthesis*, Wiley-VCH, 2008.
274 H.-P. Steinrück and P. Wasserscheid, *Catal. Lett.*, 2015, **145**, 380–397.
275 Z. Lei, B. Chen, Y.-M. Koo and D. R. MacFarlane, *Chem. Rev.*, 2017, **117**, 6633–6635.
276 K. Ghandi, *Green Sustain. Chem.*, 2014, **4**, 44–53.
277 R. Ratti, *Adv. Chemother.*, 2014, 1–16.
278 H.-K. Lim and H. Kim, *Molecules*, 2017, **22**, 536–552.
279 P. Illner, S. Kern, S. Begel and R. van Eldik, *Chem. Commun.*, 2007, 4803–4805.
280 T. D. Dolidze, D. E. Khoshtariya, P. Illner, L. Kulisiewicz, A. Delgado and R. van Eldik, *J. Phys. Chem. B*, 2008, **112**, 3085–3100.
281 T. D. Dolidze, D. E. Khoshtariya, P. Illner and R. van Eldik, *Chem. Commun.*, 2008, 2112–2114.
282 C. F. Weber, R. Puchta, N. J. R. van Eikema Hommes, P. Wasserscheid and R. van Eldik, *Angew. Chem., Int. Ed.*, 2005, **44**, 6033–6038.
283 S. Begel, P. Illner, S. Kern, R. Puchta and R. van Eldik, *Inorg. Chem.*, 2008, **47**, 7121–7132.
284 C. F. Weber and R. van Eldik, *Eur. J. Inorg. Chem.*, 2005, 4755–4761.
285 M. J. Kamlet, J. L. Abboud and R. W. Taft, *J. Am. Chem. Soc.*, 1977, **99**, 6027–6038.
286 P. Illner, S. Begel, S. Kern, R. Puchta and R. van Eldik, *Inorg. Chem.*, 2009, **48**, 588–597.
287 I. Correia and T. Welton, *Dalton Trans.*, 2009, 4115–4121.
288 M. Schmeisser and R. van Eldik, *Inorg. Chem.*, 2009, **48**, 7466–7475.
289 S. Begel, F. W. Heinemann, G. Stopa, G. Stochel and R. van Eldik, *Inorg. Chem.*, 2011, **50**, 3946–3958.
290 M. Schmeisser, A. Zahl, A. Scheurer, R. Puchta and R. van Eldik, *Z. Naturforsch., B: J. Chem. Sci.*, 2010, **65**, 405–413.
291 M. Schmeisser, F. W. Heinemann, P. Illner, R. Puchta, A. Zahl and R. van Eldik, *Inorg. Chem.*, 2011, **50**, 6685–6695.
292 K. Pokorny, M. Schmeisser, F. Hampel, A. Zahl, R. Puchta and R. van Eldik, *Inorg. Chem.*, 2013, **52**, 13167–13178.
293 M. Schmeisser, P. Illner, R. Puchta, A. Zahl and R. van Eldik, *Chem. – Eur. J.*, 2012, **18**, 10969–10982.
294 A. H. Tullo, C&EN February 3, 2020, 24–27.
295 R. H. Erlich and A. I. Popov, *J. Am. Chem. Soc.*, 1971, **93**, 5620–5623.
296 V. Gutmann, *The Donor-Acceptor Approach to Molecular Interactions*, Plenum, New York, 1976.
297 W. Linert, A. Camard, M. Armand and C. Michot, *Coord. Chem. Rev.*, 2002, **226**, 137–141.
298 Y. Marcus, *Chem. Soc. Rev.*, 1993, **22**, 409–416.
299 R. G. Pearson, *Coord. Chem. Rev.*, 1990, **100**, 403–425.
300 H. Tokuda, K. Hayamizu, K. Ishii, A. B. H. Susan and M. Watanabe, *J. Phys. Chem. B*, 2004, **108**, 16593–16600.
301 T. Cremer, C. Kolbeck, K. R. J. Lovelock, N. Paape, R. Wölfel, P. S. Schulz, P. Wasserscheid, H. Weber, J. Thar,

 

B. Kirchner, F. Maier and H.-P. Steinrück, *Chem. – Eur. J.*, 2010, **16**, 9018–9033.
302 R. Katoh, *J. Phys. Chem. B*, 2008, **112**, 14971–14975.
303 T. Fujisawa, M. Fukuda, M. Terazima and Y. Kimura, *J. Phys. Chem. A*, 2006, **110**, 6164–6172.
304 J. Estager, A. A. Oliferenko, K. R. Seddon and M. Swadźba-Kwaśny, *Dalton Trans.*, 2010, **39**, 11375–11382.
305 T. A. Zawodzinski and R. A. Osteryoung, *Inorg. Chem.*, 1989, **28**, 1710–1715.
306 J.-F. Gal and C. Laurence, *Chem. – Eur. J.*, 2013, **19**, 16832–16834.
307 R. W. Taft, N. J. Pienta, M. J. Kamlet and E. M. Arnett, *J. Org. Chem.*, 1981, **46**, 661–667.
308 Y. Marcus, *J. Solution Chem.*, 1984, **13**, 588–634.
309 M. Schmeisser, P. Illner, R. Puchta, A. Zahl and R. van Eldik, *Chem. – Eur. J.*, 2013, **19**, 16835–16836.
310 S. Begel, R. Puchta, J. Sutter, F. W. Heinemann, L. Dahlenburg and R. van Eldik, *Inorg. Chem.*, 2015, **54**, 6763–6775.
311 M. Schmeisser and R. van Eldik, *Dalton Trans.*, 2014, **43**, 15675–15692.
312 S. Kern and R. van Eldik, *Inorg. Chem.*, 2012, **51**, 7340–7345.
313 H. Konno, A. Kobayashi, K. Sakamoto, F. Fagalde, N. E. Katz, H. Saitoh and O. Ishitani, *Inorg. Chim. Acta*, 2000, **299**, 155–163.
314 R. Puchta, M. Galle, N. van Eikema Hommes, E. Pasgreta and R. van Eldik, *Inorg. Chem.*, 2004, **43**, 8227–8229.
315 E. Pasgreta, R. Puchta, M. Galle, N. van Eikema Hommes, A. Zahl and R. van Eldik, *J. Inclusion Phenom. Macrocyclic Chem.*, 2007, **58**, 81–88.
316 E. Pasgreta, R. Puchta, M. Galle, N. van Eikema Hommes, A. Zahl and R. van Eldik, *ChemPhysChem*, 2007, **8**, 1315–1320.
317 E. Pasgreta, R. Puchta, A. Zahl and R. van Eldik, *Eur. J. Inorg. Chem.*, 2007, 1815–1822.
318 E. Pasgreta, R. Puchta, A. Zahl and R. van Eldik, *Eur. J. Inorg. Chem.*, 2007, 3067–3076.
319 L. Helm and A. E. Merbach, *Coord. Chem. Rev.*, 1999, **187**, 151–181.
320 F. A. Dunand, L. Helm and A. E. Merbach, *Adv. Inorg. Chem*, Academic Press, 2003, vol. 54, pp. 1–69.
321 P. A. Pittet, G. Elbaze, L. Helm and A. E. Merbach, *Inorg. Chem.*, 1990, **29**, 1936–1942.
322 R. Puchta and R. van Eldik, *Helv. Chim. Acta*, 2008, **91**, 1063–1071.
323 R. Puchta and R. van Eldik, *Z. Anorg. Allg. Chem.*, 2008, **634**, 735–739.
324 B. Neumüller and K. Dehnicke, *Z. Anorg. Allg. Chem.*, 2006, **632**, 1681–1686.
325 S. Rachmilovich-Calis, A. Masarwa, N. Meyerstein, D. Meyerstein and R. van Eldik, *Chemistry*, 2009, **15**, 8303–8309.
326 A. Budimir, M. Walther, R. Puchta and R. van Eldik, *Z. Anorg. Allg. Chem.*, 2011, **637**, 515–522.
327 M. Galle, P. Ralph, N. van Eikema-Hommes and R. van Eldik, *Z. Phys. Chem.*, 2006, **220**, 511–523.
328 R. Puchta and R. van Eldik, *Eur. J. Inorg. Chem.*, 2007, 1120–1127.
329 R. Puchta, R. Meier and R. van Eldik, *Aust. J. Chem.*, 2007, **60**, 889–897.
330 R. Puchta and R. van Eldik, *J. Inclusion Phenom. Macrocyclic Chem.*, 2008, **60**, 383–392.
331 S. Begel, R. Puchta and R. van Eldik, *Beilstein J. Org. Chem.*, 2013, **9**, 1252–1268.
332 S. Begel, R. Puchta and R. van Eldik, *J. Mol. Model.*, 2014, **20**, 2200.
333 S. Begel, A. Scheurer, R. Puchta and R. van Eldik, *Z. Anorg. Allg. Chem.*, 2016, **642**, 395–402.
334 R. Puchta, D. Walther, M. März, S. Begel and R. van Eldik, *Z. Anorg. Allg. Chem.*, 2019, **645**, 701–705.
335 R. Puchta, S. Begel and R. van Eldik, *Adv. Inorg. Chem.*, 2019, **73**, 445–505.
336 R. Puchta, D. Ćoćić, M. Michel and R. van Eldik, *J. Coord. Chem.*, 2019, **72**, 2106–2114.
337 S. Begel, A. Scheurer and R. Puchta, *J. Coord. Chem.*, 2015, **68**, 3374–3387.
338 F. G. Cantú Reinhard, A. S. Faponle and S. P. de Visser, *J. Phys. Chem. A*, 2016, **120**, 9805–9814.